Effects of Distorted Voltages on the Performance of Renewable Energy Plant Transformers

by

Mahdi Khanali

A thesis
presented to the University of Waterloo
in fulfillment of the
thesis requirement for the degree of
Doctor of Philosophy
in
Electrical and Computer Engineering

Waterloo, Ontario, Canada, 2017

Examining Committee Membership

The following served on the Examining Committee for this thesis. The decision of the Examining Committee is by majority vote.

External Examiner	Behzad Kordi Dr
Supervisor(s)	Shesha Jayaram Dr
Internal Member	Edward Cherney Dr
Internal-external Member	Xianguo Li Dr
Other Member(s)	Siva Sivoththaman Dr

AUTHOR'S DECLARATION

I hereby declare that I am the sole author of this thesis. This is a true copy of the thesis, including any required final revisions, as accepted by my examiners.

I understand that my thesis may be made electronically available to the public.

Abstract

The significant global growth in renewable energy production has led to increasing concerns about the problems associated with electrical equipment in power plants connected with this type of energy. The crucial electrical components of renewable energy generation are step-up transformers, with respect to which, gassing problems and premature insulation failures have been extensively reported in recent years. One of the factors related to the reported problems is the presence of high-frequency high-dV/dt voltages that are created by switching operations in wind energy plants. Addressing this challenge necessitates the investigation of transformer insulation systems under high-dV/dt pulse voltages.

This thesis presents research undertaken in order to examine the performance of wind turbine step-up transformers under distorted voltages, with consideration of internal resonance phenomena and high-frequency dielectric effects. To evaluate the effect of distorted voltage on the acceleration of the ageing process in transformers, model transformers have been aged under distorted power converter voltage as well as under pure sinusoidal power grid voltage. Relevant parameters are monitored as indicators of the condition of the transformer insulation, and the results are compared throughout the ageing period. In addition, to study the transformer behavior under high-frequency high-dV/dt voltages, a detailed high-frequency model is necessary. High frequency modeling of large power transformers is complex and time-consuming due to their sizes. Therefore, as an alternative approach, this work proposes a modeling method that considers the high-frequency behavior of a scale down model transformer, and then relates it to the behavior of the actual size transformer. To verify the proposed modelling method, an experimental study investigates the correlations between the frequency responses of the two model transformers of different power ratings and sizes. Comparison of the frequency responses of the scaled and original transformers validates the proposed approach of scaling transformers for high-frequency study.

High-frequency measurements are performed on an actual wind turbine transformer to represent a linear wideband black-box model of wind turbine step-up transformer in an electromagnetic transient study. Using the simulation results for switching impulsive waveforms imposed on wind turbine transformers due to the adjacent breakers operations, this work evaluates the effects of impulsive voltage parameters such as rate of rise and repetition frequency on inception voltage and intensity of partial discharge, generally assumed to be the main long-term cause of insulation deterioration. Partial discharge parameter measurement under high-dV/dt voltages is challenging due to interferences from fast

oscillations, and difficulties of PD energy measurements. To avoid such issues, which are related to electromagnetic detection methods under pulse energization, this work uses a chemical approach to compare PD, based on the rate of hydrogen generation in a controlled test chamber with oil/paper samples. Gas monitoring of the oil containing impregnated paper samples show good linear correlation between the amount of hydrogen detected and PD energy level.

Transformers installed in renewable energy plants require specific design considerations in order to protect them from the adverse effects of abovementioned voltage distortions. A number of manufacturers practice the implementation of electrostatic shields in transformer windings to filter the transferred voltages. Although this method has shown some improvements, effectiveness of the electrostatic shielding for a broad frequency range requires further studies. The effectiveness of electrostatic shielding in alleviating the transfer of high-frequency distortions from LV winding to HV winding and vice versa is evaluated with an experimental study. To compare the internal field enhancement at different frequencies in the presence and absence of an electrostatic shield, the frequency response of the voltage distribution inside the transformer's winding is also measured and analyzed.

Internal short circuit is one of the far-reaching incidents that has been recently reported for many wind-farm transformers. Detecting the location of an internal short circuit in a transformer winding is beneficial in improving future designs by defining the critical spots for target oriented insulation reinforcement. In an effort to identify trends with inter-turn fault locations and frequency responses, this research investigates the effect of the location of deliberately initiated internal faults on parameters such as transfer voltages and input impedance by means of frequency response analysis. Finally, alternative approaches are suggested for wind-farm design based on a method for recognizing the transformer compatibility with its surrounding devices such as power converters, breakers and cables.

Acknowledgements

I would like to express my sincere appreciation and thankfulness to my supervisor, Dr. Shesha Jayaram for her guidance and exceptional support throughout my PhD. I was inspired by her motivation, patience, and the way she takes very good care of her group in all circumstances.

My thanks also go to Dr. Sivoththaman and Dr. Li, who honored me by being on the committee of my thesis examination. My sincere gratitude is to Dr. Kordi who accepted to join my dissertation from University of Manitoba and advised me with his precise comments. I would also appreciate the determining professional advice that I received from Dr. Cherney during my PhD study and thesis defence.

I would also like to thank Amir Hayati Soloot and Hans Hoidalen for providing the opportunity for me to have a fruitful research collaboration with Norwegian University of Technology. My appreciation goes to John Cheng who helped me by preparing my transformer test samples.

My special thanks go to my colleagues and friends Saleh and Desireh, with whom I started my PhD journey, and also Mohana, Refat, Alireza and Saman who all were there for me during my ups and downs. I am grateful to Chitral for his insightful inputs on my dissertation and being a great lab mate.

Amongst all the wonderful people in ECE department, I can never thank enough Susan and Brenda for their technical and moral support, and being accommodating without being asked.

My mother and my father are the blessings of my life and the ones to whom I owe all my achievements. I learned from them that the most beautiful gift of God is mercy. My deepest gratitude goes to them for their kindness and beautiful hearts.

Last but not the least, my sisters were my first mentors since my very first days. I never forget their spiritual support, caring and precious guidance.

Dedication

To Pedram,

My best friend, my brother, my cousin, … who always brought smile to my face. May the blessing of God be upon him and rest in peace.

To Fatemeh,

My sister, from whom I learned to value ideas and concepts rather than events and appearances.

Table of Contents

List of Figures

List of Tables

Chapter 1
Introduction

1.1 Introduction

Power transformers are among the most complicated and strategic components of the power system. Their active parts are composed of winding coils mounted on a grounded or floating core encompassed by liquid and/or solid insulation. This convoluted composure of dielectric, conductive, and magnetic parts results in a large network of capacitances, resistances, and inductances. As a two-port element in the electricity network, power transformers are subjected to stresses from both primary and secondary sides. When this kind of equipment is installed in renewable energy plants, stress conditions become more complex due to fluctuations in the primary source and to voltage distortions from both the generator and network sides.

Renewable energy sources, such as wind energy, in conjunction with advancements in the field of distributed generation, have become a key element of today's power generation. Wind energy – the focus of this research – is delivered to the power grid via different types of energy-conversion systems, ranging from generators equipped with gearboxes to gearless generators connected to power converters. Currently, variable speed wind turbine generators, which are connected to the power grid through full power converters, defined as Type-4 conversion systems, are increasingly being implemented in wind-farms [1]. In such arrangements, the output from the generators is fed to an AC-DC-AC converter, which in turn, feeds the wind turbine step-up (WTSU) transformer. WTSU transformers are equipped with fast circuit breakers on both the converter and grid sides to enable the energization and de-energization of the transformer, in the case of a fault event or extreme wind conditions. Figure 1-1 shows the single-line diagram of a typical wind power plant. Although this arrangement, has the positive effect of adding controllable characteristics and decoupling the generator from the grid via a DC link, the voltage sourced converters (VSCs) and frequently switching vacuum circuit breakers (VCBs) produce voltages with high-dV/dt contents that cause additional stresses on power system assets. Due to their comparatively low amplitude, such high-dV/dt voltages cannot be arrested by surge protectors but, over the medium and long term, can cause significant damages to the transformer insulation and other elements of such power plants.

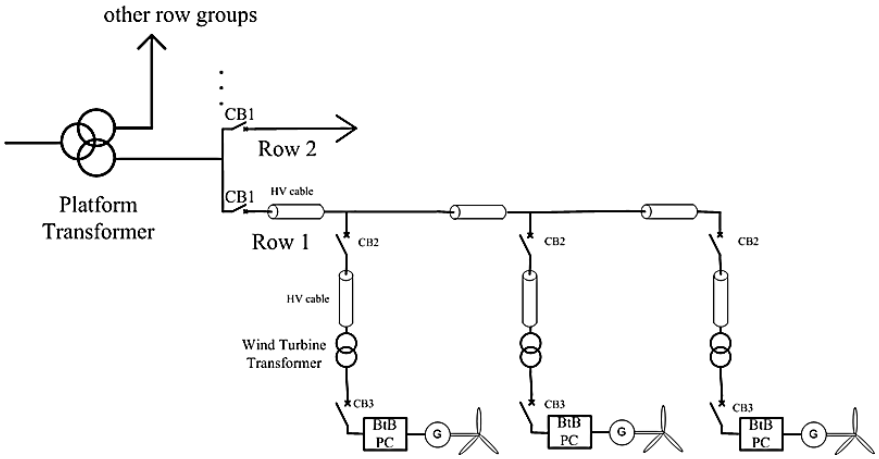

(a)

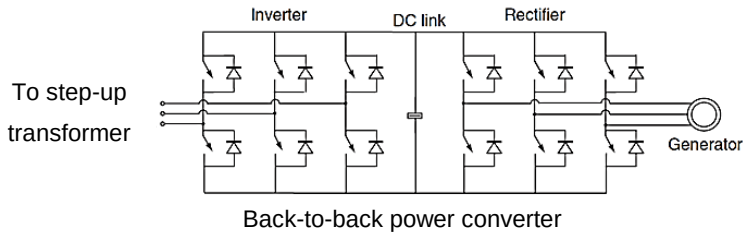

(b)

Figure 1-1: (a) A typical wind farm single line diagram (step-up transformers are connected to a power converter via circuit breakers), (b) Typical power converter topology.

Considering the average age of this type of wind energy generation, the problems associated with transformers in wind-farms are relatively new, and the majority of transformer manufacturers still prefer to keep any records and causes of failure incidents undisclosed. Therefore, there is very little published data related to the detailed analysis of such problems [2-6]. However, the relatively large numbers of high gassing issues and premature failures have been frequently acknowledged in recent publications [7-17]. For example, Figure 1-2 [6] compares the numbers of distribution transformers and WTSU transformers that contain more than 101 ppm hydrogen content (IEEE C57.104-2008 condition 2 (101 ppm to 700 ppm), 3 (701 ppm to 1800 ppm), and 4 (> 1800 ppm)). A study of more than 6000 transformers showed that 28.8 % of wind-farm transformers were characterized by conditions 2, 3, and 4 with respect to hydrogen. On the other hand, only 7.4 % of distribution transformers belonged to condition classifications 2, 3, and 4. Information was also collected from furan, acidity, and tan-delta tests, the results of which suggested the occurrence of accelerated paper ageing in such high-gassing transformers [7]. In addition, meetings and discussions with a number of transformer manufacturers

and also with wind-farm developers have confirmed that premature failures of WTSU transformers are currently causing huge problems for the wind energy industry (Figure 1-3). Insulation problems have occurred in locations where no noticeable overvoltage had been recorded so that lightning or system switching transients are not the cause of these failures. Instead, stresses from VSCs and repeated VCB operations are considered to be continuous fatiguing processes acting on the insulation of these transformers. Thus, WTSU transformers, in comparison with conventional ones, require special consideration with respect to their design, maintenance, and operation. Although the design modifications practiced by a number of manufacturers have improved the performance of WTSU transformers to some extent [8,9], high gassing and premature failures still occur. The focus of the research presented in this thesis is on the investigation of problems associated with WTSU transformers in light of the electromagnetic and dielectric effects operating at high-frequency ranges.

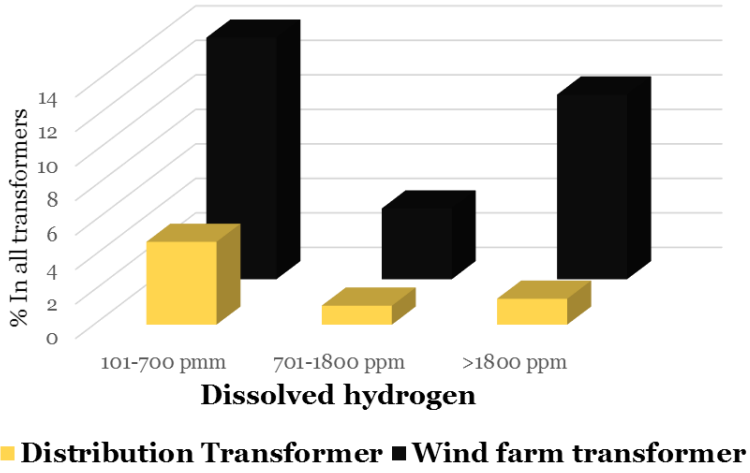

Figure 1-2: Comparison of hydrogen contents in transformers installed in wind-farm and other conventional substations [6].

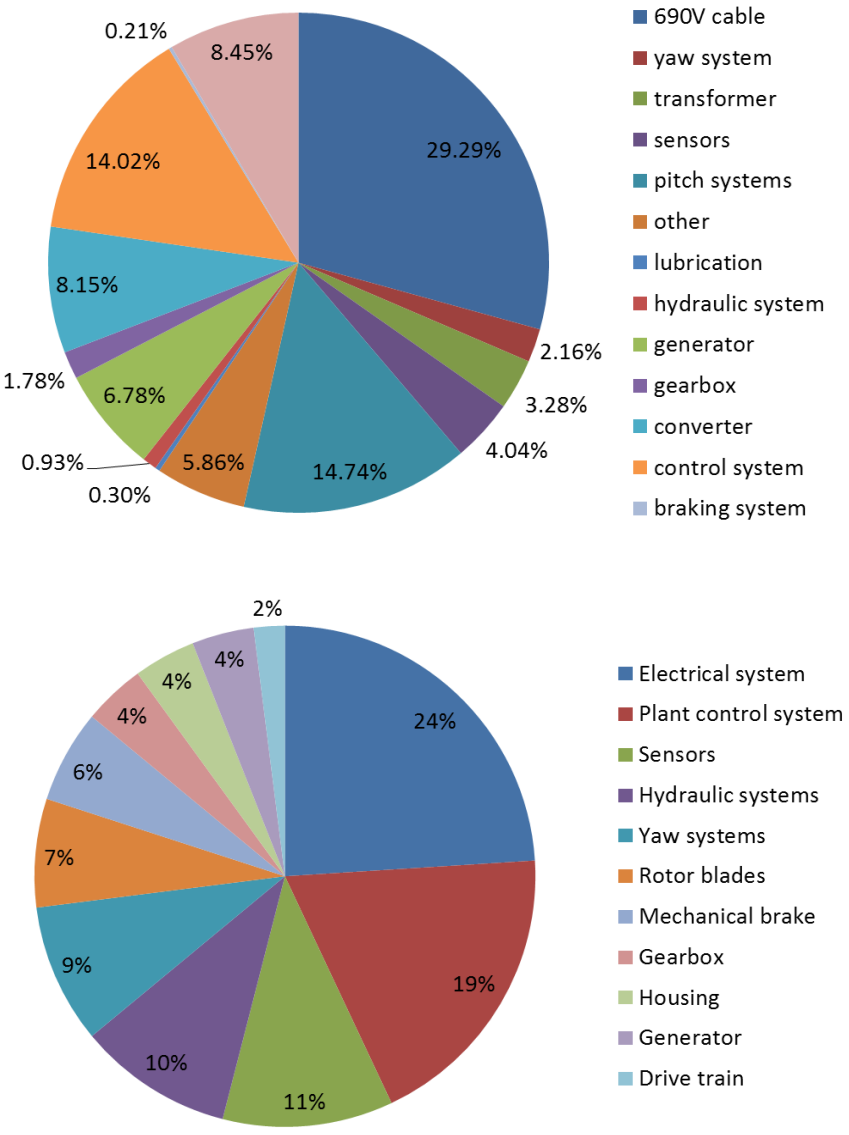

Figure 1-3: Wind turbine downtime proportions per component/system, (top) documented for 29134 Type-4 wind plants each with a capacity of 1.5 MW in the southeast coastal region in China in the first six months of 2011, (bottom) documented for Northern Europe in a survey of 1500 WTs over 15 years [10,11].

1.2 Transformers in wind-farms

The current state of the art and the specific considerations that should be taken into account in the design of WTSU transformers are briefly discussed here.

1.2.1 Load cycle

Load cycle in distribution systems has practically a constant pattern, with cycling on a daily basis (two peaks per day for most of the regions). In contrast, WTSU transformers, even in a short time period, may experience several ups and downs in the generation depending on the fluctuations in wind speed (Figure 1-4). The high number of load fluctuations on one hand, and its fast rate of changes on the other, impose excessive thermal stresses on transformer structure. Moreover, the variations in transformer oil temperature change the solubility of gasses resulting in formation of gas bubbles. It is well known that the presence of gas bubbles increases the chances of partial discharge (PD) initiation.

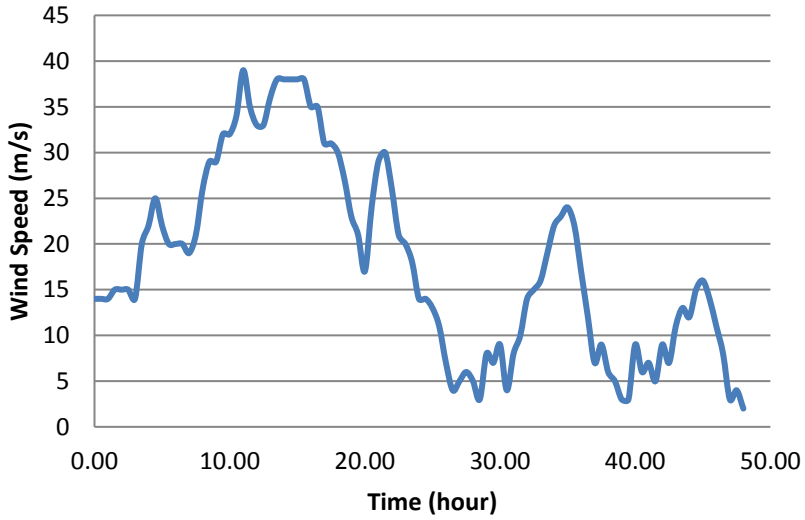

Figure 1-4: Example of recorded wind speed for a two-day span in Haldimand wind-farm, Ontario, Canada (averaged every 30 minutes) [12].

1.2.2 Harmonics and spikes

WTSU transformers are supplied by power converters which generate pulse-width-modulated (PWM) voltages. The output voltage of the converter is a sinusoidal waveform with high-dV/dt spikes repeating at the switching frequency of the converter (Figure 1-5). These spikes are very fast transients containing high-frequency components in the range of MHz due to high dV/dt, and other frequency components in the range of kHz due to the switching frequency; hence imposing additional electrical

stresses on transformer insulation system. These high-frequency contents continuously traverse through transformer windings, and can excite one or more of the windings' natural frequencies resulting in severe internal voltage amplification and damage to transformer insulation due to resonance [13]. Thus, the internally amplified tensions can develop in the windings and degrade transformer insulation without causing any significant overvoltages at transformer terminals.

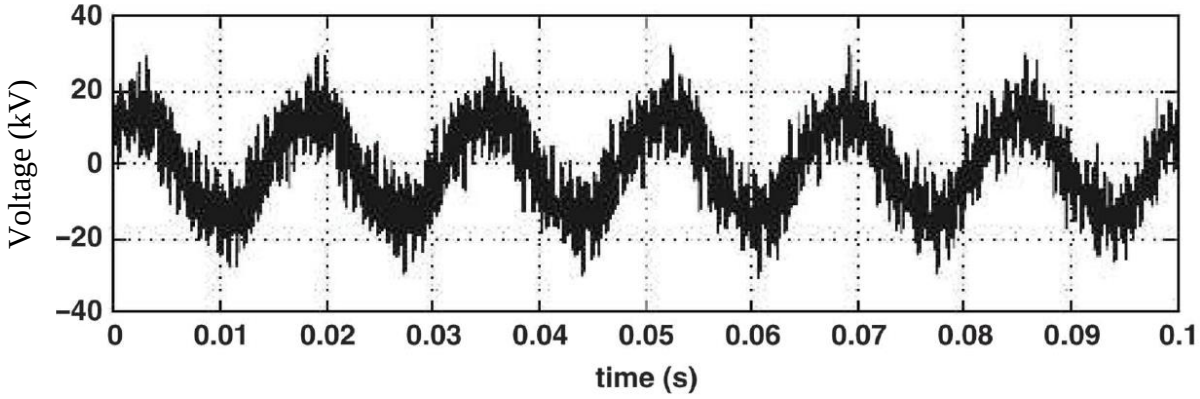

(a)

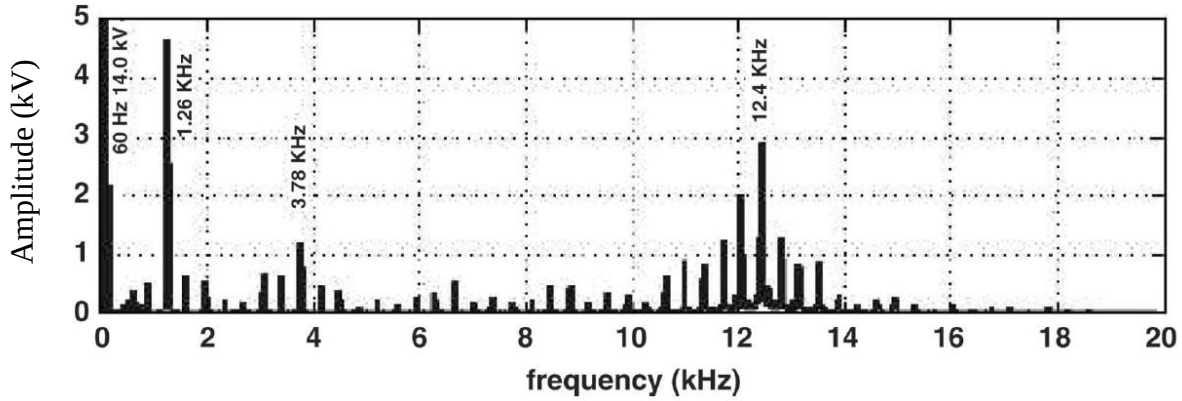

(b)

Figure 1-5: Line voltage at the terminals of a converter-fed transformer, (a): voltage waveform, (b): voltage frequency contents [14].

Other than voltage spikes, the kHz-range switching frequency contents give rise to additional eddy and dielectric losses compared to that in normal power-frequency grid sources. At critical spots in the winding, these additional losses may result in local hot-spots which may result in the generation of more gasses, PD, and insulation deterioration. Similar effects from distorted voltages have also been

observed in converter-fed cable terminations, where, due to resonance effect, the high-frequency content in voltage caused local field enhancement and temperature increase of the stress grading layers, causing significant insulation failure [15].

1.2.3 Switching operation

In addition to converter switching transients, in wind-farms, connecting and disconnecting a transformer also imposes oscillatory voltages on transformer terminals (Figure 1-6). Breakers disconnect the WTSU transformer in cases of very high or very low wind speed and also in the events of severe fault in the grid. In other words, VCB action can occur a few times in one day, thereby stressing the winding insulation to high-frequency oscillations. As it is shown in Figure 1-1, typically a WTSU transformer is connected to VCBs via cables with lengths of few hundred meters or less. The severity of such oscillations is significantly high due to the interaction of the traveling surge with capacitance and inductance of both connecting cable and transformer [4, 13, 16]. Such repeating transients affect transformer insulation through internal resonances between conductive parts [16]; traveling of voltage surge along the windings [17,18]; and the steep-front voltages intensively affecting dielectric parts [19].

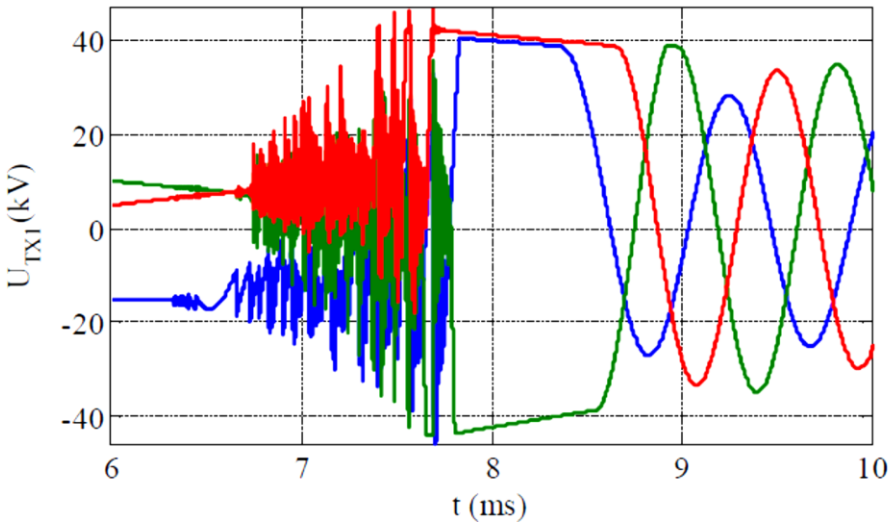

Figure 1-6: Measured overvoltages at the terminals of a 20 kV transformer due to VCB opening under inductive load with an 80 m cable [20]. ©ABB Group, 2011

1.2.4 Fault withstand

Fault ride-through capability is a requirement for WTSU transformers which puts higher electrical, thermal and mechanical stresses on them. It requires the transformers to be able to operate for up to ten

cycles under fault conditions, for network stability purposes [21]. Conventional distribution transformers are not normally subjected to or designed to endure such stresses.

Installing grounding transformers at the neutral points of wind-farm transformers is recommended to ease the stresses during the fault events. Grounding transformers, usually in zig-zag connection, lift up the voltage of the faulted phase by adding a zero-sequence impedance. This performance consequently lessens the overvoltage on the other phases [22].

1.2.5 Transfer of voltage contents

The abovementioned non-conventional voltage waveforms can also penetrate into the network and cause electrical and thermal stresses on other apparatus. Therefore, it is necessary to know how the LV generation voltage waveform is transferred to the HV network side of the transformer. On the other hand, when the circuit breaker on the HV side operates, due to the transfer of voltage oscillations to the LV terminals, connection cables and power electronic elements of the converter are exposed to harsh transient voltage strikes [23]. In this matter, a broadband transfer function of the transformer would assist to predict the voltage waveform and its high-frequency contents at HV side (when excited from LV side) and LV side (when excited from HV side). To obtain the voltage transfer function, different methods have been adopted; such as transformer analytical modelling [24], numerical modelling [25] and models based on sweep frequency response measurements [26].

1.2.6 Design modifications

To address issues discussed earlier with wind-farm connected transformers, a number of transformer manufacturers proposed a series of modifications to specially design transformers for renewable energy applications [26, 27]. One of the approaches used in renewable energy plants to reduce the volume of high-frequency content delivered to the secondary winding is the use of electrostatic shields. Since the LV winding that is connected to the power converter is generally ungrounded, it can be capacitively coupled with the HV winding. The electrostatic shield acts as a capacitive decoupler to prevent the transfer of critical voltage components onto the secondary side. The shield shall be grounded at least in a single point. This will typically supply 60 dB of common mode noise attenuation from 100 Hz through 1 MHz [29]. On the other hand, placing an electrostatic shield can shift resonance frequencies of the windings and potentially increase the voltage amplification factor at certain other frequencies. To this purpose, there are two main aspects that require investigations: effect of shielding on the distribution of electric stress inside the windings, and the performance of electrostatic shield in preventing the

transfer of high-frequency contents from one side to the other. From the power system point of view, only the delivery of high-frequency contents of the voltage from the step-up transformer to the power grid is important while, from the asset management point of view, both terminal voltages and internal voltage amplifications are of great importance as they affect the transformer insulation. Therefore, more work should be done on the design of electrostatic shield to improve its applicability.

The multiple-point grounding of the transformer magnetic core is another modification recommended by some researchers (Figure 1-7) [8]. The recommendation is founded on the idea that accumulation of static charge on the transformer core may result in electric field enhancement; hence, PD, especially at sharp edges. Since many of the WTSU transformers feature five-leg wound cores, there would be a noticeable difference between the potentials of inner and outer core layers if the core is grounded only at one point. Multiple-point or shield grounding of the core may alleviate such potential difference between the core layers.

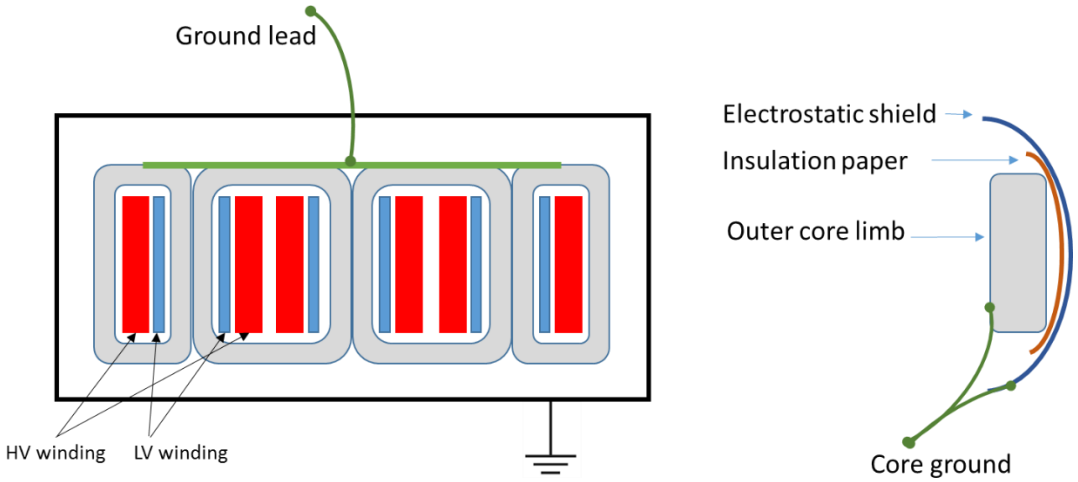

Figure 1-7: Left, conventional grounding arrangement, and right, recommended grounded shielding [8].

Another possible approach towards a competent design of WTSU transformers is the reinforcement of winding insulation. However, to perform an efficient implementation of additional insulation, it is necessary to have a reasonable approximation of field enhancement locations and the critical points of transformer windings. With such approach, instead of oversizing the transformer with more insulation throughout, only the positions with the highest probability of failure will be strengthened with suitable dielectric materials. This estimation can be performed with two procedures: using the statistical

information from the locations of the past failures in the transformer of the same design, and using transformer's high-frequency detailed model to locate the critical field enhancement points.

1.3 Research objectives

Based on the above discussion, several parameters should be considered for understanding the performance of WTSU transformers under high-frequency high-dV/dt conditions that exist in renewable energy plants. Furthermore, the implementation of new design criteria for WTSU transformers will become possible only when the distribution of electric fields and the ageing of transformer insulation at higher frequencies are thoroughly examined. The following are the objectives of this thesis:

- To investigate the phenomena associated with electrical stress due to high-frequency high-dV/dt voltages inside the transformer, considering electromagnetic resonance effects.
- To develop diagnostic schemes for examining the effect of distorted voltages on the degradation of transformer paper/oil insulation and effect of voltage waveform parameters on partial discharge.
- To evaluate the use of frequency response analysis in high-frequency transformer modeling as well as calculation of internal stress profile.
- To understand the performance of transformer design modifications and to suggest further effective design modification for more robust transformer.

The research conducted for this thesis will therefore contribute to the understanding of ageing and failure under high-dV/dt voltages through the testing of scale down models of wind-farm transformers under simulated voltage waveforms similar to those that exist at the terminals of WTSU transformers. The research is complemented by a study of the behaviour of individual transformer insulation samples under voltage pulse trains in the range of the transients that occur at transformer terminals in the case of breaker operation. The distribution of the electric field in a transformer winding is measured by means of several leads connected to different layers of the sample transformers windings. An accurate determination of the electric field distribution inside the transformer insulation system is achieved by taking into account the high-frequency spectrum of the voltage developed at a transformer terminal. For this purpose, a high-frequency simulation of an Ontario wind-farm was performed using an accurate

model of the transformer that was installed in that wind-farm along with high-frequency models of connected equipment such as breakers and cables.

The structure of this proposal is outlined here:

- Chapter 2 outlines the materials, test setups and methods utilized in this research.
- Chapter 3 presents the results of experimental studies, model verifications and design modification impacts.
- Chapter 4 discusses the results obtained in this research and recommends provisions for better utilization of WTSU transformers.
- Chapter 5 summarizes this research and offers a conclusion along with potential contributions. The thesis ends with suggestions for future work.

Chapter 2
Literature Survey

In this section, literature related to this work is reviewed. The first part reviews the literature which studied the degradation of dielectric materials under high-frequency distorted voltages, and compared it with that under sinusoidal power-frequency voltages. The next part discusses partial discharge, as the dominant root of insulation deterioration, and its measurement methods under high-dV/dt voltages. To focus on the specific impacts of high-dV/dt voltages on transformers, the third section reviews resonance effects in transformers and how high-frequency stresses affect transformer insulation system. Fault detection methods using FRA analysis are explained, and finally, transformer modelling methods are presented and compared with each other.

2.1 Insulation materials under distorted voltage

Generally, it is accepted that dielectric materials get affected more severely by pulsed or high-frequency voltages than the power-frequency voltages. This phenomenon and the associated mechanisms behind an accelerated ageing process has been the focus of many researchers. To evaluate ageing acceleration under high-frequency distorted voltages, it is required to study the ageing of individual insulation specimens. A challenge in such studies is to produce a criterion to estimate the degradation level of an aged dielectric material.

Gao *et al.* [30] used the loss factor and PD as indications of the materials ageing. Therefore, changes in these two factors under sinusoidal voltages were compared with those under square-wave voltages. Using thermally stimulated current [31], it has been shown that square wave pulses cause more damage to the insulation materials than the AC voltage of even a higher peak value (Figure 2-1). It was concluded that under square-wave pulse conditions, not only the damage due to partial discharges but also the damage from space charges increase with the increment of voltage, frequency, and temperature.

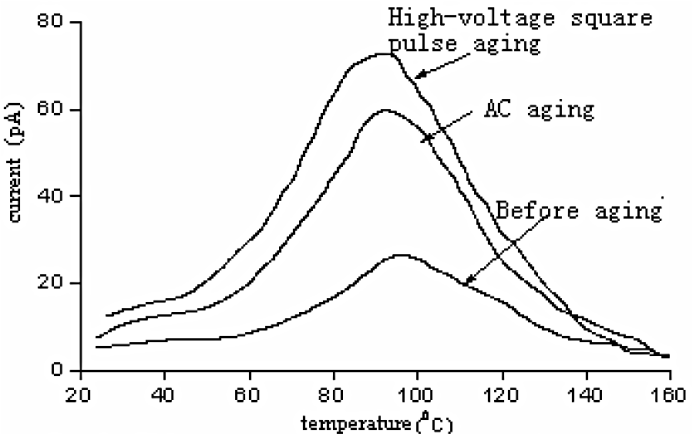

Figure 2-1: Thermally simulated current of motor insulation before and after ageing under square-wave and AC voltage [31]. © IEEE 2001

Koltunowicz, in cooperation with an international team, conducted a research on the influence of square voltage waveforms on transformer insulation breakdown voltage (Figure 2-2) [32]. The group was motivated by the fact that the use of VSCs in high voltage DC (HVDC) transmission and, more commonly, in flexible AC transmission systems (FACTS), raises concerns over the endurance of turn/turn insulation of grid/converter interface transformers. It was pointed out that mixed sinusoidal/repetitive surge voltages may impact the transformer insulation endurance. The results of tests on oil-impregnated paper specimens showed that increasing the repetition frequency and/or shortening the rise time of square waves decreases the breakdown voltage. The main cause of breakdown voltage reduction was associated with partial discharges, which appear to be incepted more easily with faster slew rates. In addition, once PD is incepted, higher repetition rates promote faster degradation [33], [34].

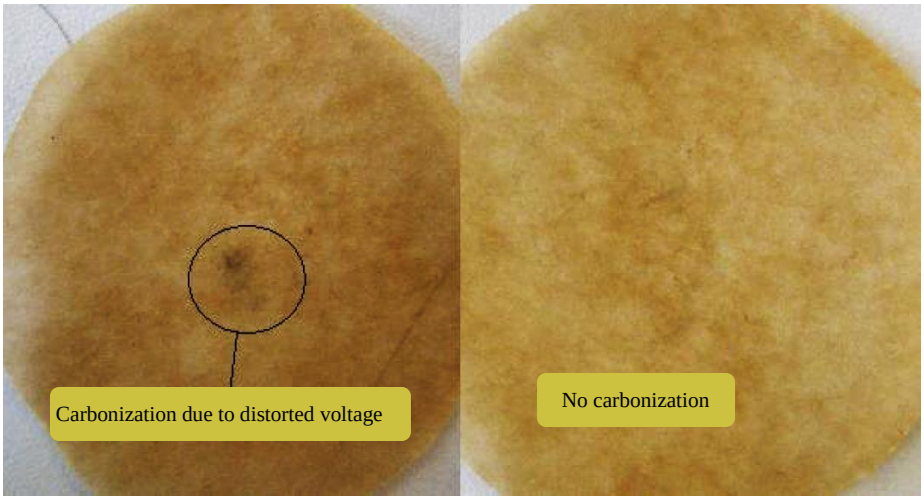

Figure 2-2: Ageing of paper-oil insulation samples, (right) under power-frequency sinusoidal voltage, (left) under high-frequency distorted voltages [32]. © IEEE 2010

In addition to the abovementioned ageing analysis, degree of polymerization [35] and tensile strength [36] are also parameters that can be used for the assessment of transformer paper/oil insulation. Measurement of such parameters requires laboratory tests on individual samples. Since the collection of paper samples from a transformer in operation is not feasible, the by-products of the cellulose degradation, such as furfural content in oil, are taken as the indirect indications of paper ageing [37].

To achieve higher precision and reliability with a lower expense, various alternative methods have been considered by researchers. As a substitute approach, insulation assessment is traditionally performed by DC insulation resistance test [38] and/or dissipation factor measurement at power-frequency [39]. Although these methods proved to be helpful for transformer condition monitoring and basic qualification of insulation systems, such single-frequency measurement methods provide limited information and may not be able to assist with differentiating between ageing, contamination, moisture etc. On the other hand, dielectric frequency response (DFR) test can reveal accurate information about the degradation level of the transformer insulation system and its probable origins [40].

2.2 PD under high-frequency distorted voltages

Under electric stress, different ageing mechanisms are active on any insulation, but when the magnitude of the electric field is over the PD inception level, PD becomes the leading cause of ageing in most insulation materials.

To have a good comparison between the partial discharge characteristics under different voltage waveforms, a consistent standardized method should be considered for PD measurements. The

applicability of IEC-60270 standard guide for PD measurement [41] is, however, questionable for high-dV/dt voltage sources because the standard measurement frequency range is limited to 1 MHz, which overlaps the frequency spectrum of the voltage source. The study of PD under pulse voltages has therefore been carried out using methods such as low-resistance non-inductive resistors, capacitive detectors, Rogowski coils, and broadband antennas [42]. Adopting these methods, Florkowska *et al.* conducted three parallel measurement procedures using electric field detection sensors, current measurement with Rogowski coil, and voltage measurement across a non-inductive resistor to study the impact of rise-time and switching frequency of pulse voltages on PD duration and PDIV. Although the authors measured the PD duration successfully, they admitted that exact monitoring of PDIV under impulse voltages that are close to the ionization threshold is challenging because of the transient development of ionization. Other studies ([43], [44]) showed that ultra-high-frequency (UHF) antennas with high-pass filters can perform well as means of indirect PD measurement, while authors of [45] adopted a direct measurement approach using mixed resistive/capacitive dividers with differential amplifiers for recording PD current waveforms. The results of abovementioned methods, however, could not be compared with each other to examine their validity because the experimental setups and test objects have been different.

Literature data regarding the behaviour of partial discharge inception voltage (PDIV) under repetitive impulse waveforms reveals some contradictions about the effects of pulse parameters on the PD characteristics. One of the possible reasons for the contradicting reported observations is that different researchers used different voltage sources, and the rise time and the frequency of the source waveform could affect partial discharge spectra. PD measurement methods that involve electromagnetic approaches are therefore subjected to noise and other forms of interference.

As an alternative to electrical detection methods, dissolved gas analysis (DGA) can be used to detect the occurrence of PD in cases that PD occurs in a bounded fluid medium. This method has been adopted widely for transformer condition assessment, based on the correlation between the dissolved gasses and the type and severity of transformer fault, e.g., overheating, arcing, and partial discharge. Muller *et al.* [46] investigated the correlation between DGA and UHF PD measurements for a power transformer under AC voltage. UHF measurements were taken using sensors inserted into the transformer tank, and taking advantage of the ability of the tank to provide electrostatic shielding from outside noise. Results indicated that the hydrogen level increased almost linearly with time due to PD under normal transformer operation. Overall, for the power transformer tested, the UHF measurements showed good

agreement with DGA measurements. On the other hand, in the case of a significantly higher excitation voltage causing a high level of PD, the amount of hydrogen and other combustible gasses increased significantly.

Despite the wide use of DGA for transformer fault detection purposes, due to the large sizes and complexity of transformers, a number of uncertainty parameters are involved in such measurements. To understand the basics, Fumihiro *et al.* [47] tested oil-immersed pressboard samples placed between rod-plane electrodes in a controlled test chamber. The authors used both PD current measurement and offline DGA for comparing PD under AC voltages in different oil viscosities. Their study also observed that hydrogen is the dominant gas in the case of partial discharge and that there is a good relationship between the measured PD energy and the level of dissolved gasses.

2.3 High-frequency stresses due to resonance in transformer

Previous studies have analyzed the dielectric stresses that can occur in transformer windings in the case of high dV/dt voltage transients. Some of these papers, such as [26], investigated surge-travel while others focused on internal resonance phenomenon [48]. Resonated voltage oscillations at transformer terminals and enhanced electrical stresses inside transformer windings are reviewed in this section.

The inherent MHz-range contents due to high slew rate spikes combined with the kHz-range contents due to switching repetition make the VSC output, potential of exciting internal resonances inside transformer windings. In addition, when VCBs are connected to transformers via few-hundred-meter cables, the generated surges have traveling frequencies that may overlap transformer resonance frequencies. In this light, a number of studies [49] analyzed the dielectric stresses that can occur in transformer windings due to high-frequency transients. Lopez-Roldan *et al.* [50] studied the transfer of lightning overvoltages between windings and showed that energizing an unloaded transformer via a cable may cause excessive overvoltages on the secondary side due to a resonant overvoltage phenomenon.

In an effort to compare the influences of periodic and aperiodic voltage surges on a power transformer, Abhinandan *et al.* [51] analyzed the voltage stresses developed in the windings of a 400/220/33-kV grid connected transformer where natural frequencies of the transformer winding were triggered by oscillatory switching transients. The authors compared developed stresses under oscillatory voltages with those under standard laboratory dielectric tests voltages. For this purpose, the

response of a 400 kV transformer connected to the Eastern Regional Power Grid of India has been analyzed under a number of probable events. Case studies showed that winding resonance produces severe voltage stresses in the tap changer coils located near the neutral end, which normally experience much lower stresses under aperiodic surges. It has been concluded that windings' response to certain oscillatory voltages can be worse than the response to any form of aperiodic voltages, whether lightning impulse, slow-rising switching impulse or steep front-long tailed switching surge (Figure 2-3). Fast front surge test may help to evaluate transformer withstand capacity, but it is evident from the study that the potential hazard associated with oscillatory system waves and winding resonance cannot be ignored. The authors stated that a reliable transformer design can only be ensured if suitable oscillatory overvoltage tests are devised and winding designs are suitably modified to handle the voltage stresses developed under such oscillatory voltages.

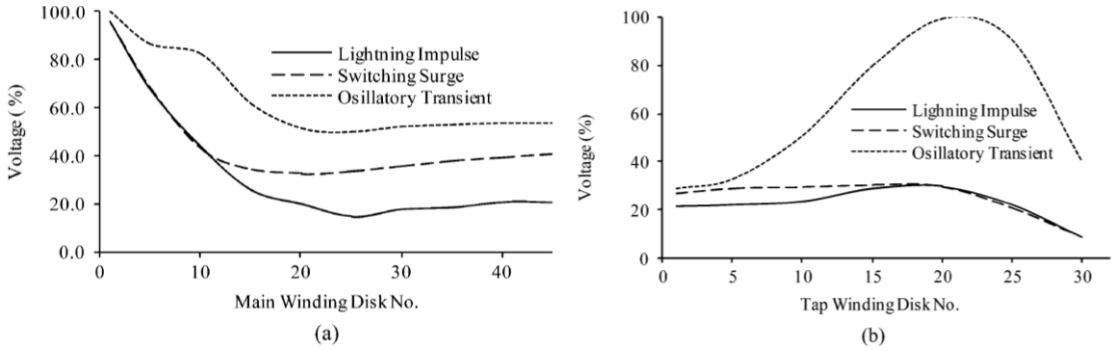

Figure 2-3: Comparison of the voltage stresses on disk coils under different incident waves (a): main winding disks and (b): tap winding discs [51]. ©IEEE 2009

Van Craenenbroeck *et al.* [52] explained the possible occurrence of internal winding resonances using experimental investigations and numerical analysis together. The experimental part of the investigation consisted of laboratory experiments and on-site measurements in a substation. The numerical analysis was carried out using a pre-processing program that translates the geometrical transformer data into a model that converts magnetic parameters to their duals in electric parameters. The duality-based model was prepared for use in an electromagnetic transient program. The authors supported the conclusion that all failures were caused by similar combinations of electrical transients, leading to internal resonances inside the transformer windings and material deterioration by PD. The insulation deterioration by partial discharges explains why many of the failures were not directly related to a switching maneuver or a lightning strike, and why the transformers failed while they all complied with the present standards.

Through FRA measurements, Soloot *et al.* investigated the winding design influence on the electric field resonance in a transformer [25]. Voltage gradients between adjacent layers and discs of transformer windings were measured with the use of FRA in a wide range of frequency. The results showed that depending on the design of the windings, transformers show different patterns of internal stresses. It was concluded that, comparing disc, layer and pancake windings, the highest internal stress at resonance frequencies happens for disc winding while the highest resonance voltage at winding terminals happens for layer structure. Further, it has been shown that resonances that occur with many frequency components can lead to high stresses and eventually cause layer-to-layer or disc-to-disc short circuits. Such resonance-initiated stresses in transformers connected to wind-farms are also reported by Banda *et al.* [53].

2.4 Standard guides

The International Electrotechnical Commission (IEC) has developed two documents to provide guidance on the qualification of electric motor's stator insulation systems subjected to voltage surges from PWM drives. IEC 60034-18-41 discusses the qualification and acceptance tests for random windings not expected to see PD during normal operation. IEC 6003418-42 covers form-wound stators, whose insulation design is expected to withstand PD in operation. On the other hand, only a short part of IEC 60076-16 standard on transformers for wind turbine applications is dedicated to the concerns about harmonics and high-dV/dt voltages. Regarding the harmonic distortion of the input voltage, the latest edition of IEC 60076-16 standard [54] outlines that if the total harmonic distortion (THD) of the transformer input voltage is higher than 5%, all the harmonic voltages and their magnitudes shall be announced to the transformer manufacturer by the purchaser. Accordingly, transformers shall be designed considering the specified input voltage spectrum or 5% THD (whichever is higher). This standard does not demand any high-frequency content specification for voltages with THD less than 5%, regardless of the frequencies of the associated voltage contents. Current regulations on the THD of transformer input voltage are based on the consideration of only limited voltage harmonics, usually up to 50^{th}, which does not cover above few kHz; hence higher frequency contents are neglected.

IEC 60076-16 acknowledges the occurrence of insulation failures attributed to VCB operations in several wind-farms; stating that the transformers exposed to the highest stress are the first and last ones in the wind-farm chain, especially at light loads. The IEEE guide on the occurrence and mitigation of switching transients induced by transformers and switching devices (IEEE C57.142) relates this issue to the vulnerability of transformers to current chops and high dV/dt voltage restrikes initiated by VCBs.

The phenomenon is not discussed in details in IEC 60076-16, and it recommends the client to perform a system study ahead of the purchase. If the system study flags a critical situation, alleviation provisions shall be taken by the wind-farm developer.

Furthermore, according to IEC 60076-16, additional tests for wind turbine transformers are specified as: lightning impulse test including chopped wave on every new design and also a PD test in accordance with IEC 60076-11 or C57.12 if required by the purchaser.

2.5 Frequency response analysis for transformer fault detection

Detection of transformer faults using frequency response analysis (FRA) has been introduced and developed as a method that adopts changes in frequency responses to diagnose physical and/or chemical changes in transformer. Today, FRA is widely used in the industry for the detection of transformer mechanical defects, such as core displacement or winding deformation. There are numerous studies that investigated the application of FRA in the identification of transformer mechanical faults explaining a number of aspects that must be considered with respect to the implementation of FRA, including frequency range and connection of non-tested terminals [54, 23].

In addition to the well-established work related to mechanical failures, detection of inter-turn short circuits has been recently studied by research groups. Wilk and Adamczyk [56] found that as an inter-turn short circuit progresses from a high-impedance connection to a total short circuit between the faulty turns, the amplitude of the winding response at its resonance frequency shows a U-shape drift (Figure 2-4). This phenomenon is attributed to the fact that the resonance amplitude is related to the energy loss in the winding which starts growing in the premature stages up to a certain maximum and then reduces when the fault develops further towards the complete short circuit.

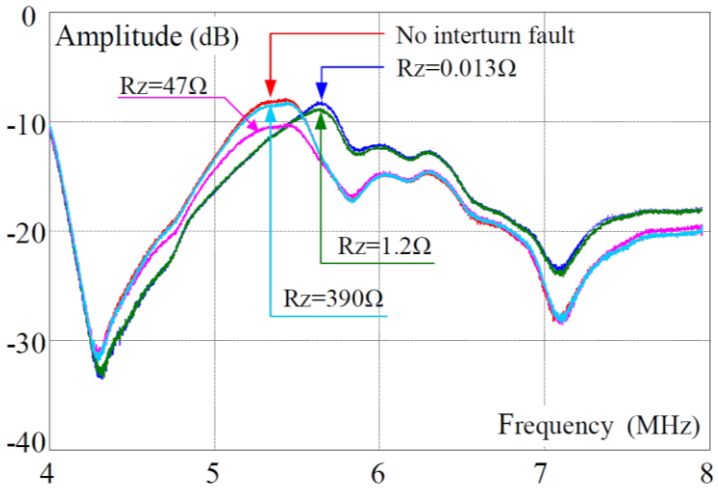

Figure 2-4: Frequency response of a model transformer winding for four stages of the short circuit development, from high connection resistance (R_z) to very low connection resistance [56]. © IEEE 2011

Detection of internal fault occurrence is the first step of fault diagnosis. In addition to the detection, knowing the location of an internal fault can also benefit operators and manufacturers by reducing cost and time required for repair, and providing statistical information about the areas of the windings in which internal faults occur more often. The latter would be useful for more effective insulation reinforcement in future designs. Furthermore, due to the exposure of wind turbine transformers to high-dV/dt voltages from frequent switching, inter-turn and inter-layer insulation of such transformers are under higher stress compared to their power-grid counterparts, as an internal short circuit is more likely to happen. However, recognizing the location of internal faults has been of less focus in recent research despite its importance.

2.6 Transformer modelling

Network components respond differently to impulsive and high-frequency oscillatory transients than to the normal power-frequency voltages. To a first approximation, these effects can be modeled using discrete element circuits. At high frequencies, the distributed capacitances of the transformer dominate the turns-ratio and hence they determine the magnitude of the transient that passes through the transformer. There are various high-frequency models proposed for transformers which have advantages over each other depending on their applications, generally classified into two main categories: internal winding models and terminal models.

2.6.1 Internal winding models

This type of model comprises large networks of capacitances and coupled inductances that can be obtained by discretization of distributed self and mutual winding inductances. The calculation of partial capacitances and inductances involves the solution of complex electric field equations and requires information about the physical layout and construction details of the transformer. This information is not generally available as it is considered proprietary by transformer manufacturers. These models have the advantage of accessing intended points inside the windings, permitting the calculation of internal winding stresses. In general, internal winding models can predict transformer resonance frequencies but cannot reproduce the associated magnitudes. This makes this class of models suitable for the calculation of initial voltage distribution along a winding due to high-frequency excitation, but unsuitable for the calculation of transients involving the interaction between the transformer and its surrounding network. Furthermore, the size of the matrices (typically 100 x 100 or larger) makes this kind of representation impractical for electromagnetic transients program (EMTP) system studies.

Gomez *et al.* [57] combined mathematical calculations with finite element method for high-frequency modelling of power transformers. The authors worked on a finite-element approach to calculating the stray capacitances, and self and mutual inductances. Based on those calculations, the dielectric stresses produced by PWM type waveforms on medium voltage transformer windings were calculated. From the results of the simulation, it was observed that the rise time of the PWM waveform has an important effect not only on the overshoots presented in the dynamic response but also on the regions of winding in which the maximum voltage stress develops.

2.6.2 Terminal models

In the majority of problems related to power system transients, transformers are considered as black-box components [58], which are modeled based on the simulation of frequency and/or time domain characteristics at the terminals of the transformer. Frequency domain data consist of terminal impedance or admittance characteristics; whereas, the time domain data is basically acquired from impulse voltage tests.

For the calculation of external overvoltages, black-box-type models are usually preferred as they do not require information about the transformer geometrical structure, and they are capable of reproducing the transformer terminal behaviour with a high degree of accuracy. Gustavsen conducted a series of studies with this approach. Measurement setup and vector fitting modelling technique were

utilized to obtain a linear wideband frequency-dependent black-box model of a two-winding power transformer, for the purpose of calculating electromagnetic transients in power systems [59]. The measurement setup was made of a network analyzer, shielded cables, and a connection board. The accuracy of the data set was increased by using a combination of current measurements and voltage transfer measurements (Figure 2-5). Vector fitting process was coupled with a rational approximation in the range of 50 Hz to 1 MHz and subjected to passivity enforcement to obtain a stable model which can be included in (EMTP)-type simulation programs. The accuracy was validated both in the frequency domain and in the time domain.

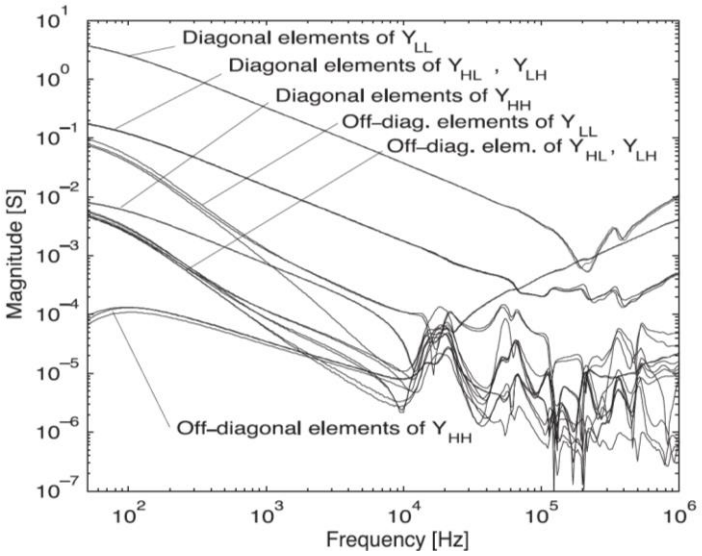

Figure 2-5: Measured frequency response of admittance matrix elements [60]. © IEEE 2004

2.7 Literature review summary

A brief summary of the reviewed literature is outlined as follows:

- Ageing degree of dielectric materials, in general, and transformer insulation, in particular, can be studied by measuring partial discharge level, dissipation factor, tensile strength, degree of polymerization, insulation resistance, dielectric frequency response and modeling studies. Dielectric frequency response test reveals more reliable information about the insulation condition compared to power-frequency dissipation factor test.
- Partial discharge measurement methods that involve electromagnetic approaches are subjected to noise and other forms of interference, and the reported results from different researchers for partial discharge measurement under high-dV/dt voltages are contradictory. Dissolved gas

analysis is immune to electromagnetic noise; hence can be used for PD detection under pulse voltages and noisy test environments.

- Pulsed voltages leave more negative effects on transformer insulation compared to AC voltages. Moreover, the repetition frequency and rise time of the repetitive pulse waves affect the breakdown voltage of insulation materials, and also affect the overshoots present in the transformer dynamic response and the locations of winding in which the maximum electric stress develops.
- Winding failures caused by a mixture of electrical transients, internal resonance, and insulation degradation are observed commonly. The fact that many of the WTSU transformer failures were not directly related to a switching maneuver or a lightning strike can be explained by gradual insulation deterioration under partial discharge.
- Resonance phenomenon due to oscillatory waveforms may result in dangerous overvoltages inside transformer windings and on the secondary side of a WTSU transformer, particularly when it is energized via a short cable. Transformer winding response to such oscillatory spikes of certain frequencies may be more harmful than aperiodic voltages such as lightning and switching impulse.
- The main categories of transformer modelling are detailed internal modeling and terminal modeling. The former is more suitable to calculate transformer internal stress while the latter is more useful for high-frequency system simulations.
- Frequency response analysis can be used for detection of internal faults and mechanical defects as well as high-frequency terminal modeling of transformer.
- According to IEC 60076-16 standard on transformers for wind turbine applications:
    - The purchaser is obliged to outline the harmonic content of the voltage only if the total harmonic distortion of the transformer input voltage is higher than 5%.
    - Voltage contents with frequencies higher than few kHz are neglected.
    - The frequent occurrence of insulation failures due to VCB operations is recognized.
    - Additional test of chopped-wave lightning waveform is recommended for WTSU transformers.

In summary, effects of distorted voltages with high-dV/dt contents on insulation systems, to a good extent, are discussed for converter-fed motors and cables in earlier studies. However, studies on the influences of voltage distortion on transformers are generally limited to overvoltages generated by lightning, or decaying transients caused by switching or faults. Although these studies have valuable inputs for analyzing the voltage distribution in transformer due to a single impulse, many important factors, e.g. internal resonances and the effects of repetitive pulses on the material degradation require more detailed studies.

Chapter 3
Materials and Methods

This chapter explains the materials specifications, the experimental setups, and the modelling and design modification methods that were implemented for this research. The first section describes the design and preparation of the test samples as well as the reasons for the specific features of each model transformer. Section 2.2 outlines the generation of the voltages applied on the test specimens, identifying the real voltage waveforms they represent. The next sections present the ageing setups for a comparative study of the effects of distorted voltages on oil-filled transformers and the investigation of the PD in paper/oil samples under impulse trains. Transformer modelling, an examination of the effects of electrostatic shielding, and a fault location study are included in the last three sections, adopting frequency response analysis methods.

3.1 Model transformers

Details of custom designed model transformers are presented here. Two identical 1-kVA transformers (T1 and T2) were built for ageing study under distorted voltages and observing electric field resonance inside the windings. Two similar but non-identical 9-kVA transformers (T3 and T4) were built for studying: effect of scaling on transformer response and use of scaling in modelling; and effect of electrostatic shielding on transformer high-frequency behaviour. A 500-kVA transformer, built in Norwegian University of Technology, was also used in a joint study on fault location estimation in WTSU transformers.

3.1.1 Model transformers for ageing study

All four model transformers built for this research (T1, T2, T3 and T4) feature the same voltage ratio and similar materials to that used in conventional wind-farm transformers. Table 3-1 shows the general specification of two identical model transformers, T1 and T2. T1 and T2 are the same in their construction as conventional pole-mount transformers except for two additional features: multiple embedded connection leads and temperature sensors (Figure 3-1). In order to analyze voltages inside the windings, 10 additional connection leads, one in each layer, are inserted in HV windings to facilitate the monitoring of generated voltages between layers of the windings (Figure 3-2). Five thermal sensors are also installed for measuring the winding temperature profile during ageing. The thermal sensors are inserted in the middle position of layers, and evenly distributed from the innermost layer to the

outermost one. To avoid any electromagnetic interference, fiber optic sensors with no metal parts are utilized.

Table 3-1: Specifications of model transformers T1 and T2.

T1 and T2 Specifications	
Rated Output	1 kVA
Type	Single phase, Oil filled
Voltage	115 V / 6.6 kV
Connection leads (10)	One in every layer
Thermal sensors (5)	Accuracy: 1 °C In layers 1, 3, 5, 7, 9
Nominal frequency	60 Hz
Number of turns for LV winding	130
Number of turns for HV winding	7480

Figure 3-1: Photograph showing model transformers T1 and T2.

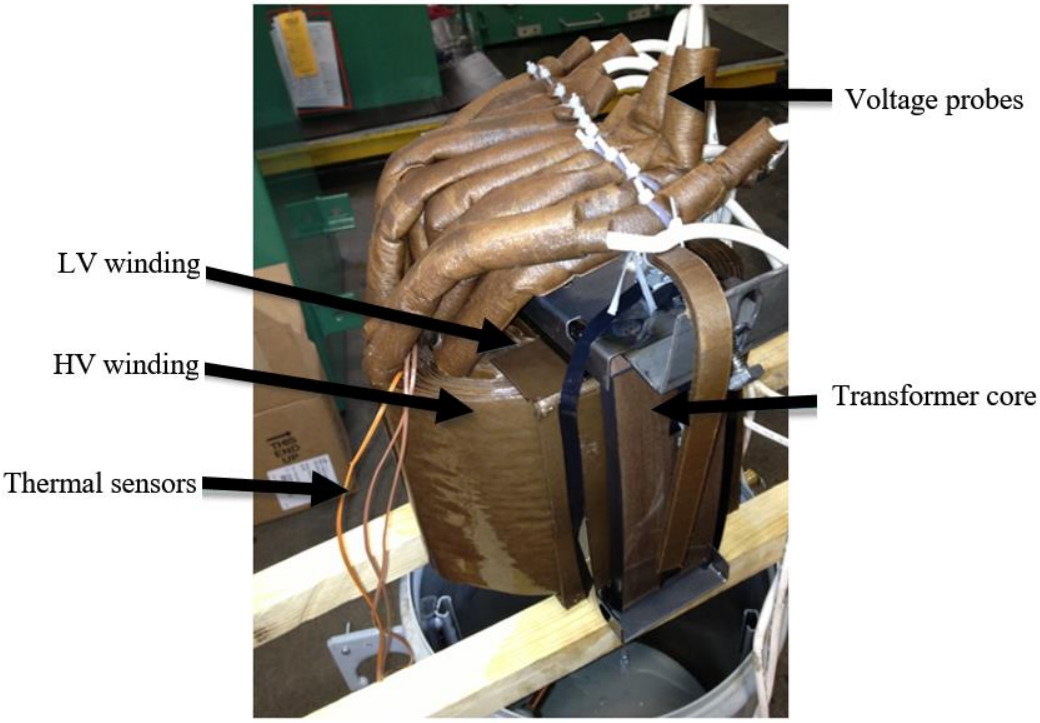

Figure 3-2: Active part of T1 (out of tank).

3.1.2 Model transformer for scaling effect study

Transformer T3 is a scaled version of T1 in terms of size, voltage and current capacity, and was built using same materials and design as T1 and T2 (Figure 3-3). T3 is designed with the same turns ratio as that of T1, which also matches the typical turns ratio of wind turbine transformers used in Ontario, Canada. The crucial part of designing the scaled model transformers is selecting appropriate components sizing based on the desired scale factor.

Principles of the scaling method are described here for a scaled version transformer (T3) based on original (reference) transformer (T1), by a scale factor called *Scl*. In this work, *Scl* is defined as the ratio of any one-dimensional geometrical parameter of a scaled transformer to that of the original transformer. The primary step of scaling procedure is to define the sizes of scaled transformer components in a way that basic design parameters remain the same in both transformers. As such, core material and core structure, magnetic flux density in the core, current density in the windings, and type of transformer (oil-filled or dry-type, number of phases, number of windings) should be the same in both transformers (Table 3-2). On the other hand, all one-dimensional parameters, even the thickness

of insulation, are scaled with the same *Scl* factor, which in turn, scales the cross section areas and volumes by Scl^2 and Scl^3 respectively.

Table 3-2: Specifications of model transformer T3.

T3 Specifications	
Rated Output	9 kVA *
Type	Single phase, Oil filled
Voltage	345 V / 19.8 kV **
Connection leads (10)	One in every layer
Nominal frequency	60 Hz
Number of turns for LV winding	130
Number of turns for HV winding	7462

$*:\ Original\ model\ transformer: 1\ kVA\ (T1) \rightarrow\ Scaled\ model\ Transformer: 9\ kVA\ (T3)$

$**:\ Linear\ scale\ factor, Scl = \sqrt{3}\ ;\qquad volt.ampere\ scale\ factor, Scl^4 = 9$

Figure 3-3: A photograph of model transformers, (left): original transformer, T1 (right): scaled transformer, T3.

Because of the limited standard sizes available in the market, for the LV foils and HV wires, it was not possible to use the conductors with the exact sizes as dictated by *Scl* scale factor, rather, the closest matching dimensions have been used. This procedure also applies to insulation paper thickness and

core dimensions. Table 3-3 shows the detailed data of the transformer design with the deviation of actual dimensions from the desired values calculated based on *Scl*.

Table 3-3: Transformers T1 and T3 design data.

	Original Transformer	**Scaled-up Transformer**	**% Deviation from values dictated by *Scl*=$\sqrt{3}$**
Capacity	1kVA	9kVA	0
LV voltage	115V	345V	0
LV turns	130	130	0
HV voltage	6617V	19850V	0
HV turns	7480	7480	0
C*	3	5	4%
D*	0.5625	1.05	-7%
G*	7.39	12.5	2%
A*	8.625	14.85	0.5%
LV conductor section area (mils^2)	4572	14742	-7%
HV conductor section area (mils^2)	503	1612	-6%
design flux density (T)	1.572	1.516	4%

* C, D, G and A define the core dimensions.

Parameters C, D, G and A that define the core dimensions are shown in Figure 3-4.

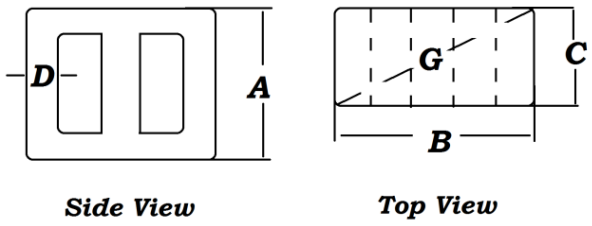

Figure 3-4: Schematic depicting the parameters of the core dimensions.

3.1.3 Model transformer for shielding effect study

Transformer T4 is built for a comparative study on the effects of electrostatic shield on the transfer of high-frequency voltage contents as well as its effects on the voltage gradient, i.e. electrical stress

inside the windings. T4 is designed identically to T3 in all aspects except that T4 comprises an electrostatic shield, inserted between LV and HV layers. In addition, to evaluate the electrical stress between the layers of windings, both T3 and T4 are equipped with 10 connecting leads like that used with T1 and T2 for measurement of voltages at middle turn of every layer of HV winding (Figure 3-5).

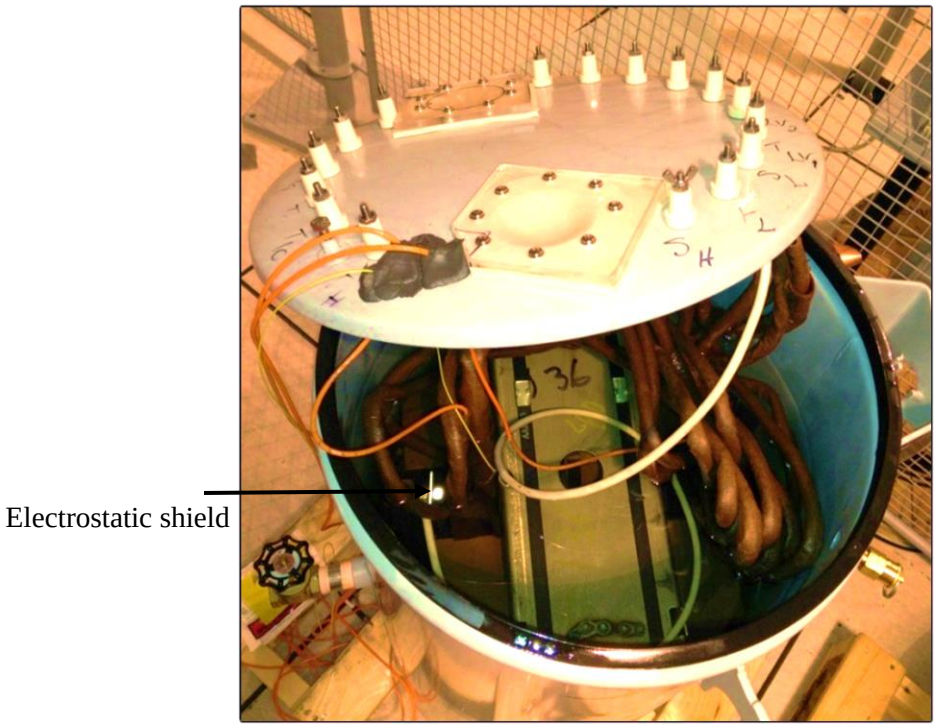

Figure 3-5: T4 model transformer active part with multiple connection leads and a high-voltage teflon insulated wire (white one) for grounding the electrostatic shield.

3.1.4 Model transformer for fault location study

A 500-kVA model transformer (Figure 3-6) is also used in this study. The transformer was initially built by NTNU University for the purpose of investigating the effect of winding design on both internal and external voltage transfer; hence consists of a layer winding on the left limb, a pancake winding on the middle limb and a disc winding on the right limb. The connection leads which were initially considered for internal voltage measurements, are used in this research for creating intentional short circuits at several locations of the windings. A detailed design of T5 is described in [61].

Table 3-4: Specifications of transformer T5.

T5 Specifications	
Rated Output	500 kVA
Type	Three phase, Oil filled
Voltage	240 V / 11 kV
Connection leads (24)	Two in each layer
Nominal frequency	50 Hz
Number of turns for LV winding	25
Number of turns for HV winding	1334

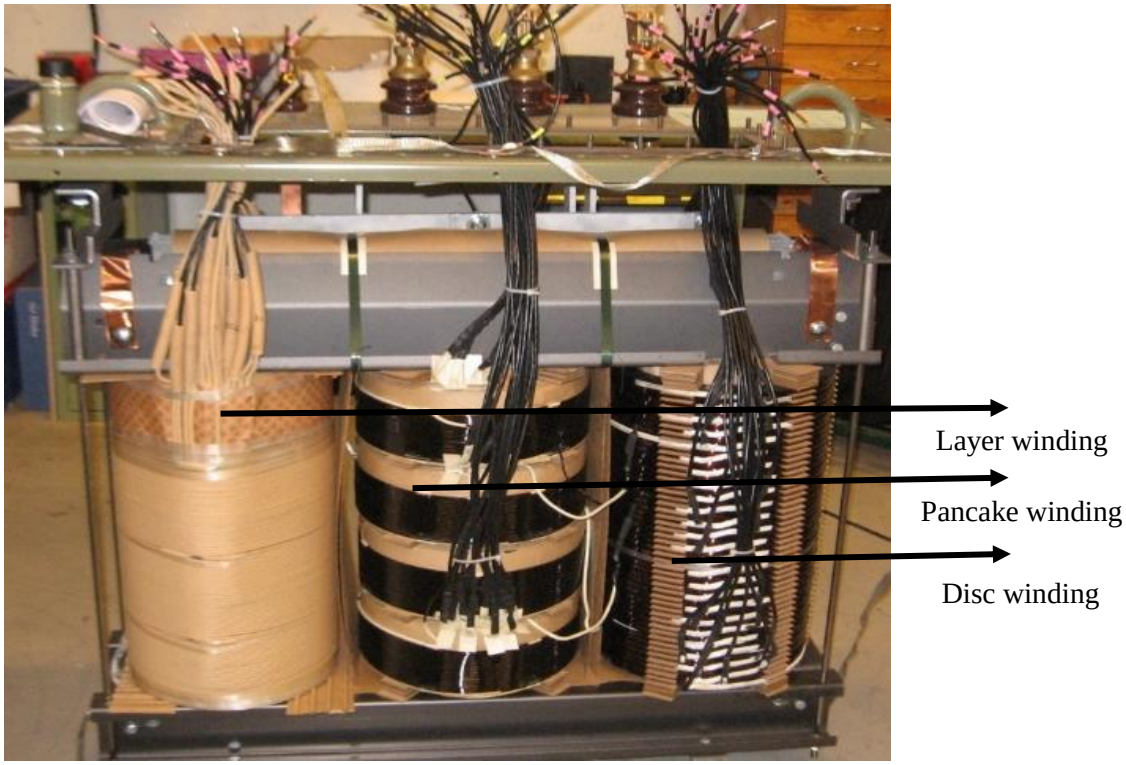

Figure 3-6: T5 model transformer (un-tanked), showing different winding types and connection leads.

3.2 Paper/oil samples

Paper samples were prepared by the same procedure as that typically used by WTSU transformer manufacturers; whereby, paper samples are vacuumed and heated prior to being placed in oil. This

process extracts moisture from the paper and also prepares it for better oil absorption. Both oil and paper samples were provided by a transformer manufacturing company in Ontario, Canada. Size and materials of circular paper samples used in the present fundamental study are defined in Table 3-5.

Table 3-5: Description of circular paper samples.

Paper diameter	Paper thickness	Paper material	Oil material
150 mm	0.127 mm	Diamond coated Kraft paper 75 kV/mm breakdown strength	Voltesso 35 40 kV/mm breakdown strength
25 mm	0.250 mm		

3.3 Voltage waveform generation

3.3.1 Sinusoidal and PWM voltage for transformer ageing

To study the effect of voltage source converter on transformer insulation, ageing tests on T1 and T2 were conducted in parallel, using two separate sources for energization. Source-1 is a conventional 60 Hz voltage regulator connected to the laboratory AC supply. Voltage regulator is used to set the input voltage to 138V; 120% of transformer's nominal primary side voltage. Source-2 is a voltage sourced converter with a switching frequency of 3 kHz and 1.4 kV/µs rate of voltage rise, generating PWM signals. The output voltage of the converter is adjusted in such a way that it has same peak value as that of source-1. Total harmonic distortion (THD) of source-1 is less than 2% while source-2 has a maximum THD of 14% including a wide range of frequency components that exist in wind-farms. A typical voltage waveform of source-2 is shown in Figure 3-7.

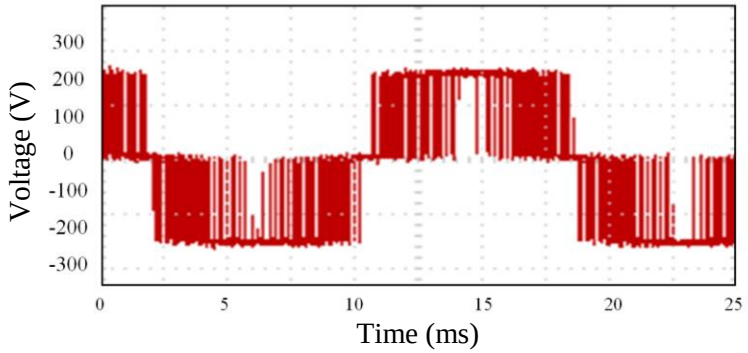

Figure 3-7: Output voltage waveform of source-2.

3.3.2 Impulse voltage for paper/oil sample ageing

Analysis of transformer insulation performance under switching transient voltages is only possible by having the characteristics of such waveforms at transformer's terminals. Despite all the efforts made for approaching several wind-farm developers, reluctances were shown against performing online measurements at transformers terminals. In addition, even with continuous measurement of voltage at transformer terminals, not all the different types of events could be expected to occur and be recorded during a short measurement period. Therefore, voltage profiles at transformer terminals calculated by PSCAD® simulations are used [62]. High-frequency black-box model of transformers used in simulations are based on the frequency responses measured on a full scale WTSU transformer (explained in section 3.7.1).

Applied test voltage waveforms on paper/oil samples (section 3.5) represent fast rise time impulses simulated in the abovementioned simulation study for the operation of circuit breakers on LV and HV sides of wind turbine transformers in different operation scenarios. Results of the simulations revealed impulse waveforms with rate of rise (ROR) varying from 1.1 kV/µs to 12 kV/µs and repetition frequencies ranging from 450 Hz up to 22 kHz. Although both power-frequency voltage and high-frequency switching spikes exist in the real voltage waveform, because of the focus of this research on the effects of high-dV/dt components, only the spike train was generated and applied to the test samples. The pulse train was generated by a high-voltage pulse modulator fed by a 0-30 kV DC source, with a continuous current rating of 540 mA (Figure 3-8). Figure 3-9 illustrates a pulse train with its associated timings. To capture these steep-front waveforms, high-frequency sensors (a 75 MHz high-voltage probe and a 40 MHz current transformer (CT)) and a wide-band high-sampling-rate oscilloscope, with a 2 GHz bandwidth and a 5 GS/s sampling rate, were used.

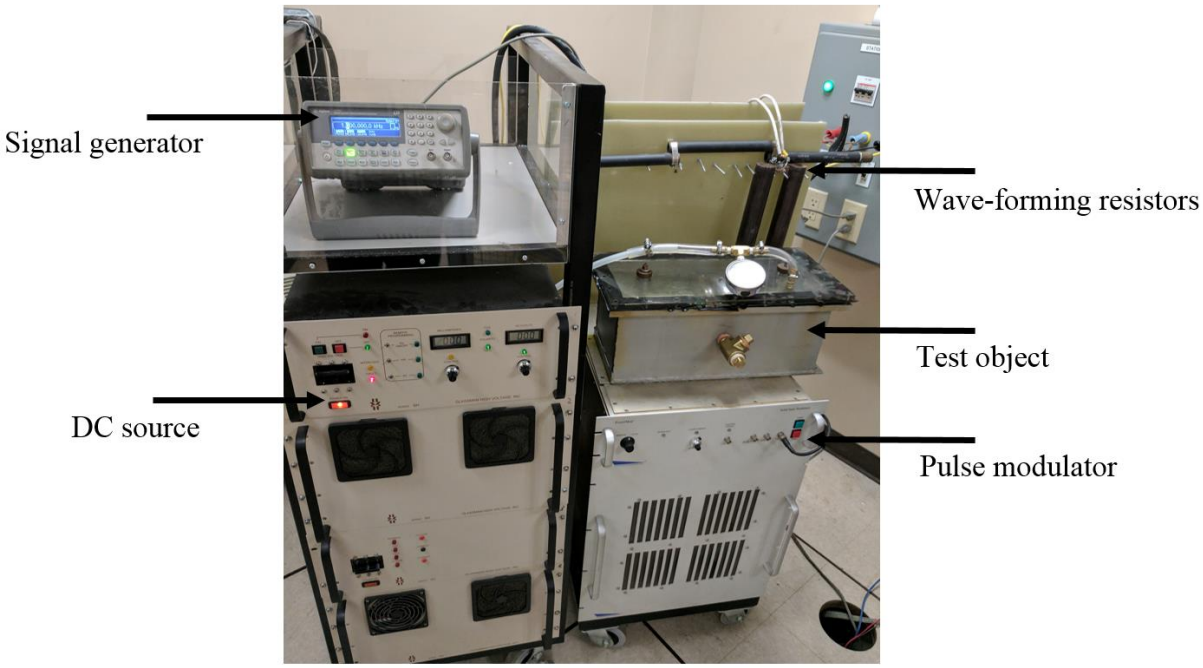

Figure 3-8: Test setup for voltage pulse generation.

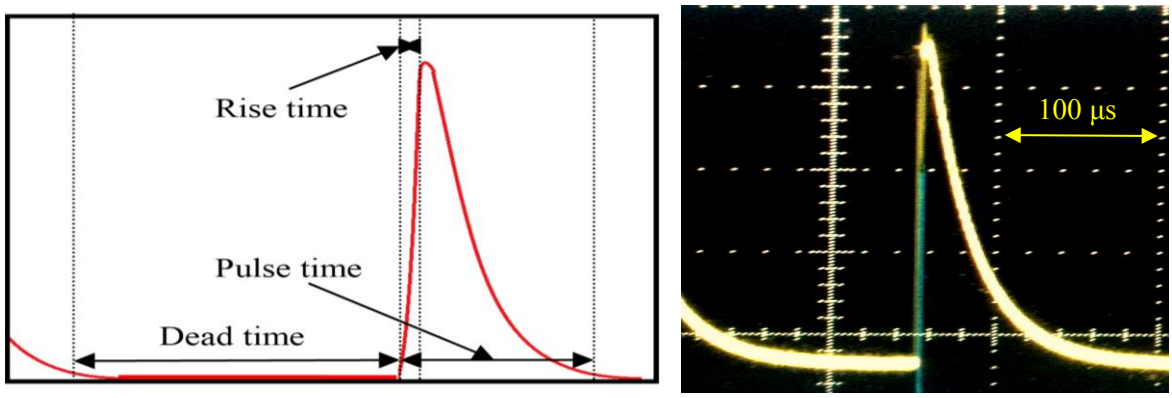

Figure 3-9: Exponentially decaying impulse train waveform and the associated times (for the purpose of illustration, the time periods used in left figure are not to scale) *(Dead time) = (1/f) - (pulse time).*

3.4 Transformer ageing experiment

Transformers T1 and T2 were subjected to stresses from two different types of voltage sources (explained in section 3.3.1) to evaluate the effect of high-frequency high-dV/dt voltages on transformer. A variety of parameters are considered as indicators of the insulation conditions, which have been monitored periodically during the ageing process. The results are then analyzed in order to recognize

the properties that are affected by high-frequency high-dV/dt distorted voltages and the ageing process under distorted voltage waveforms.

3.4.1 Experimental Procedures

Transformers T1 and T2 were energized for 960 hours at 120% of their nominal voltage. Both transformers were loaded by non-distorting resistive loads at 40% of their rated value (Figure 3-10). Use of reduced load has two benefits: preventing no-load over-voltages on the secondary side of the transformer, and avoiding overheating that may occur at higher loads. By avoiding overheating, it is possible to investigate the effect of electrical stress on transformer insulation, independent of thermal ageing.

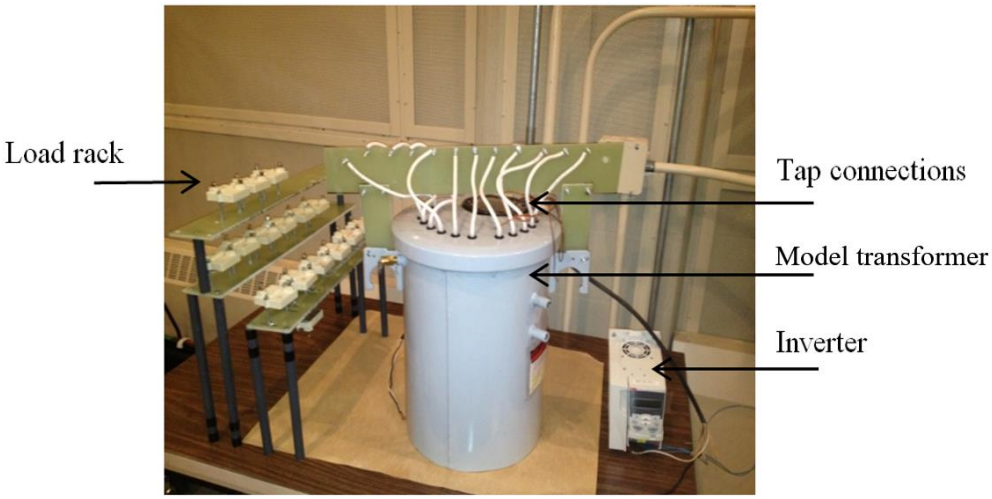

Figure 3-10: Test transformer with voltage sourced converter (inverter) and resistive load.

3.4.2 Monitored Parameters

Dielectric measurements on transformers are functions of humidity, temperature and ageing degree of paper/oil insulation system. In a laboratory experiment, as the humidity and temperature are kept within a certain range, the following parameters can be indicators for the ageing degree of transformer insulation. In this research, dissolved gas analysis, dielectric frequency response, winding temperature and partial discharge are investigated as representative indices of the transformer insulation conditions, before, during and after ageing period.

3.4.2.1 Partial Discharge

One of the indicators of insulation health used in most high-voltage equipment is partial discharge. Periodic measurements of PD were done on both T1 and T2 using Hipotronics® PD test setup with PD noise level of less than 2 pC. Initial PD tests were carried out to ensure the good condition of model transformers, and to have a reference PD level. Additional PD tests were done after 100, 200, 500 and 960 hours of ageing respectively.

3.4.2.2 Dissolved gas analysis

Oil samples are taken from both transformers, and dissolved gases were extracted from oil samples, using the flame ionization detection technique as per ASTM D3612 standard test method.

3.4.2.3 Dielectric frequency response

Dielectric frequency response, also known as frequency domain spectroscopy, is based on measurement of material's dielectric parameters such as total and imaginary part of capacitance (C and C″), dissipation factor (DF) and power factor (PF). The method is basically founded on measurements of system input impedance over a wide range of frequency (0.1 mHz to 10 kHz in this thesis), from which parameters such as real capacitance, imaginary capacitance, dissipation factor and power factor can be extracted.

Currently, with the progress in wide-band capturing of very low amplitude signals, and powerful data acquisition systems, sophisticated instruments are commercially available for DFR measurements. However, the interpretation and comparison of DFR output curves are complicated tasks which require in-depth knowledge in the field. Although there are discussions about accurate interpretation of trends in DFR curves, the general concept of the effects of insulation ageing on the DFR pattern of transformer insulation system is well established [63]. Changes in high and very low frequency ranges of dielectric response curves can be related to the moisture levels while changes in medium range are mostly correlated with the insulation degradation level (Figure 3-11).

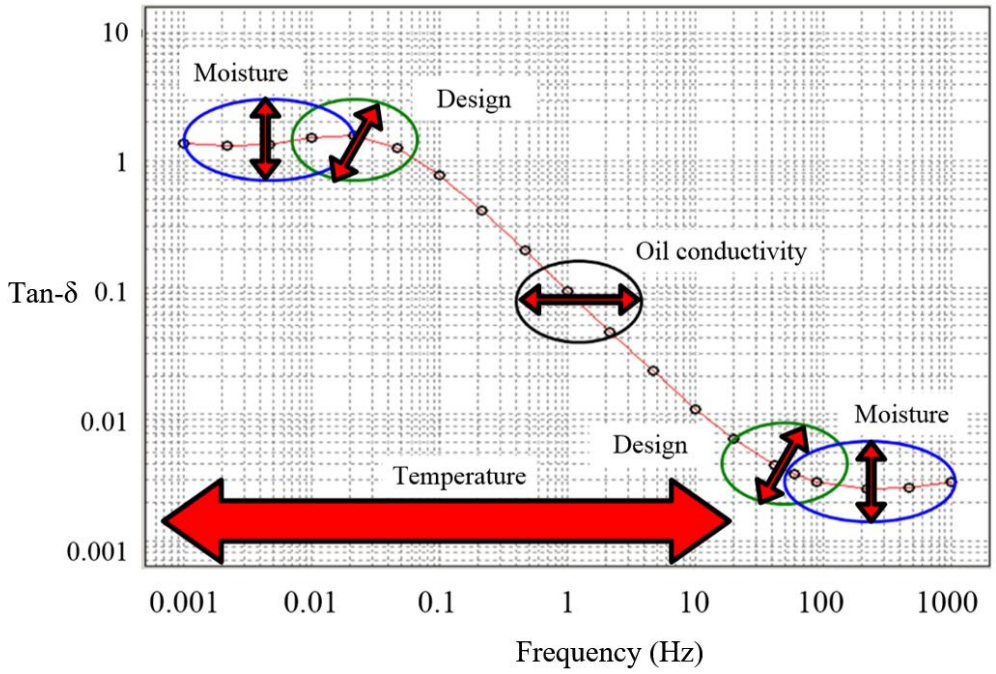

Figure 3-11: Typical dielectric frequency response of a transformer, showing the regions of each parameter's effect. (temperature change shifts the whole graph horizontally) [63].

Using DFR tests, ageing progress is investigated by comparing the performance of T1 and T2 under pure and distorted voltage waveforms (Figure 3-12). At certain intervals during the ageing cycle, sample transformers are diagnosed with DFR analyses to compare their dielectric responses. DFR tests are performed by IDAX-300® insulation diagnostic analyzer, which is a high-accuracy automated measurement unit featuring a variety of test modes for insulation assessment [64]. The peak voltage of IDAX 300 test signal is 200 V which can be amplified to 2 kV by adding an amplifying module named VAX020®.

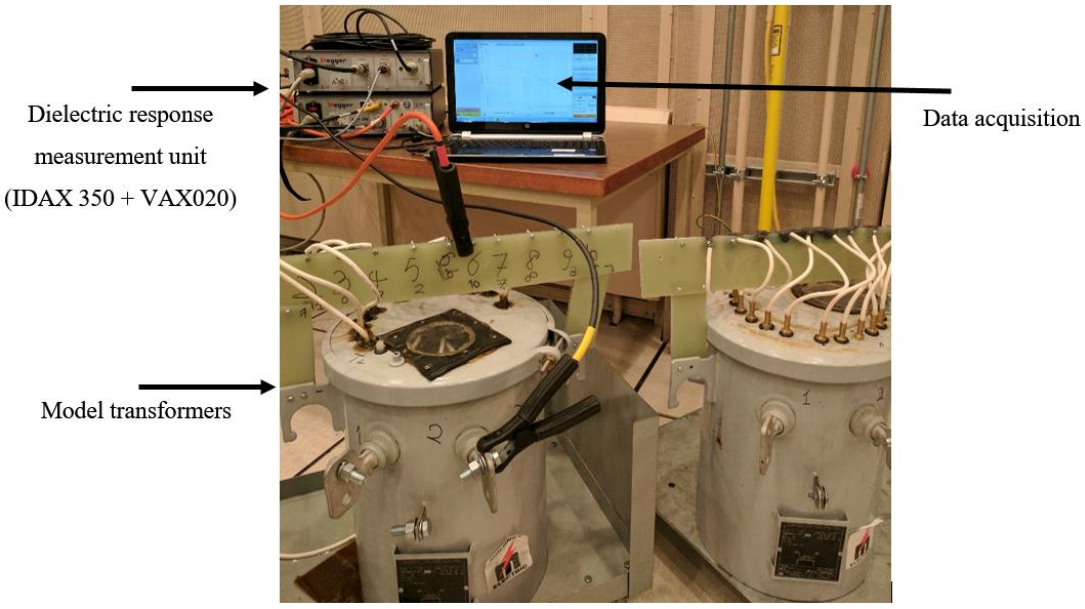

Figure 3-12: DFR test setup: model transformers, dielectric response measurement unit with high-voltage amplifier and computer for data capture and analysis.

A DFR test can be done in two modes: un-grounded specimen test (UST) mode or grounded specimen test (GST) mode (Figure 3-13). This research adopts the UST mode for condition assessment of the insulation between LV and HV windings, and the GST mode for assessment of transformer total insulation system which takes the insulation between grounded parts and energized parts of the sample transformer into account.

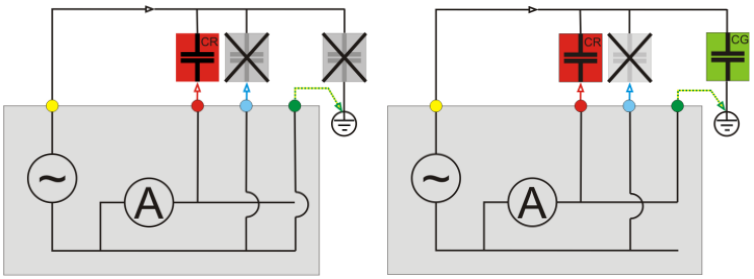

Figure 3-13: DFR test connections schematics; (left): UST mode, (right): GST mode

All DFR tests are performed in relatively consistent ambient conditions for obtaining a good comparison (T= 22 ± 1 ºC, % relative humidity = 30 ± 5).

3.5 Ageing of paper-oil samples

The experimental study of this section employs online monitoring of dissolved hydrogen for investigating the performance of oil/paper insulation systems under high-dV/dt pulsed voltages generated by switching operations (described in section 3.3.2). The proposed DGA method relates accumulated PD energy of impulse trains to the amounts of hydrogen gas generated over the ageing period. Using the hydrogen/PD relationship, PD is monitored through the measurement of dissolved hydrogen by subjecting impregnated paper samples to voltage impulses with different rates of rise (RORs), peak values, and repetition frequencies. Moreover, with controversies about the parameters for defining the insulation destruction effect of PD, what becomes clear is that a parameter directly related to total PD energy is needed for comparing levels of damage inflicted by voltage waveforms on test samples. Because of the direct relation between PD energy and hydrogen content, destructiveness of different pulse waveforms can be compared by trending dissolved gas levels.

Preparation of test cells, and online monitoring of dissolved hydrogen in oil are described below.

3.5.1 Test chambers and electrodes

Two types of test chambers (chamber 1 and chamber 2) were built for studying PD of impregnated paper samples immersed in transformer oil.

Chamber 1 used a set of Rogowski-profile plane-plane electrodes with a transformer paper sample sandwiched between the electrodes (Figure 3-14). The diameter of the paper sample exceeded the diameter of the energized electrode to ensure that PD would initiate on the surface of the paper where the energized electrode contacts the paper (Table 3-6, Figure 3-14). This geometry provides a large interface between paper and oil under uniform field with smooth electrodes.

Table 3-6: Description of electrode dimensions.

Energized electrode diameter	Ground electrode diameter
100 mm	200 mm

For a fair comparison of test results under different voltage waveforms, the paper-to-oil mass ratio is kept constant for all test samples. A small free space (8% of the test cell volume) was maintained on top of the oil and under the lid of the chamber so that the gases generated in the oil could create

equilibrium with the free gases. Chamber 1 was operated in isobaric conditions with a barometric pressure of 102.7 kPa.

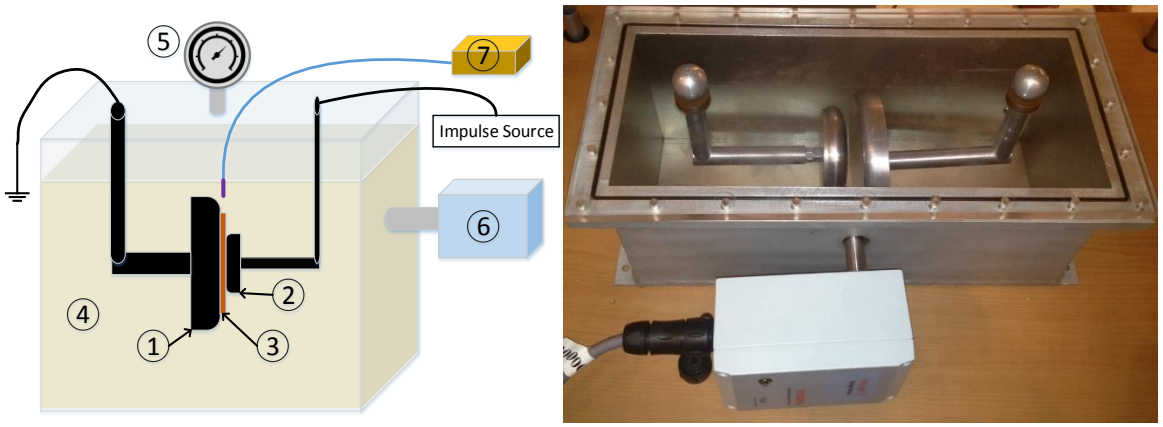

Figure 3-14: (left): Illustration of test chamber 1; 1: ground electrode, 2: energized electrode, 3: paper sample, 4: oil bath, 5: pressure controller, 6: dissolved gas monitor, 7: fiber optic thermal probe with recording instrument, (right) : actual test chamber.

Chamber 2 contains six pairs of rod-plane electrodes with paper samples placed between them (Figure 3-15). Ambient temperature, moisture, and initial pressure were the same as for chamber 1, but chamber 2 was operated under sealed conditions unlike the isobaric conditions in chamber 1. The enhancement in electric field at sharp corners of rod electrodes has an impact on PD and consequently on the generated gas, simulating multiple sources of PD in large transformer tanks.

For both chambers 1 and 2, tests were repeated five times and the reported readings are the mean values.

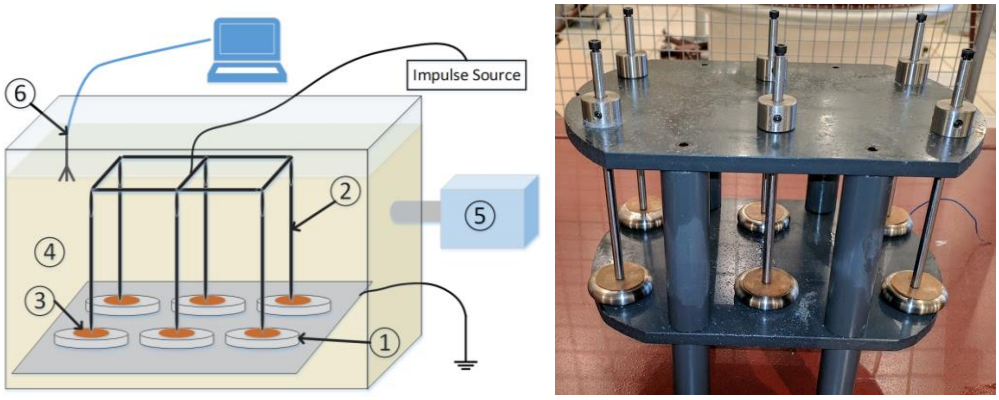

Figure 3-15: (left): Illustration of test chamber 2; 1: ground electrodes, 2: energized electrodes, 3: paper samples, 4: oil bath, 5: dissolved gas monitor, and 6: RF antenna, (right) : actual test electrodes (out of oil chamber).

To monitor the local temperature of the sample being tested, a fiber-optic thermal sensor which meets the electromagnetic compatibility requirements is placed in the vicinity of the energized paper sample (Figure 3-16). To monitor the average temperature of oil bath, the thermal built-in sensor of the DGA unit has been utilized.

Figure 3-16: Optic thermal sensors (in yellow) connected to the measurement unit.

3.5.2 Hydrogen Monitoring

Under high electrical stresses, due to the bombardment of molecules by electrons, oil/paper insulation generates small quantities of gases, including hydrogen. The amounts and types of gases found in the oil are indicative of the severity and type of discharges occurring in the oil/paper insulation system. However, a full gas analysis is costly and not feasible to be iterated for one measurement point and entails long time intervals between samplings. Dissolved hydrogen can be measured online by means of a monitoring unit connected to the test chamber. This research utilized the InsuLogix® hydrogen monitor with a measurement range of up to 5000 ppm, with 25 ppm accuracy.

3.6 Frequency response analysis

Frequency response analysis (FRA) was used in the studies presented in the following sections, which include transformer modelling, effects of electrostatic shielding, and detection of fault location. Since the conventional method is well known and explained in literature [64, 65], just a brief explanation of frequency response measurement used in the present work is given here.

A schematic diagram of FRA test connections are shown in Figure 3-17. The network analyzer generates a sinusoidal waveform with variable frequencies at the source terminal (S). The source signal excites transformer with voltage magnitude ranging from 5-20 V. Connections of reference (R) and

transfer (T) channels are determined based on the parameter for which the frequency response is measured. For example, to measure LV/HV voltage transfer function, R and T channels are connected to HV and LV terminals respectively (Figure 3-17a). On the other hand, as it is demonstrated in Figure 3-17b, R and T channels are respectively connected to the current sensor and HV terminal to measure input impedance. For admittance measurement, everything is the same as impedance measurement except that R and T connections are reversed. To measure voltage transfer functions from LV terminals to the connection leads inserted inside the layers of HV windings, similar connections as shown in Figure 3-17a are used while T channel is connected to the connection lead associated with each measurement.

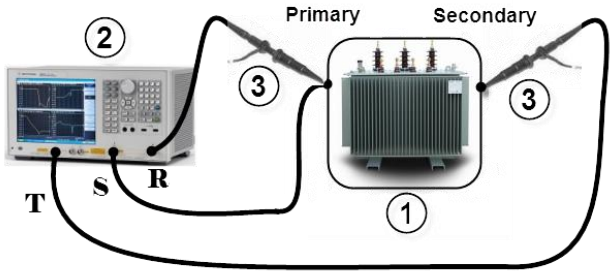

a)

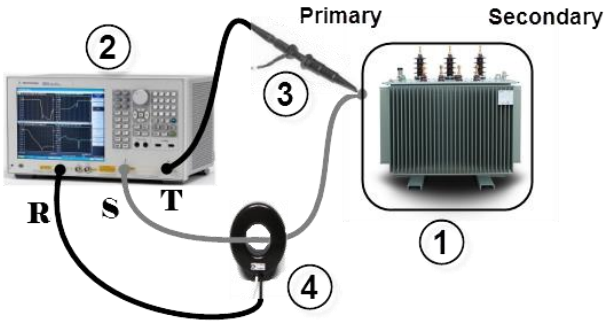

b)

Figure 3-17: Test setup for FRA measurement, (a): transfer function, (b): input HV impedance (1- transformer with grounded tank and core, 2- network analyzer, 3-high-frequency voltage probe, 4- high-frequency current sensor).

3.7 Transformer modelling

Transformers in power flow analysis and steady-state power system management are modeled as leakage inductance and resistance in series for the windings, and a parallel inductance and resistance for the core, which is valid only for power-frequency studies. However, transformers respond

differently to high-dV/dt high-frequency oscillatory transients compared to the normal power-frequency voltages. At higher frequencies, the interaction of distributed capacitances and inductances of transformer influence the magnitude of the voltage waveform that passes through the transformer.

Analytical and numerical models of transformers are used for high-frequency modelling of transformers but such methods are too sensitive to the geometry and materials used in the transformer, and require access to the detail design of each transformer. Two alternative methods are presented in this research: a black-box model for network simulation purposes, and a gray-box model for the study of internal resonance effects and voltage transfers.

3.7.1 Black-box modelling using terminal measurement

To analyze the switching transients in a wind-farm, appropriate implementation of a wideband transformer model is crucial. Of numerous proposed models, black-box high-frequency model of transformer is a rather realistic model for analyzing the high-frequency transients [67]. The idea adopted is to find rationally approximated functions as summation of partial fractions. The partial fractions are extracted from admittance frequency response of an actual transformer installed in the simulated wind-farm. Figure 3-18 shows the use of FRAX 101® frequency response analyzer on a 2.65 MVA, 690V/34.5 kV WTSU transformer ready to be shipped to wind-farm.

Once the parameters are expressed as rational functions, the black-box module of PSCAD® software creates a multi-port frequency-dependent equivalent circuit from given characteristics. The advantage of being terminal-based makes the black-box model implementable for any transformer even without accessing its internal design, ensuring that the model of the transformer in the simulation resembles transformer real response even when dealing with high-frequency voltage contents. Modelling of transformer for wind-farm simulation is described with more details in Appendix A.

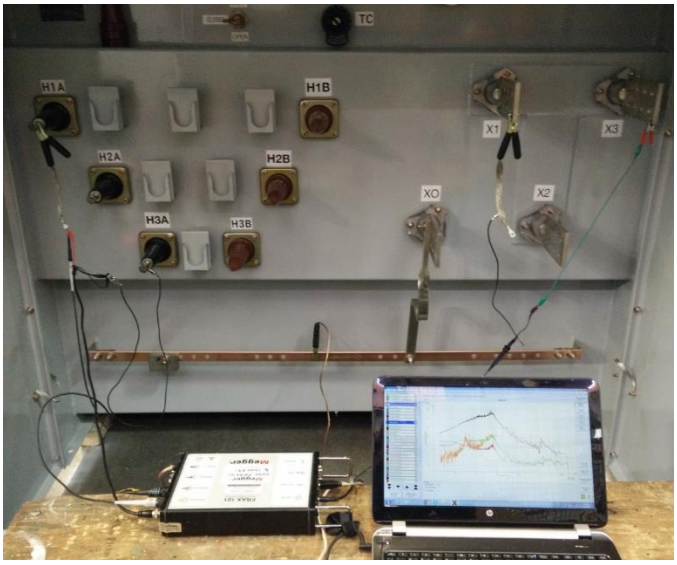

Figure 3-18: Experimental Setup for frequency response measurements of a WTSU transformer.

3.7.2 Gray-box modelling using scaling method

A gray-box modelling method is proposed in this thesis as an addition to the discussed transformer modelling approaches such as detailed internal modelling and black-box modelling. Gray-box modelling has characteristics from both aforementioned methods. Like black-box modelling, this method is based on FRA measurements, but instead of only terminal measurements, FRA measurements are done at multiple locations of transformer windings. It has also similarities to detailed internal modelling because it reveals information about voltage distribution inside the winding, and can help with the calculation of internal electric stresses.

FRA measurements at terminals and internal points of the transformer windings are required for the proposed gray-box modelling. Performing FRA on actual power transformers however can be challenging because of their large size, limited access, and associated costs. In contrast, performing FRA on a scale down model transformer of the same design is feasible and can be done in a laboratory setup. Scale down model transformers can be easily built with additional connection leads inserted in desired positions of the windings. Such model studies can thus help the manufacturers to predict the high-frequency behaviour of power transformers in their design stage.

3.7.2.1 Scaling Rules

Principles of the scaling method are described here for an original transformer (T1) and its scaled version (T3) by a scale factor of *Scl* (chosen as $\sqrt{3}$ in this research). The primary step of the scaling

procedure is to define the materials and dimensions of different components of scaled transformer T3 in a way that certain properties remain the same for both transformers. The parameters that should remain constant when a transformer is scaled are:

- Transformer type (oil-filled or dry-type, number of phases, number of windings)
- Core material and core structure
- Magnetic flux density in the core
- Current density in the windings

It is well known that in practice, when it is required to scale down the voltage level of a transformer by e.g. 3 times, the basic design parameters of the transformer such as its number of turns changes. However, here, for research purposes, the basic design parameters are kept the same while all the linear dimensions, even the thickness of insulation parts, are scaled with the same factor, *Scl*. This, in turn, scales cross section areas and volumes by Scl^2 and Scl^3, respectively.

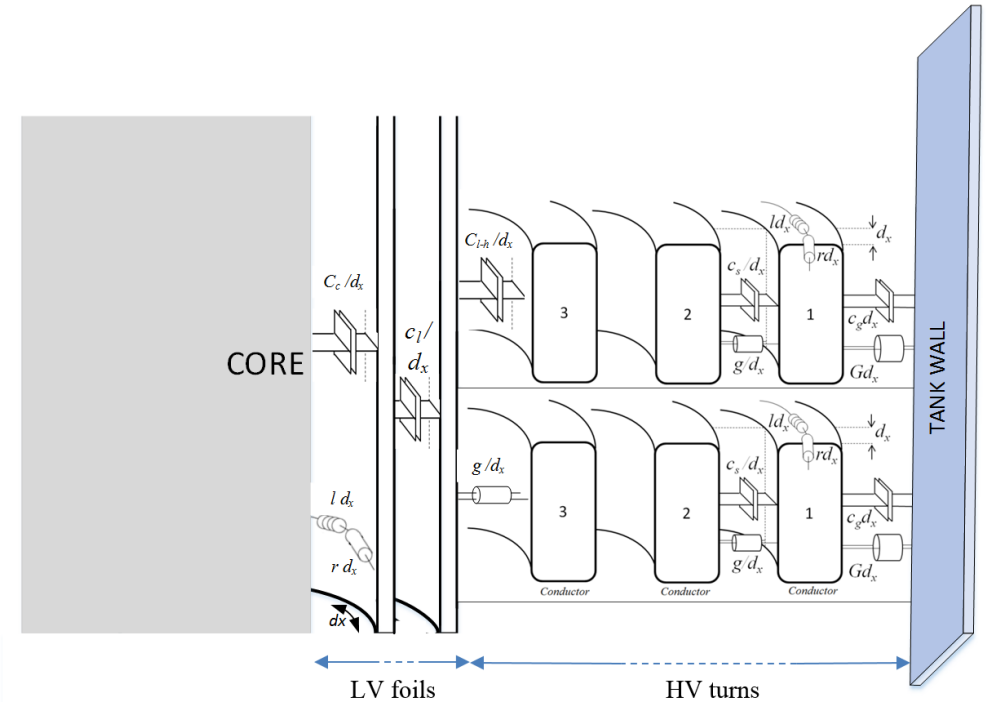

Figure 3-19: Schematic illustration of distributed resistive, capacitive and inductive parameters in transformer winding.

The most basic parameters of a transformer that change by scaling are rated voltage and current. Below, it is described how these parameters change when a transformer size scales by *Scl*.

$$V = 4.44\, N\varphi f \qquad (2.1)$$

The fundamental machine equation is derived as above, considering *V* as the rms value of the sine wave voltage with a frequency of *f*. Since *N* (number of turns) and *f* remain constant during the scaling, the voltage changes only with φ (magnetic flux).

The magnetic flux is derived as multiplication of magnetic flux density and core area:

$$\varphi = B \,.\, A \qquad (2.2)$$

Because both transformers are comprised of the same core material, the magnetic flux density (*B*) should be equal for both transformers when operated at the magnetic knee-point:

$$B_{Scaled} = B_{Original} \xrightarrow{yields} \frac{\varphi_{Scaled}}{\varphi_{Original}} = \frac{A_{core_{Scaled}}}{A_{core_{Original}}} \qquad (2.3)$$

The cross section areas are scaled by Scl^2:

$$\frac{A_{core\ Scaled}}{A_{core\ Original}} = scl^2 \xrightarrow{yields} \frac{V_{Scaled}}{V_{Original}} = scl^2 \ (= 3 \ \ in\ this\ case) \qquad (2.4)$$

On the other hand, for the input current, since the current density is supposed to remain constant:

$$J_{Scaled} = J_{Original} \xrightarrow{yields} \frac{I_{Scaled}}{I_{Original}} = \frac{A_{copper_{Scaled}}}{A_{copper_{Original}}} = scl^2 \qquad (2.5)$$

$$(= 3 \ \ in\ this\ case) \qquad (2.6)$$

(2.4) and (2.5) $\xrightarrow{yields}$ $\frac{(volt.ampere\ capacity)_{Scaled\ transformer}}{(volt.ampere\ capacity)_{Original\ transformer}} = scl^4$ (2.7)

$$(= 9\ in\ this\ case) \qquad (2.8)$$

T1: 1 kVA, T3: 9 kVA (2.9)

The above equations show that to satisfy the fundamental scaling rules, the capacity of scaled transformer multiplies by a factor of Scl^4 when its linear size scales by *Scl*.

Focusing on the frequency response analysis, parameters that define the frequency response of transformers are turns ratio, stray capacitances, inductances and resistances. While capacitances and inductances affect the frequencies of resonances and anti-resonances, the turns ratio and resistances mostly affect the magnitude of resonances in the frequency responses. The concept of the electrical circuits theory suggests that uniform scaling of all the elements of the transformer equivalent circuit will result in the scaling of the resonance frequencies of the circuit by the same scaling factor. The following equations show how the equivalent circuit elements change when a transformer is scaled.

By scaling the size of a transformer the cross sections scale by Scl^2 while the distances scale by *Scl*. Consequently, the whole stray capacitance matrix scales by *Scl*.

$$C = \frac{\oiint ds}{\bar{d}} . \epsilon \quad , \quad ds_{Scaled} = Scl^2 . ds_{Original} \quad , \quad \bar{d}_{Scaled} = Scl . \bar{d}_{Original} \tag{2.10}$$

$$\rightarrow \frac{[C]_{Scaled}}{[C]_{Original}} = Scl \tag{2.11}$$

To calculate the approximate effect of the scaling on self and mutual inductances, it can be stated that:

$$M_{ij} = \frac{\mu}{4\pi} \oint \oint \frac{ds_i . ds_j}{|d_{ij}|} \tag{2.12}$$

Or more generally:

$$L = \mu \frac{N^2 . A}{l} \tag{2.13}$$

Constant values of μ and N due to the scaling rules, and below relationships between the inductive area and winding length of original transformer, and those of scaled transformer:

$$A_{Scaled} = Scl^2 . A_{Original} \quad , \quad l_{Scaled} = Scl . l_{Original} \tag{2.14}$$

Result in scaling the distributed inductance matrix by a factor of *Scl*.

$$\rightarrow \frac{[L]_{Scaled}}{[L]_{Original}} = scl \tag{2.15}$$

Since the voltage transfer at higher frequencies is mostly defined by the stray capacitances and partial inductances rather than turns ratio, it can be concluded that the resonance frequencies of the transfer function also scale by (*1/Scl*):

$$\frac{[f_{res\ Scaled}]}{[f_{res_{Original}}]} = \frac{\frac{1}{2\pi}\frac{1}{\sqrt{[L]_{Scaled} \cdot [C]_{Scaled}}}}{\frac{1}{2\pi}\frac{1}{\sqrt{([L]_{Original}) \cdot ([C]_{Original})}}} = \frac{\frac{1}{\sqrt{([L]_{Original} \cdot Scl) \cdot ([C]_{Original} \cdot Scl)}}}{\frac{1}{\sqrt{([L]_{Original}) \cdot ([C]_{Original})}}} = \frac{1}{Scl} \tag{2.16}$$

To examine the accuracy of the above calculations for the shifts in the resonance and anti-resonance frequencies, frequency response measurements were performed on T1 and T3, as an original transformer and its scaled version respectively.

3.8 Shielding

To investigate the influence of electrostatic shielding, this study compares the results of frequency response analysis on T3 and T4 to analyze how the implementation of an electrostatic shield modifies the electric field resonation in high-frequency range; hence the stresses on winding insulation.

3.8.1 Shielding mechanism

Installation of an electrostatically grounded shield between primary and secondary windings has been recently recommended by transformer study groups for renewable energy converter-fed transformers [68]. The main functionality of the electrostatic shield is a capacitive decoupling of primary and secondary windings. The purpose of this method is the suppression of high-frequency voltage contents transfer from each side of the transformer to the other side. This decoupling action is more important in converter-fed transformers because generally the terminals that are connected to the inverter are not grounded through a star point, resulting in a floating capacitive coupling between primary and secondary windings.

3.8.2 Terminal voltages and voltage gradients

The electrical stress on the insulation of a transformer is defined by terminal voltages, and voltage gradient between the winding turns or layers. Frequency responses of the abovementioned parameters are measured over a wide range of frequency (power-frequency up to MHz range) to obtain an estimation of the stress that is imposed by high-dV/dt voltage components.

To find the electrical stress response at different layers of the winding, voltage gradients between the middle turns of adjacent layers are measured (Figure 3-20). In other words, the frequency response of the differential voltage along the winding is computed by measuring the frequency response of voltage transfer at each layer and then subtracting the responses of two adjacent layers. The resultant frequency responses are the distribution profile of electrical stress as a function of excitation frequency.

$$TF_{layer\ i}(f) = \frac{V_{layer\ i}(f)}{V_{input}(f)} \qquad (2.17)$$

$$\frac{VG_{layer\ i,i+1}}{V_{input}(f)}(f) = TF_{layer\ i}(f) - TF_{layer\ i+1}(f) \qquad (2.18)$$

Where $TF_{layer\ i}$ is voltage transfer function at layer *i* of the winding, $V_{layer\ i}$ is the voltage spectrum at layer *i*, V_{input} is the excitation voltage from the primary side and $VG_{layer\ i,i+1}$ is the voltage gradient between layers *i* and (*i+1*).

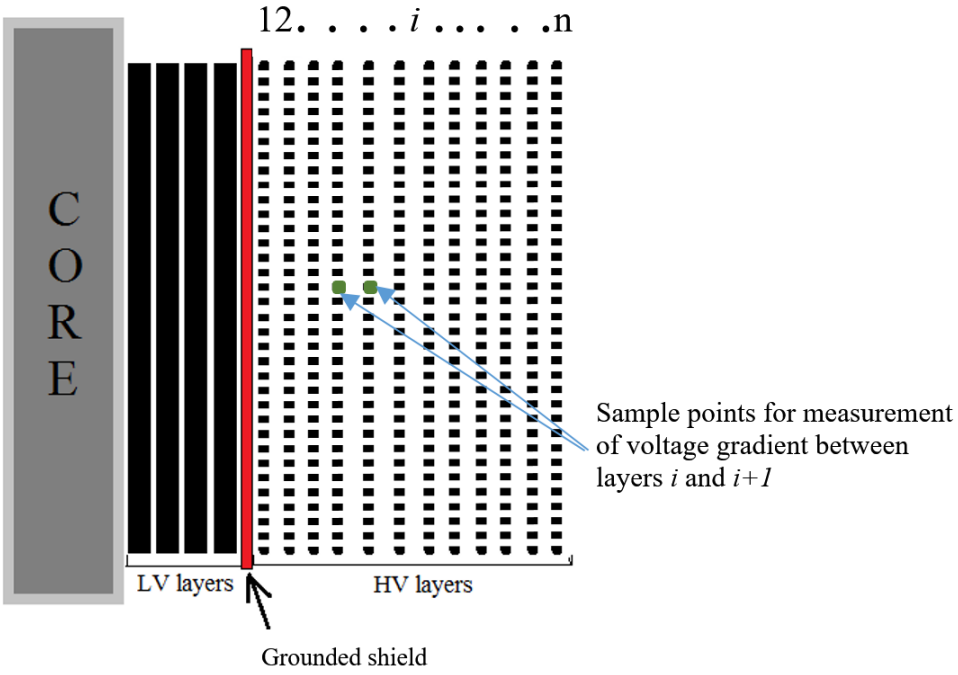

Figure 3-20: Numbering of layers and the position of a shield with respect to the windings.

3.8.3 Measurement setup

Transformers T3 and T4 are used for a comparative study on the effects of the electrostatic shield on the transfer of high-frequency voltage contents as well as its effects on the voltage gradient along the windings.

A FRAX101® FRA unit is used to measure the voltage transfer function for the following: a) transferred voltage from LV terminal to HV terminal; b) transferred voltage from HV terminal to LV terminal; c) transferred voltage from LV terminal to each layer of HV winding for calculating voltage gradients between the winding layers, i.e. stress on inter-layer insulation (Figure 3-21).

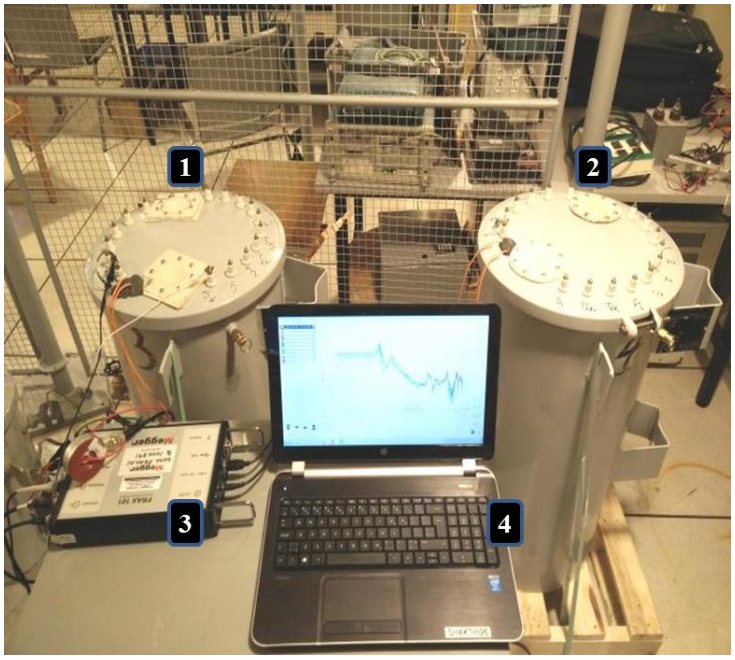

Figure 3-21: Experimental setup, 1- shielded transformer (T4), 2- unshielded transformer (T3), 3- frequency response measurement unit, 4- data acquisition.

3.9 Detection of fault location

A possible modification in wind-farm transformer design is reinforcing the insulation in the positions with the highest probability for failure. Having statistical data about the locations of internal faults in failed transformers can help in recognizing the vulnerable positions in a certain transformer design. With an experimental approach on model transformers, the aim of this section is to identify the relationship between locations of an internal fault and patterns of transformer frequency responses. To estimate the location of short circuits, the FRAs of faulty windings, with short circuits positioned at different locations, are compared with one another and also with healthy winding as a reference. The comparison is based on the use of statistical parameters along with visual observations of trends in frequency spectra. This research also compares sensitivities of different parameters with respect to the location of the fault.

In an attempt to establish a method for locating internal faults, this study investigates the effects of fault location on the frequency response of transformer parameters, e.g. input impedance and transfer voltage. It is shown that moving the fault to different locations in the winding changes the frequency response of transformer parameters with certain patterns. These systematic changes in the frequency responses can be utilized to predict the location of internal faults.

Artificial short circuits are implemented in the transformer winding to simulate the internal faults at different layers. For each short circuit, frequency responses of transfer voltage (V_{out}/V_{in}) and input impedance (V_{in}/I_{in}) are measured. To find the patterns of frequency response change as function of fault location, the frequency responses of faulty transformers are compared with each other. The trends are analyzed by both qualitative and quantitative approaches. Also, all the frequency responses of the transformer with different fault locations are compared with the frequency response of the healthy transformer. The comparison is done using statistical parameters along with visual observations of frequency spectra.

3.9.1 Measurement procedure

Both transfer functions; *HV/LV* and *LV/HV* are measured, respectively, from HV and LV terminals while the other side is excited. In addition, input HV impedances with LV terminals shorted are also utilized to correlate measured impedances with defect locations. An Agilent® E5061B network analyzer and high-frequency oscilloscope probes P2220 are used for voltage transfer measurements, as well as special Ionphysics® current sensors CM-100-6L-IR50 for wide-band impedance measurements.

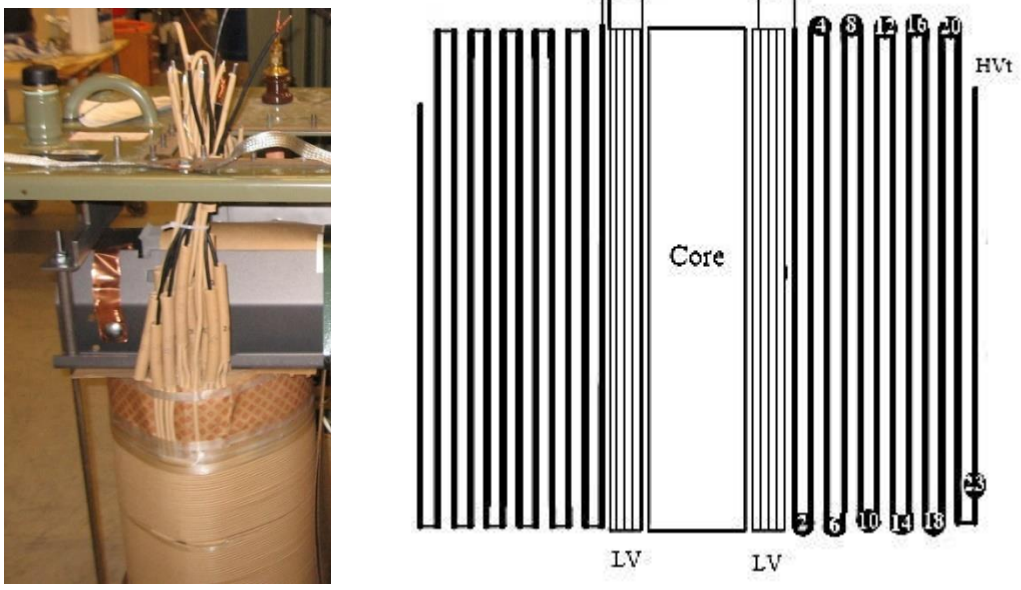

a) *b)*

Figure 3-22: T5 details (left): transformer winding with connection leads from different locations, (right): winding schematic and positions of connecting leads.

Variations that occur in transformer frequency responses due to changes in the location of fault are investigated. Unlike conventional FRA tests on transformers wherein the responses are used to detect faults such as winding deformations or core dislocations, in this investigation, frequency responses of different parameters are measured against a simulated defect. For this purpose, nine short circuits were created at different locations by shorting a certain number of HV winding turns. It is also presumed that access to the terminals of each individual winding is available for measurement. It should be noted here that although model transformer T5 is a three-phase design, only one phase is considered in this study, while the unused phase windings are short-circuited. As the effect of the core for magnetic coupling between windings of different legs (phases) is negligible for frequencies above 10 kHz (due to the huge drop in core permeability) [69], windings of different legs have insignificant mutual effects on each other.

Transformer T5 is designed in a way that the number of turns between each two consecutive connections is 56 except for the taps (21-26) which have 32 turns between one another. This means that, in terms of number of short-circuited turns, all implemented faults have the same number of turns (112) except the fault in the outermost layer, which has eight more turns. Fault numbering along with short circuit locations are given in Table 3-7.

Table 3-7: Fault numbering based on the position of short circuits based on Figure 3-22.

Fault Number	Location of Short Circuit (Between Connection Leads)
1	2 and 6
2	4 and 8
3	6 and 10
4	8 and 12
5	10 and 14
6	12 and 16
7	14 and 18
8	16 and 20
9	18 and 23

3.9.2 Fault Analysis

To analyze the FRA measurement results, both qualitative observations on trends and quantitative analysis are used. Trends in frequency responses based on patterns in the shifts of resonance frequencies and changes in resonance magnitudes have been investigated in detail. On the other hand, quantitative analysis, which derives numeric values for comparing FRA measurements, is based on the "difference factor" which is defined below.

A measure that can be adopted to compare faulty windings with the reference healthy winding is a criterion derived from the absolute sum of logarithmic errors; hereafter referred to as the difference factor. The higher the difference factor is, the larger are the differences between responses; hence it is easier to differentiate between graphs.

$$\delta_{ASLE}(R_{sc\_k}, R_0) = \sum_{f=f_{\min}}^{f_{\max}} \frac{\left|20\log_{10} R_0 - 20\log_{10} R_{sc\_k}\right|}{N} \qquad (2.19)$$

Where N is the number of readings, δ_{ASLE} is a quantitative indication of the difference between R_{sc_k}, responses of transformer winding with a short circuit at location k, and R_0, the response of a healthy transformer. This difference factor can also be generalized to include other types of faults. Compared to other mathematical criteria, the difference factor calculated using the above formula was found to be the most sensitive criterion to diagnose even badly scaled responses irrespective of fault type [70].

Considering $R_{0(f)}$ as the frequency response of a healthy transformer and $R_{sc\_1(f)}, R_{sc\_2(f)}, \ldots, R_{sc\_k(f)}, \ldots, R_{sc\_n(f)}$ as frequency responses of that transformer with fault numbers $1,2,\ldots,k,\ldots,n$, the formula for computing the correlation coefficient can be derived as:

$$CF(k) = \frac{\sum_{f=f_{min}}^{fmax} R_{sc\_k}(f) \cdot R_0(f)}{\sqrt{\sum_{f=f_{min}}^{fmax} (R_{sc\_k}(f))^2 \cdot \sum_{f=f_{min}}^{fmax} (R_0(f))^2}} \qquad (2.20)$$

Wher f_{min} is the lower frequency limit of the measurement and f_{max} is the upper frequency limit of the measurement. The correlation coefficient always ranges between -1 and 1, with 1 or -1 indicating perfect correlation (all points would lay along a straight line in this case). A correlation value close to 0 indicates no association between the variables.

Chapter 4

Results

This chapter presents the results of this work, classified in the following categories: ageing experiments, validations of models and methods proposed in this research, and analysis of design modifications suggested for transformers.

4.1 Transformer ageing under distorted voltage

Results of ageing tests on transformers T1 and T2 are presented. Four parameters are monitored as indications of transformer's insulation condition: partial discharge, oil temperature, dissolved gas content and dielectric frequency response. T1 is aged under sinusoidal voltage (source-1) while T2 is aged under PWM voltage of a converter (source-2).

4.1.1 PD

PD was periodically measured for both transformers during ageing experiment. The first PD tests were done before the start of ageing, as the initial qualification tests. Subsequent PD tests were done after 100, 200, 500 and 960 hours of ageing. The results of PD tests at 10 kV are shown in Figure 4-1.

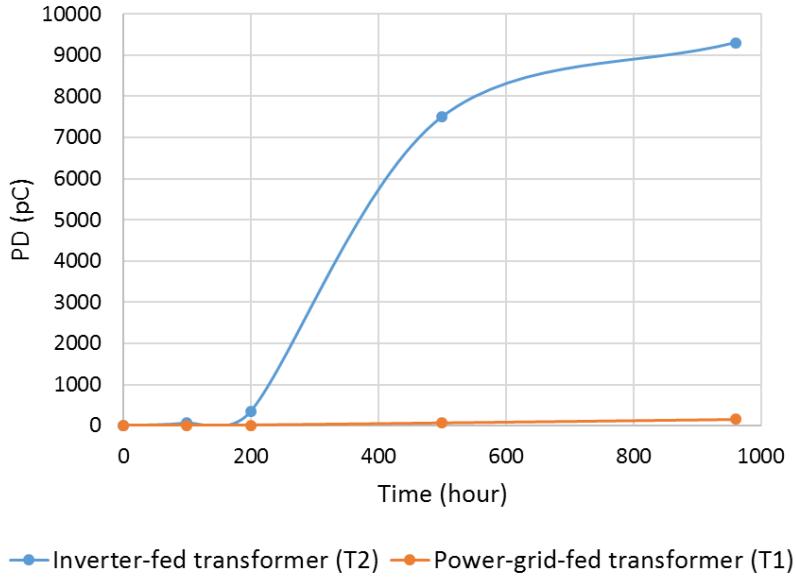

Figure 4-1: PD test results on sample transformers during ageing under sinusoidal and PWM voltages.

With ageing, the difference between PD of the inverter-fed and power-grid-fed transformers increased significantly. After 960 hours, the level of PD reached 9300 pC for T2 while the corresponding PD level in T1 was 21 pC. Trends observed in PD of T1 and T2 indicate severe degradation in the insulation of T2 confirming accelerated ageing under high-frequency distorted voltage.

4.1.2 Oil temperature

The temperature of the bulk oil was measured during the ageing while ambient laboratory temperature was in a range of 24±1° C. Oil temperature was recorded every day, and its average value for each 100-hour period is plotted in Figure 4-2. It can be observed that the difference between temperatures of T1 and T2 does not exceed 15%, and they are both considerably below the temperature limit of transformer operation. Figure 4-3 shows winding temperatures measured at layers 1, 3, 5, 7 and 9 of T1 and T2 windings. For T1, winding temperature gradually increased by moving towards inner layers. For T2, the overall trends are similar to what was observed for T1 except that the differences between the measured temperatures of adjacent layers for T2 are higher than those for T1, and the temperature measured for T2-Layer 9 is higher than T2-Layer 7 even though the latter is an inner layer.

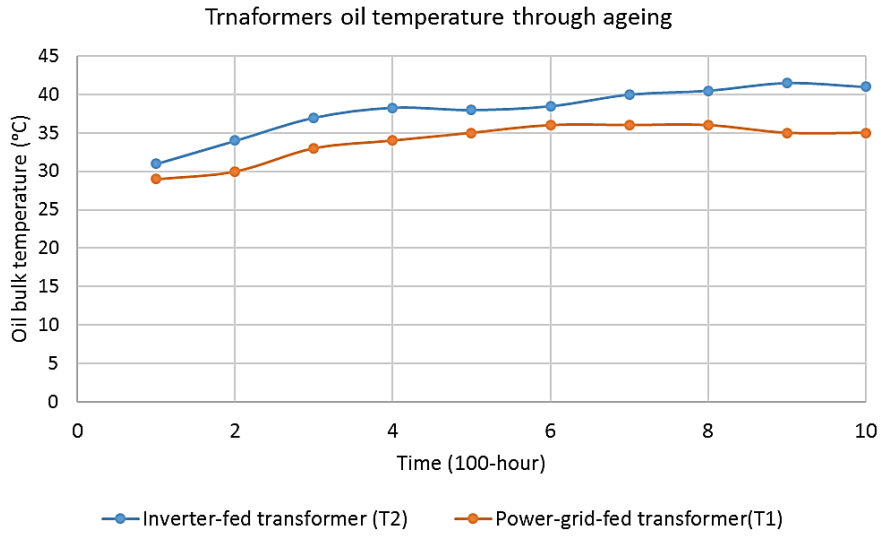

Figure 4-2: Bulk oil temperature of sample transformers during the ageing.

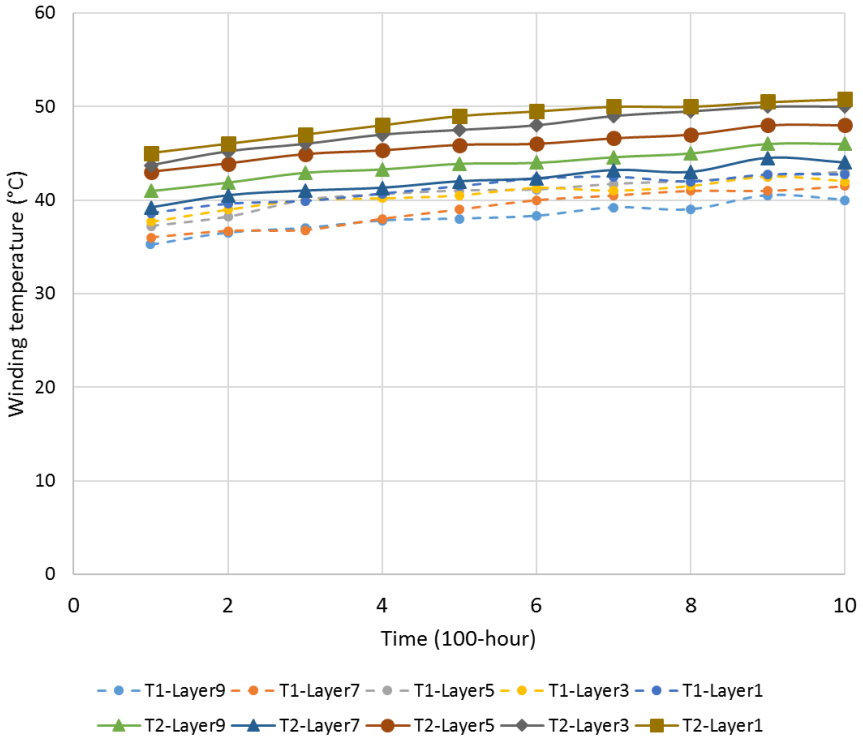

Figure 4-3: Winding temperature of sample transformers during ageing measured at five different layers of HV winding.

4.1.3 Dissolved gas analysis

Table 4-1 shows the results of DGA for the power-grid-fed and inverter-fed transformers. The gases were extracted from transformers' oil and analyzed using the standard test method. The result for the transformer energized by power grid sinusoidal voltage shows only air gases, while the inverter-fed transformer oil has higher hydrogen, carbon monoxide, methane, carbon dioxide, ethylene and acetylene. Thus, there are more fault gases present, indicating that inverter-fed transformer's insulation has considerably degraded. The gas of real concern is acetylene because its level is above the threshold warning level. The other gas contents are still below the warning levels.

Table 4-1: Dissolved gas content in T1 and T2 after 500 hours ageing.

Dissolved gas (ppm)	Power-grid-fed transformer (T1)	Inverter-fed transformer (T2)
Hydrogen	<10	52
Carbon Monoxide	43	259
Methane	<5	13
Carbon Dioxide	1120	5780
Ethylene	<2	4
Ethane	<2	<2
Acetylene	<2	7

4.1.4 Dielectric frequency response

The frequency response of dielectric parameters are presented for T1 and T2. Total capacitance (C), imaginary capacitance (C") and percentage dissipation factor (%DF) are the parameters used to compare the ageing of T1 and T2. Measurements are performed at two levels of excitation voltage: 200 V and 2 kV. Each test has been repeated three times, and the average values are plotted.

4.1.4.1 Un-grounded specimen test mode

The frequency response of the capacitance between HV and LV windings obtained in Un-grounded specimen test (UST) mode test (Figure 4-4) is shown in Figure 4-5 for both transformers. As it is shown, the capacitance values are the same for both transformers from 10 kHz down to 0.1 Hz. For the frequencies below 0.1 Hz, the capacitance of T2 is slightly higher than that of T1. The capacitance that is measured in the UST mode involves only the winding insulation between the HV and LV windings.

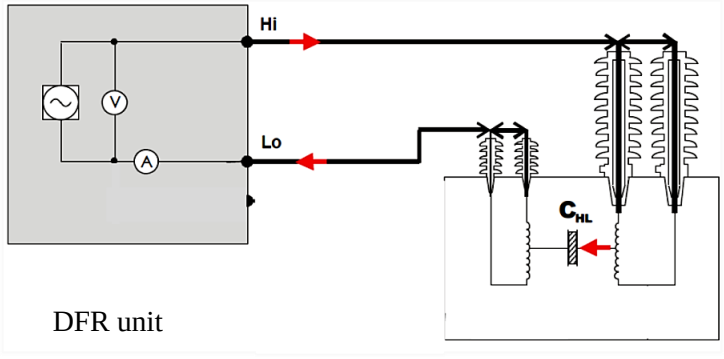

Figure 4-4: Schematic diagram of circuit connections in un-grounded specimen test (UST) mode.

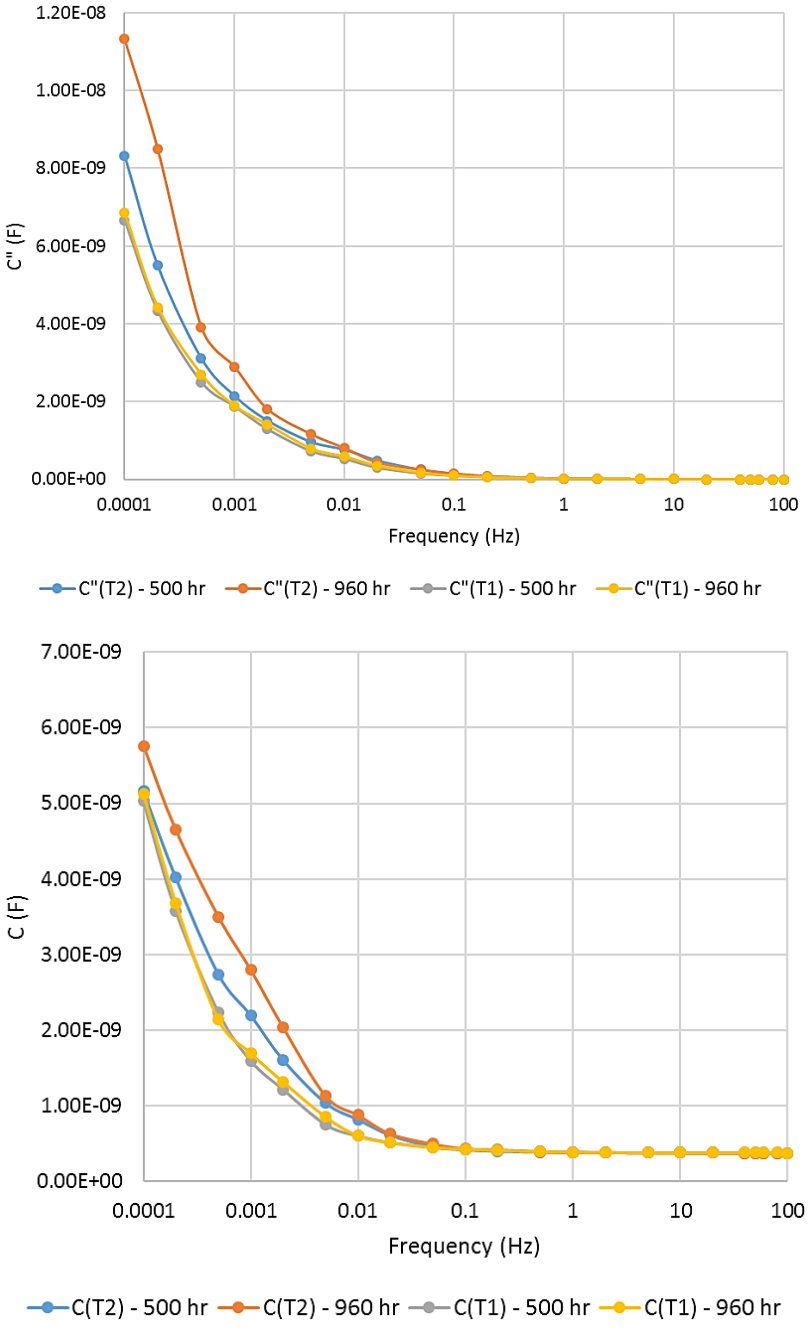

Figure 4-5: Imaginary and total capacitance versus frequency in UST mode (200 V) for T1 and T2 after 500 and 960 hours of ageing.

Figure 4-6 shows the %DF curves for both transformers. A horizontal shift between the curves in the medium frequency range is observed.

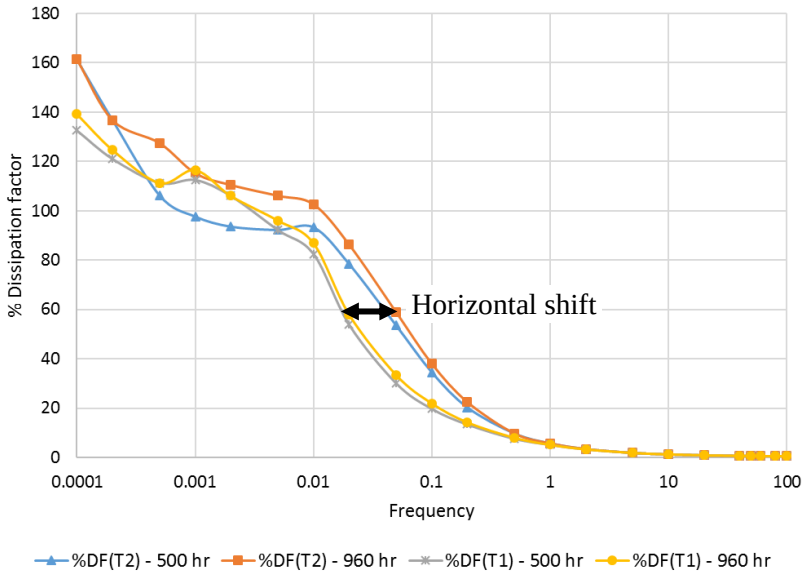

Figure 4-6: Percent DF versus frequency in UST mode (200 V) for T1 and T2 after 500 and 960 hours of ageing.

4.1.4.2 Grounded specimen test mode

As it is shown in Figure 4-8, in 4.1.4.2 grounded specimen test mode (GST) mode (Figure 4-7), there are discrepancies in the measured capacitances in medium-frequency range as well as in low-frequency range. The difference emerges more clearly in GST mode measurements where the bulk of oil is also involved under energization.

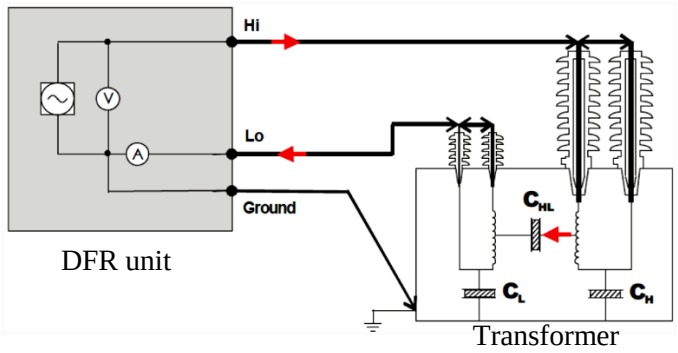

Figure 4-7: Schematic diagram of circuit connections in grounded specimen test (GST) mode.

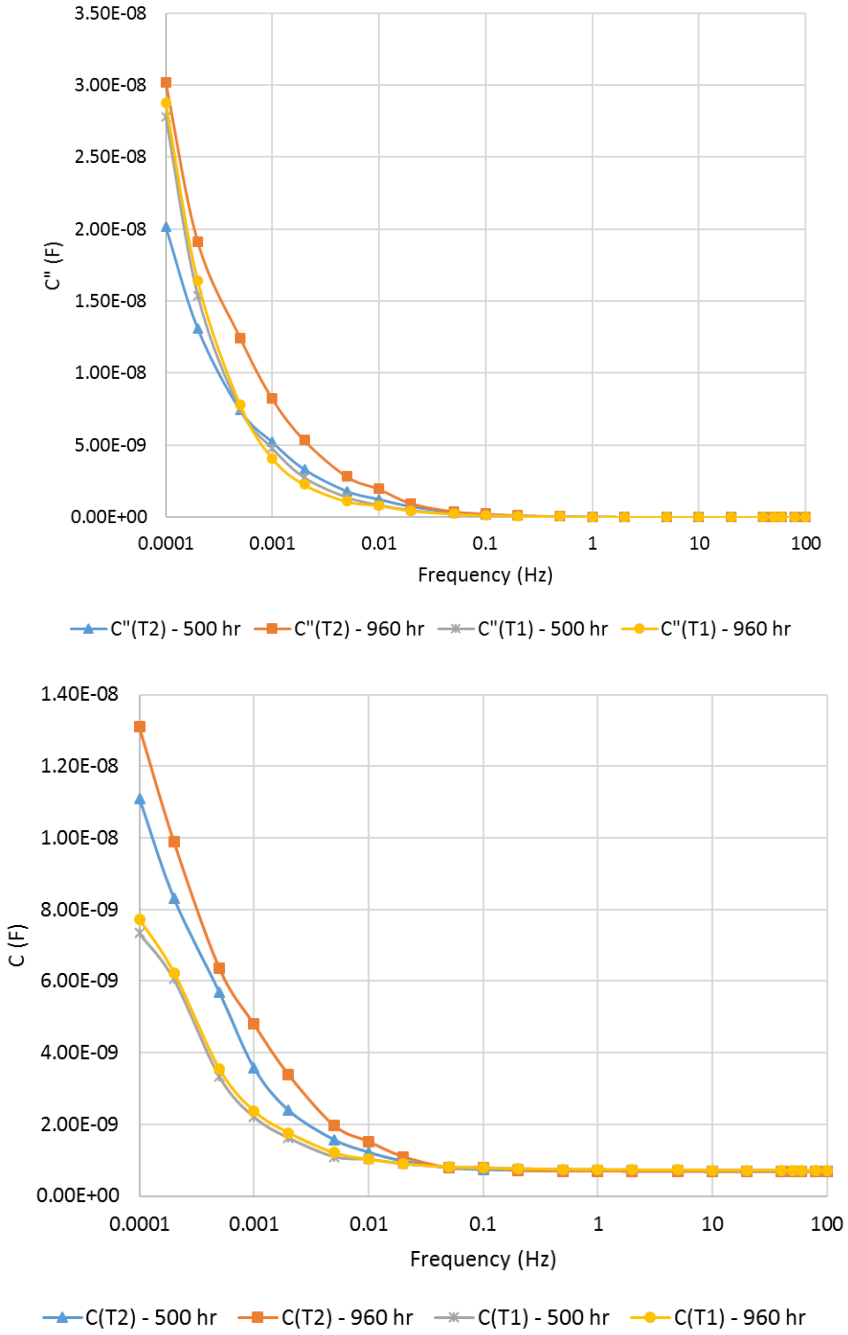

Figure 4-8: Imaginary and total capacitance versus frequency in GST mode (200 V) for T1 and T2 after 500 and 960 hours of ageing.

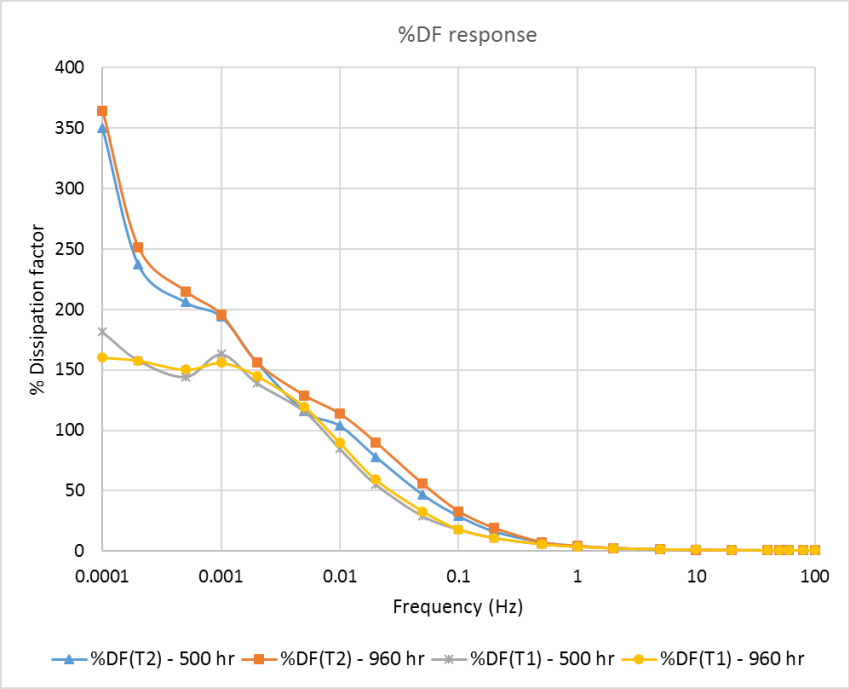

Figure 4-9: Percent DF versus frequency in GST mode (200 V) for T1 and T2 after 500 and 960 hours of ageing.

4.1.4.3 Effect of applied voltage on dissipation factor

To measure the dissipation factor at a higher voltage, the same UST measurements are performed under 2 kV peak voltage. Figure 4-10 reveals more consistent %DF in the low-frequency range compared to the results under 200 V (Figure 4-6).

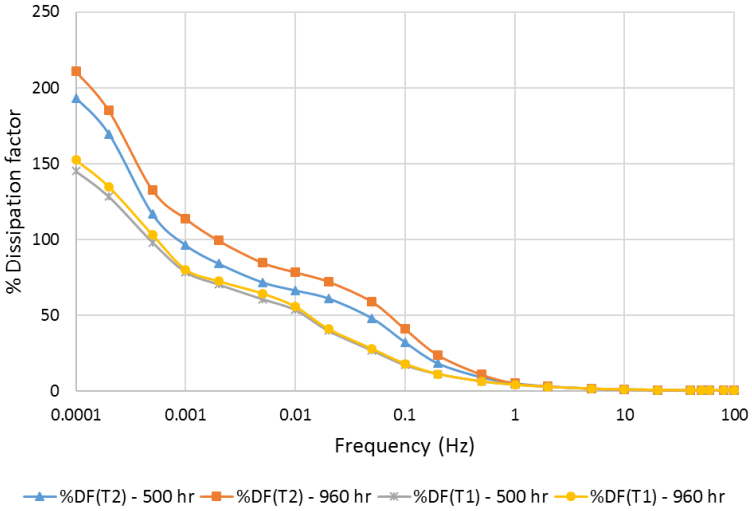

Figure 4-10: Percent DF versus frequency in UST mode (2 kV) for T1 and T2 after 500 and 960 hours of ageing.

4.2 Transformer modelling

To examine the validity of the proposed scaling method for transformer modelling, the frequency response of scaled transformer (T3) and original transformer (T1) are compared. The parameters analyzed for studying the effect of scaling on terminal characteristics of transformers are *HV/LV* transfer function, *LV/HV* transfer function, and Z_{HV} when LV terminal is shorted. Furthermore, to study the effect of scaling on internal voltage resonance and electric field distribution inside the windings, frequency response of each layer's voltage and gradients of voltages between adjacent layers are measured and compared between T1 and T3. All the results are presented over 100 Hz to 1 MHz range for the purpose of uniformity. It is important to note that, at very high frequencies (>500 kHz), frequency responses are highly influenced by the stray capacitances and inductances of probe connections.

4.2.1 HV/LV Transfer function

Figure 4-11, using normalized voltage transfer ratios, shows transfer function spectra for the delivery of voltage contents from the LV terminal to HV terminal. As expected, from 100 Hz to 1 kHz, the voltage ratio is the same for both transformers and equal to the transformer nominal turns ratio with a normalized value of 1. The first resonance for T1 occurs at 3.75 kHz while that for T3 occurs at 2.22 kHz, showing a shift to the lower frequency in the resonance frequency of scaled transformer. Similarly,

the occurrences of second and third resonance peaks are also shifted to the lower frequency for T3. This observation is in compliance with the expected results based on the following relation (explained in section 3.7.2.1):

$$\left[f_{resonance\ Scaled\ (T3)}\right] = \frac{\left[f_{resonance\ Original\ (T1)}\right]}{Scl} \quad , \qquad (Scl = \sqrt{3})$$

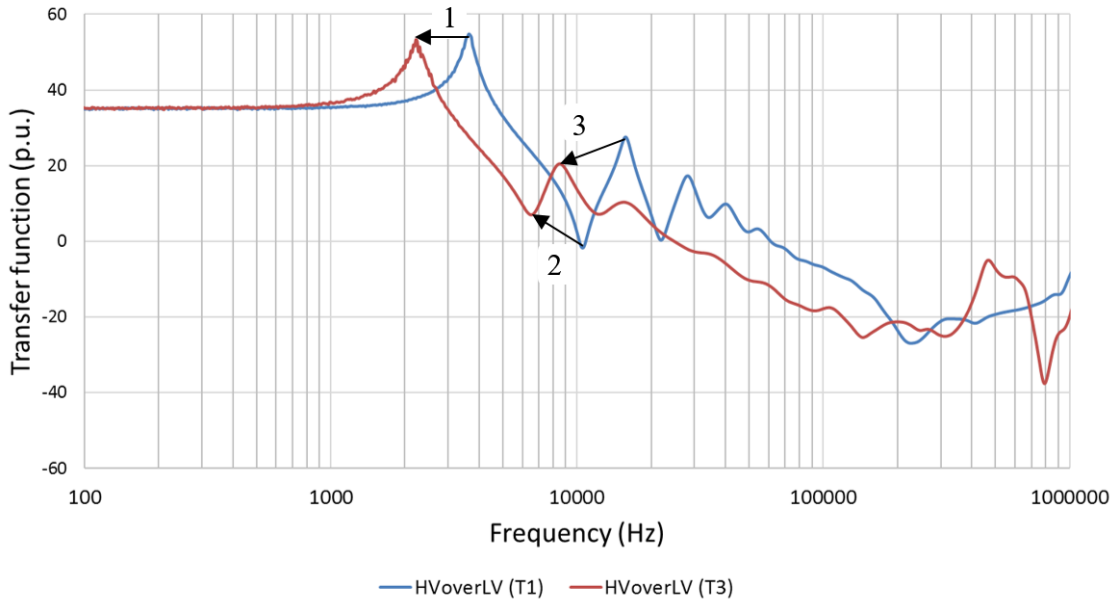

Figure 4-11: *HV/LV* transfer function for original (T1) and scaled (T3) transformers.

Table 4-2 lists the measured frequencies of the first three resonances for both T1 and T3. For comparison purpose, for T3, the calculated resonance frequencies based on the proposed scale factor, *Scl*, are also listed. It is noteworthy that the resonance frequencies of T3 calculated based on the frequency scale factor match closely with those measured; and for the first resonance, which is also the most significant resonance condition, frequency deviation is as low as 2.4%.

Table 4-2: Measured and calculated frequencies of the first three extrema for T1 and T3 (*HV/LV*).

Shift number	Resonance frequency (Measured for T1)	Resonance frequency (Measured for T3)	Resonance frequency (Calculated for T3)	% Deviation between calculated and measured frequency for T3
1	3.75 kHz	2.22 kHz	2.16 kHz	2.4%
2	10.9 kHz	6.7 kHz	6.29 kHz	6%
3	14 kHz	8.7 kHz	8.1 kHz	7%

4.2.1.1 LV/HV Transfer function

The transfer function for the delivery of the voltage from HV terminals to LV terminals showed similar behaviour with shifts like what was observed in *HV/LV* transfer function; with the highest peak occurring around 200 kHz. The deviation between calculated shifts of resonance frequencies and measured shifts are shown in Table 4-3 for three resonance points. An excellent correlation between the measured and calculated resonance frequencies has been observed, with less than 3% deviation.

Table 4-3: Measured and calculated frequencies of the first three extrema for T1 and T3 (*LV/HV*).

Shift number	Resonance frequency (Measured for T1)	Resonance frequency (Measured for T3)	Resonance frequency (Calculated for T3)	% Deviation between calculated and measured frequency for T3
1	9.2 kHz	5.3 kHz	5.31 kHz	-0.2%
2	14.3 kHz	8.2 kHz	8.25 kHz	-0.6%
3	380 kHz	225 kHz	219.3 kHz	2.5%

4.2.1.2 Input impedance, Z_{HV}

Figure 4-12 shows the frequency response of input impedance from HV side while LV terminal short-circuited. An overall shift in frequency response is seen between the response of original transformer and response of scaled transformer. Within the range of 100Hz to 1MHz, the dominant resonance peak has been observed at 21 kHz for T3 and at 37 kHz for T1; with a deviation of 1.6% from the calculated resonance frequency. A constant ratio equal to *Scl* exists through the whole frequency response between the magnitudes of Z_{HV} for T1 and T3.

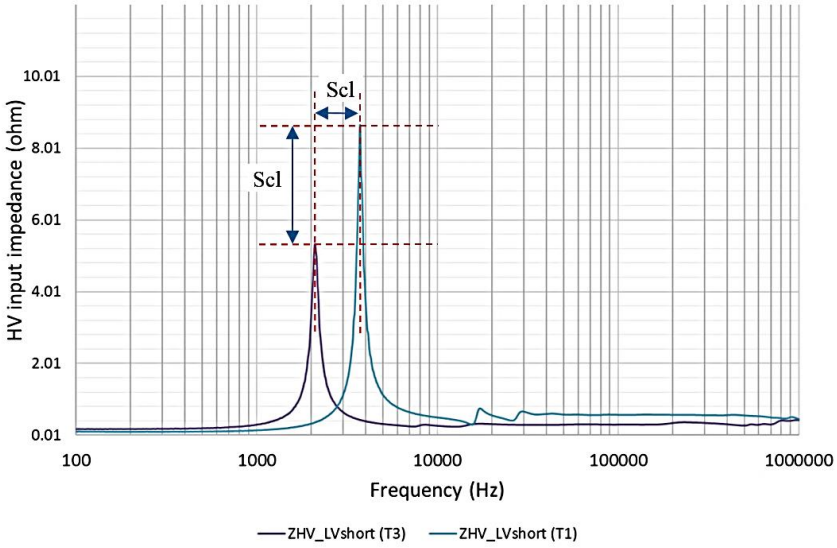

Figure 4-12: Input impedance Z_{HV} as a function of frequency with LV shorted.

4.2.1.3 Effect of scaling on internal resonance

In addition to the terminal voltage study which deals with transformer behaviour observed from the terminals, the development of internal electrical stress due to resonance is investigated as an important factor in the performance of winding insulation. To achieve this goal, frequency response of transferred voltage at each layer of HV winding is measured for T1 and T3. To calculate the frequency spectrum of electrical stress on interlayer insulation, responses of adjacent layers are subtracted from each other. Although only frequency response magnitudes are shown here, in the subtraction operation, both magnitude and phase of frequency responses are taken into account. The result of electric stress calculation between HV layers is presented in Figure 4-13. Comparing interlayer electric stresses of T1 and T3 reveals that the frequency shift is in agreement with the scaling factor.

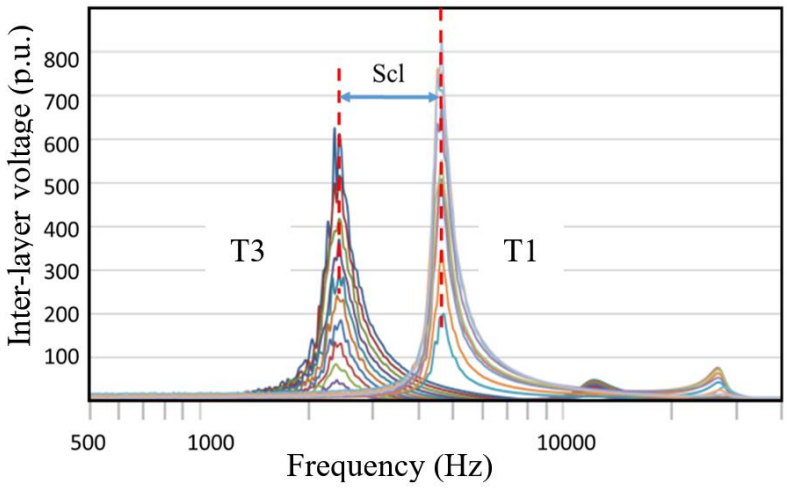

Figure 4-13: Frequency response of voltage gradient between layers of T1 and T3 (normalized based on inter-layer voltage gradient at power-frequency)**.**

4.3 PD in paper/oil under impulse voltage

Paper/oil samples are tested for PD under impulse train waveforms with different frequencies, rise times and peak voltages, using the results of wind-farm modelling and characteristics of simulated transient waveforms. Validation of the proposed method of PD measurement, and effects of frequency and rise-time on PD of paper/oil samples are presented in this section.

4.3.1 Temperature

Oil temperature, in the vicinity of the energized samples and in the oil bulk, were measured for 10 hours of voltage application. The average values listed in Table 4-4 show that the temperature in the vicinity of the energized samples is very close to the average oil temperature (Table 4-4).

Table 4-4: Average oil temperature, 10 hours after application of 6 kV impulse (chamber 1).

Rates of rise (RORs) (kV/µs)	Oil bath temperature (° C)	Oil temperature close to samples (° C)
11	24.3	26.8
5	24.8	26.1
2	24.6	26.2
1	24.5	26.3

4.3.2 PD on the surface of paper

It is important to ensure that the studied PD occur on the surface of paper samples rather than in the surrounding oil. To verify this, carbonization tracks on the paper samples were examined in a view magnified by a factor of 200 (Figure 4-14). It was observed that trackings started from the surface of paper and expanded over time. The final photo shows a punctured paper after being subjected to impulse stress for 78 h.

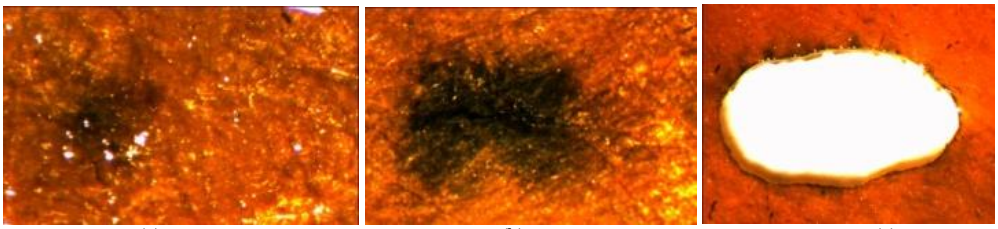

(a) (b) (c)

Figure 4-14: Trend of carbonization from PD on the surface of Kraft paper, (a): after 20 hours, (b): after 40 hours, (c): after 78 hours.

4.3.3 Hydrogen and PD energy

Comparing the energy levels of PD caused by different impulses based on the amount of dissolved hydrogen generated by PD would be a valid approach only if the hydrogen contents were proven to be linearly related to PD energy in the controlled test compartment. The first step of this experiment was to examine the trends in the relationships between PD energy and dissolved hydrogen content. To achieve this objective, the amounts of hydrogen generated must be compared for pulse trains whose relative power ratios can be analytically pre-established. To this end, pulse voltages with the same pulse characteristics but with different frequencies were applied for validation of the proposed method. Samples were energized for four hours, following which the hydrogen content was recorded for each test. Repetition frequencies were chosen to be in the range of 200 Hz to 2 kHz so that their associated dead times between impulses (in the range of 0.5 ms to 5 ms) are much greater than the durations of decaying impulses (around 70 μs). Under such conditions, it can be assumed that the total PD energy of the pulse train is proportional to its repetition frequency. This procedure was repeated for three rise-times and two peak voltages in order to confirm the linearity of the trends under a variety of impulse waveforms. Each test was conducted three times, and average values are depicted in Figure 4-15, which indicates the relationship between frequency and hydrogen content in the oil. The bars, in all graphs, represent the ranges of measured values for each data point, along with the mean value.

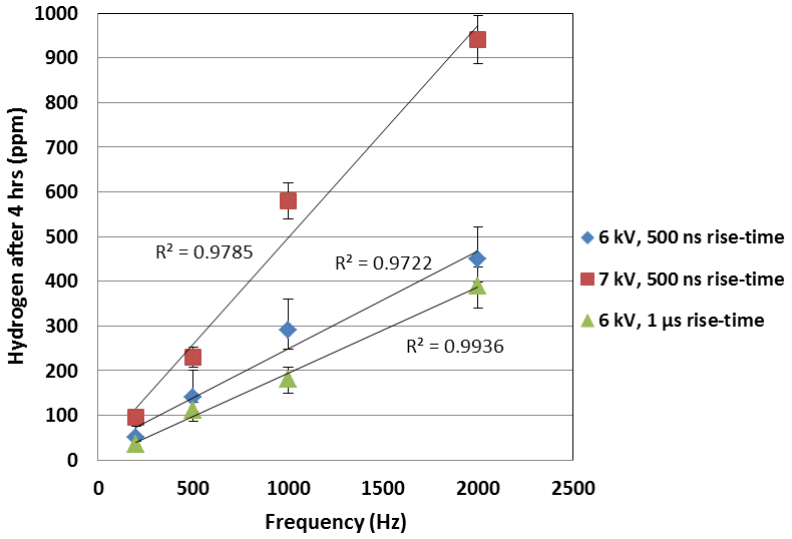

Figure 4-15: Hydrogen generation as a function of impulse frequency at different test conditions. The R-squared factors are also given (beside the plot for each series) to show the linear trends observed. (max standard deviation = 11 %).

4.3.4 Effect of rise-time and frequency on PD inception voltage

Hydrogen generation rate depends on partial discharge intensity, and is at its lowest when the PD is just above the inception level. For voltages slightly higher than the inception voltage, hydrogen reached detectable levels after a long energization time. In contrast, below the inception voltage, even after a long time (20 hours), no significant increase in hydrogen level was observed. Based on this observation, this section adopts dissolved hydrogen content to detect PD initiation for paper samples stressed under impulse voltages with various rise-times and frequencies.

Figure 4-16 shows hydrogen content for pulse trains with different rise-times but at equal peak voltages. The peak voltage of 4.4 kV is chosen as an example peak voltage that initiates PD for two of the studied rise-times but not for the other two. For a peak voltage of 4.4 kV, slower rise-time pulses show increased hydrogen content with the increased time of pulse application. Conversely, faster rise-time impulses exhibit no noticeable hydrogen generation, and hence no significant PD. Although measurement of low hydrogen contents might be subject to accuracy issues, the experimental result shown in Figure 4-16 is rather a comparative study, which focuses on the trend of hydrogen under different pulse waveforms.

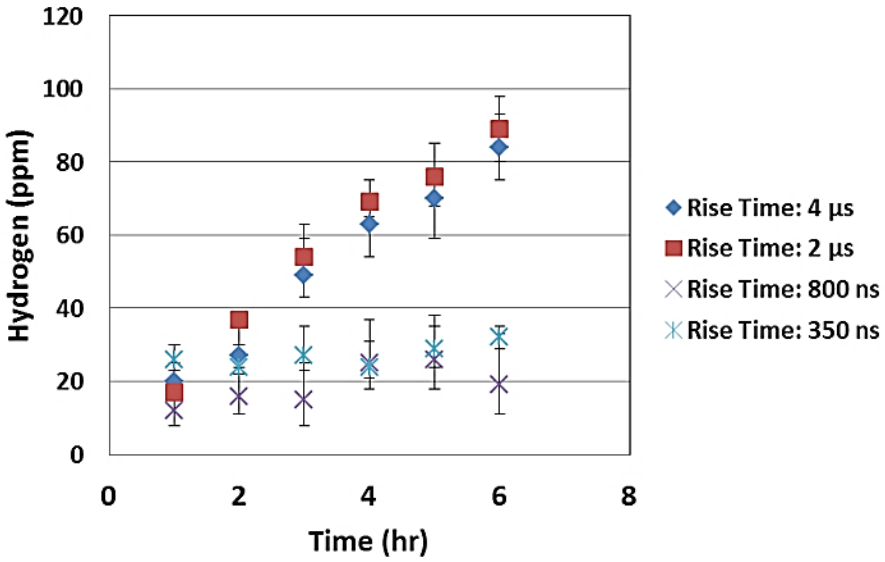

Figure 4-16: Hydrogen content (in chamber 1) versus time, for pulse trains with 4.4 kV peak voltage at 200 Hz. (max standard deviation = 6 %)

To find the PD gas initiation voltage associated with each rise-time, the peak voltage was increased in 50 V steps, and the samples were energized under each voltage level for six hours. The first voltage level at which a measurable hydrogen growth could be observed within six hours was recorded as the hydrogen initiation voltage. The test was repeated for five identical paper samples, and the average of the recorded hydrogen initiation voltages was taken as the PD gas inception voltage (PDGIV) for that particular impulse rise-time.

A comparison of the PDGIV trends for different rise-times shown in Figure 4-17 and Figure 4-18 reveals that slower rise-times result in lower PDGIV, especially for rise-times slower than 1 µs, for which the effect of rise-time is stronger.

Another parameter whose effects on PDGIV were studied is the impulse frequency. To determine the PDGIV associated with each repetition frequency, the same procedure as for the rise-time study was followed for five frequencies, and the voltage at which hydrogen content started to increase was recorded for each frequency. The average PD initiation voltage for each frequency was taken as the PDGIV. Figure 4-17 and Figure 4-18 demonstrate the PDGIV as a function of frequency for various rise-times in chambers 1 and 2. In chamber 1, with plane-plane electrodes, changing the frequency makes no significant difference (less than 4%) in the PDGIV. On the other hand, in chamber 2, the PDGIV exhibits a decreasing trend, starting to fall more than 15% after 1 kHz.

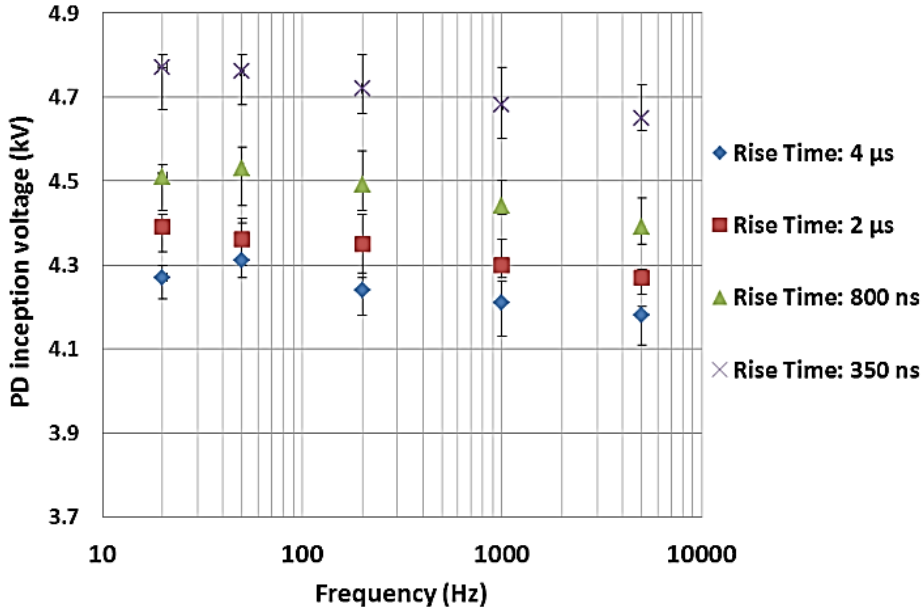

Figure 4-17: PD inception voltage versus frequency for chamber 1 (plane-plane electrodes) (max standard deviation = 8 %).

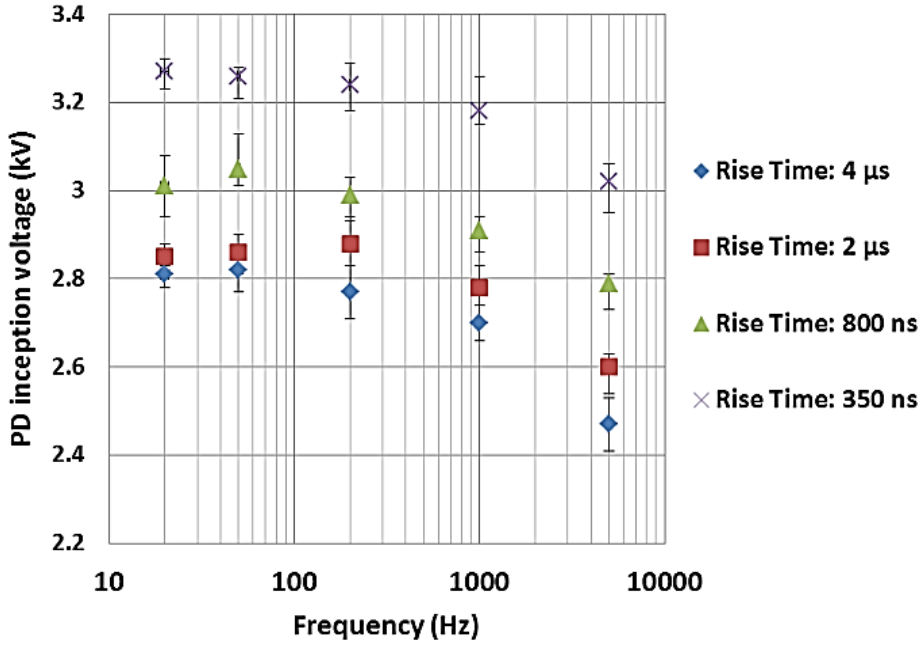

Figure 4-18: PD inception voltage versus frequency for chamber 2 (rod-plane electrodes) (max standard deviation = 8 %).

4.3.5 Effect of rise-time on PD energy

PD energy is the parameter that has been analyzed to influence hydrogen content. The effect of PD energy at different rise times has been evaluated, keeping pulse amplitude constant. Data is presented at different RORs, as modifying rise-time while keeping peak voltage constant alters ROR values. Peak voltage was chosen to be high enough to initiate PD for all RORs in the study range. PD energy levels of impulses with different RORs were compared based on analysis of hydrogen content for the duration of the experimental period. Hydrogen content readings were recorded every minute and then averaged on an hourly basis. Results are provided for chamber 1 and chamber 2, under isobaric and sealed conditions, respectively.

The curves shown in Figure 4-19 indicate hydrogen content in chamber 2 for 0.25 mm paper samples under 6 kV at 1 kHz impulse trains. Due to the sealed conditions, amounts of hydrogen increase continuously at an almost constant rate for hydrogen contents below 3500 ppm; whereas, above 3500 ppm, the rate of increase in the hydrogen content is slightly slower. The equations of the lines fitted to the curves have also been derived for each curve. The tangential slopes of the fitted lines are given to facilitate a comparison of hydrogen generation rates.

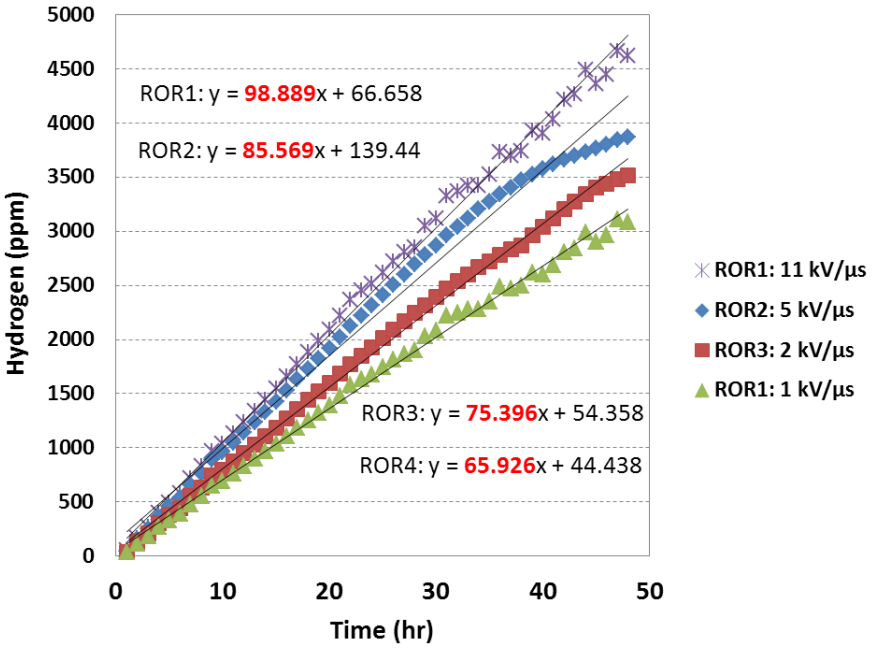

Figure 4-19: Hydrogen content in chamber 2 over time for different RORs under 6 kV at 1 kHz (max standard deviation = 10 %).

Figure 4-20 shows the hydrogen content in chamber 1 for the first 48 hours after application of a pulse train of 6 kV at 1 kHz on the paper samples. In contrast to the results obtained under the sealed conditions of chamber 2, under the isobaric conditions in chamber 1, hydrogen contents converged to specific levels rather than increasing continuously. The effect of different hydrogen generation rates can be seen in hydrogen-increase slopes and also in levels where the curves finally end. The tangential slopes of the curves for their linear parts (before their saturation point) are 80.5, 61.5, 47.2 and 34.8 for ROR1, ROR2, ROR3 and ROR4 respectively. Both Figure 4-19 and Figure 4-20 show that higher RORs, in the range associated with this study, result in higher hydrogen generation rates, interpreted as higher PD energy levels.

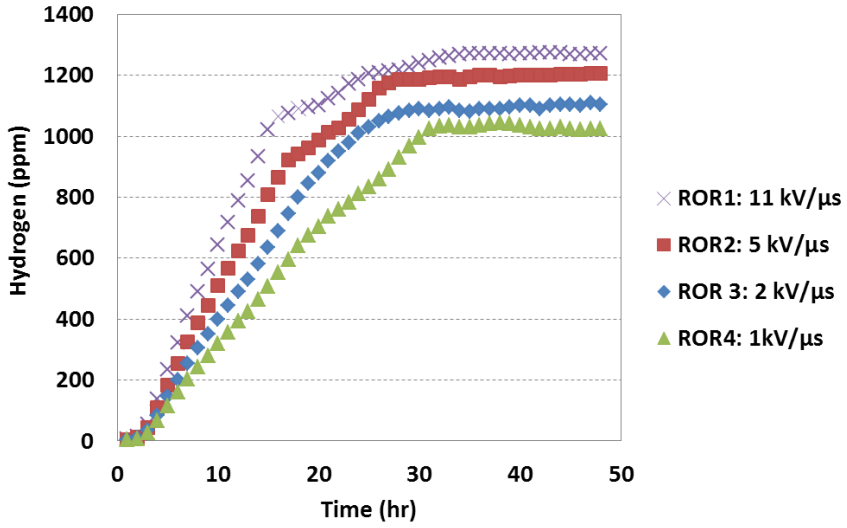

Figure 4-20: Hydrogen content in chamber 1 over time for different RORs under 6 kV at 1 kHz (max standard deviation = 5 %).

4.4 Evaluation of electrostatic shield effectiveness

Further to previous sections investigating the effects of high-frequency distorted voltage on transformer insulation system, transformer modelling for calculating internal stresses, and paper/oil samples under high-dV/dt impulses; this section addresses a modification method by presenting the results of a study on the effect of electrostatic shielding on transformer behaviour. To this purpose, voltage transfer functions across transformer terminals, and voltage gradients between the layers of HV winding are analyzed and compared for both cases of shielded and unshielded designs.

4.4.1 Voltage transfer functions at terminals

Frequency responses of voltage transfer function from LV terminal to HV terminal is presented in Figure 4-21, for the shielded (T4) and unshielded (T3) transformers. It can be observed that from power-frequency (60 Hz) up to nearly 170 kHz, both shielded and unshielded transformers behave the same in terms of transfer of voltages of different frequency contents. In contrast, for higher frequencies in a range of 170 kHz to 600 kHz, the shielded transformer showed a better filtering functionality compared to the unshielded transformer with a difference of up to 18 dB. For frequencies higher than 600 kHz, the frequency responses are practically the same and much lower than nominal turns ratio (normal power-frequency value).

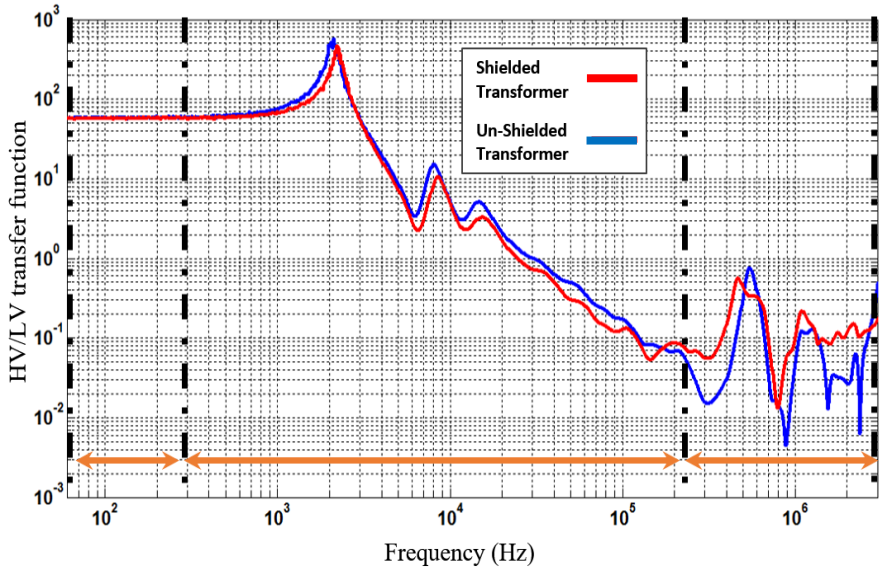

Figure 4-21: Frequency response of voltage transfer function from LV to HV terminals for shielded and un-shielded transformers.

Figure 4-22 demonstrates the comparison between HV-to-LV transfer functions of shielded and unshielded model transformers. The responses of two model transformers drift away from each other starting from 2 kHz. Insertion of the electrostatic shield results in attenuation of the transferred voltage from HV to LV side by a factor of 5 dB over the frequency range of 8 kHz to 100 kHz. The other noticeable difference between the curves occurred around 400 kHz where the voltage transfer ratio of the shielded transformer is higher than that of the unshielded transformer by a significant factor of 20 dB while they are higher than nominal turns ratio (normal power-frequency value).

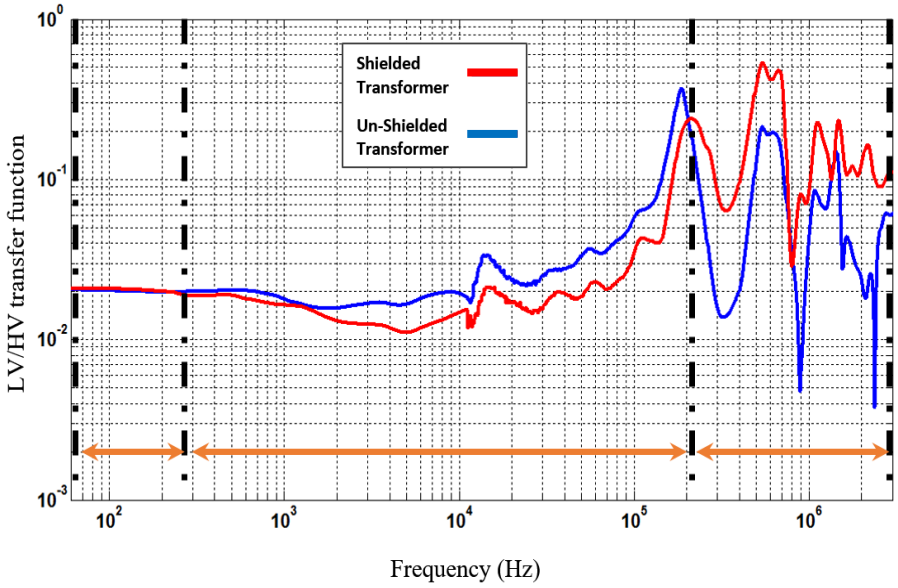

Figure 4-22: Frequency response of voltage transfer function from HV to LV terminals for shielded and un-shielded transformers.

4.4.2 Voltage transfer functions inside transformer

To find the frequency response of electric stress on layer insulations, it is first required to measure the voltage transferred to each layer of transformer winding. As an example, Figure 4-23 shows transferred voltage spectra at all layers of HV winding measured for T4. Although transferred voltages to adjacent layers have differences all along the frequency range, the frequency range that is critical is the period in which the transferred values are higher than their normal power-frequency values, because those are the ones that can cause excessive stress on layer insulation. Taking into account both magnitude and phase of transferred voltages to each layer for T3 and T4, Figure 4-24 and Figure 4-25 are derived.

$$Transfer\ Function_{layer\ i}\ (f) = \frac{V_{layer\ i}\ (f)}{V_{input}\ (f)} \tag{4.1}$$

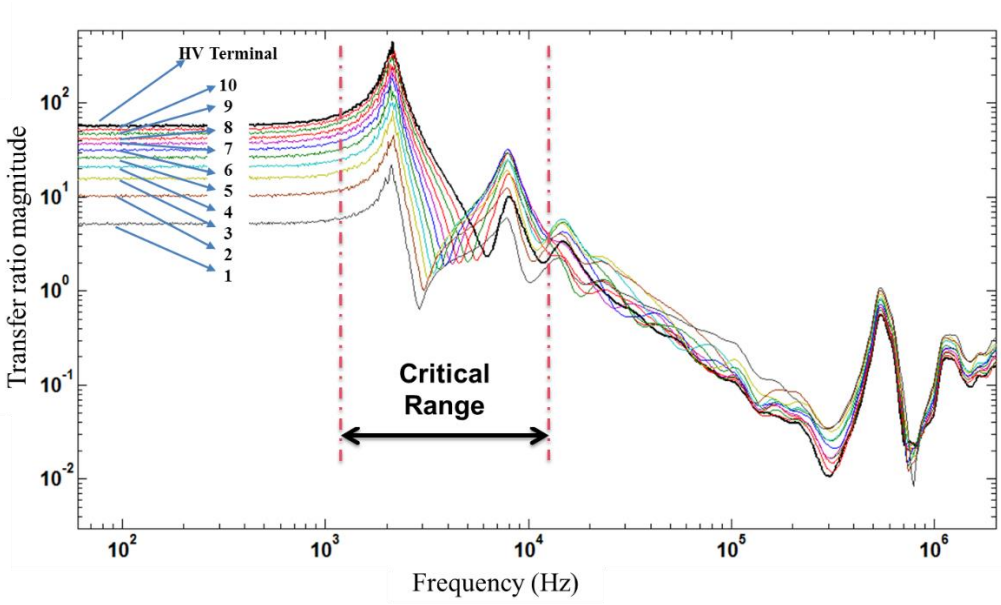

Figure 4-23: Frequency response at all layers of transformer winding.

Figure 4-24 and Figure 4-25 show the voltage gradient between two adjacent layers of the HV winding for shielded and unshielded transformers respectively. Y axis indicates the per-unit value of differential voltage between two adjacent layers. The per-unit values are normalized based on the voltage difference that appears between the same adjacent layers at power-frequency which also can be defined as *turns-ratio/number of layers*. Each curve represents one interlayer voltage gradient. That is, curve *i* on X axis represents the voltage difference between the middle turns of layer *i* and layer *(i+1)*.

A comparison between the graphs shows that for both transformers, the peak value of internal stress occurs at about 2.2 kHz. The amplitude of transferred voltages in the unshielded transformer is 20% higher than those in the shielded transformer. The peak voltage difference which happens between layers #9 and #10 is significantly high (more than 100 p.u.). This means that if the input voltage from the LV side contains only 1% of 2.2 kHz frequency content, the resulting voltage difference between the first two layers will have 1 p.u. content of 2.2 kHz superimposed on the 1 p.u. power-frequency voltage. This will result in at least doubled stress on the insulation just with %1 distortion of 2.2 kHz in the LV side voltage. In addition, it can be observed that voltage gradient between layers drastically increases by moving towards the outer layers.

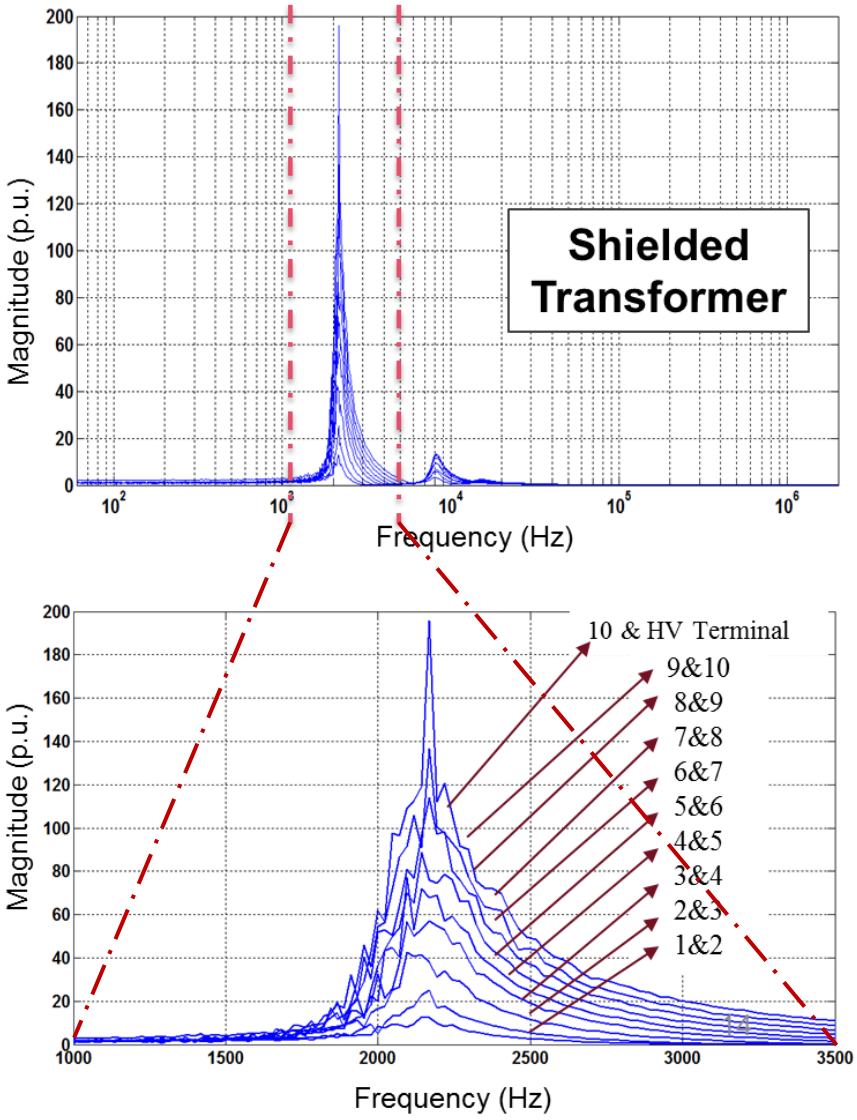

Figure 4-24: Frequency response of voltage gradient between HV winding layers (shielded transformer) – (top): For a broad frequency range, (bottom): Zoomed in view of the critical frequency range.

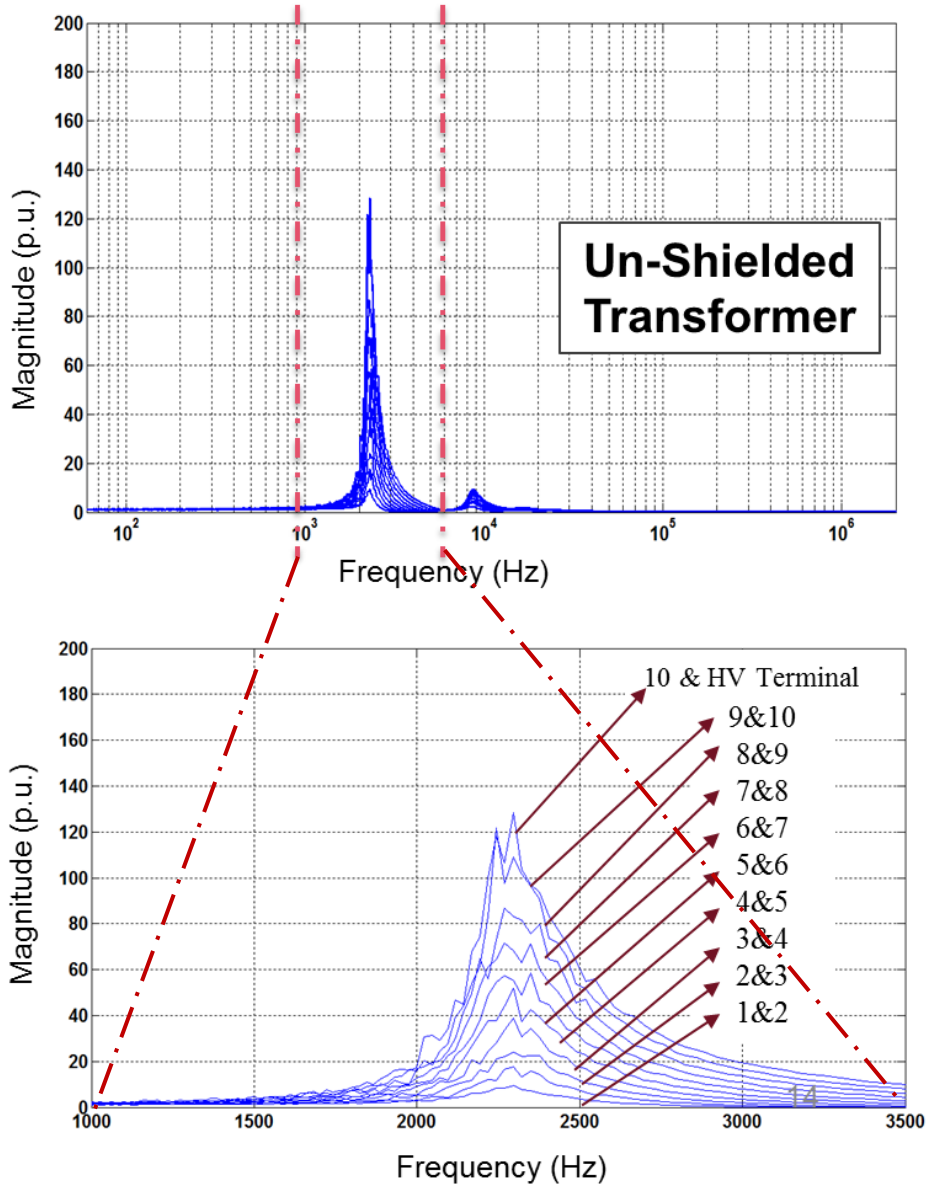

Figure 4-25: Frequency response of voltage gradient between HV winding layers (Un-shielded transformer) (top): For a broad frequency range, (bottom): Zoomed in view of the critical frequency range.

4.5 Fault location

This section presents the results of the study on locating the internal faults based on transferred voltage and input impedance spectra that are measured using procedures described in 3.6. The results are presented using 3D and 2D plots. In 3D plots, X, Y, and Z axes represent frequency, location of the short-circuit (fault number as per Table 3-7), and magnitude of the parameters, respectively. For clarity, along with 3D plots, the magnitudes of parameters are indicated by colored maps wherever it is helpful for illustration. Together, 2D and 3D plots facilitate identifying the effects of fault location on transformer frequency response patterns. Sub-sections 4.5.1, 4.5.2 and 4.5.3 represent the results for T5 while 4.5.4 shows complementary validation results for T1 and T3.

4.5.1 HV/LV Transfer voltage

Figure 4-26 shows HV voltage over LV voltage transfer function (voltage transfer from LV side to HV side) for faults at different locations in the winding. The 2D graph of Figure 4-26 presents normalized value of the frequency response in a logarithmic scale. Values are normalized with respect to transformer's original turns ratio (*HV/LV*=83.375 @50Hz) to yield a comparison between response values and transformer rated voltage ratio. It can be seen that compared to a healthy transformer response; represented using a solid curve, when the location of fault is in the inner layers, first resonance occurred at lower frequencies. The most evident characteristic of the graph is that for fault #1, transfer voltage tends to be enormously high (58 dB more than its normal value) at 11.8 kHz. For faults in subsequent layers (#2, #3, and #4), magnitudes of transfer voltage at their first resonance frequencies are respectively 29 dB, 15 dB, and 6 dB more than their normal value, revealing a decreasing trend. Although *HV/LV* voltage transfers for the outer layers do not indicate a specific trend, some standalone critical frequencies, such as 180 kHz with a resonance magnitude of 51 p.u. for fault #7, was noted. Such standalone peaks can be further employed as a means of matching fault more precisely.

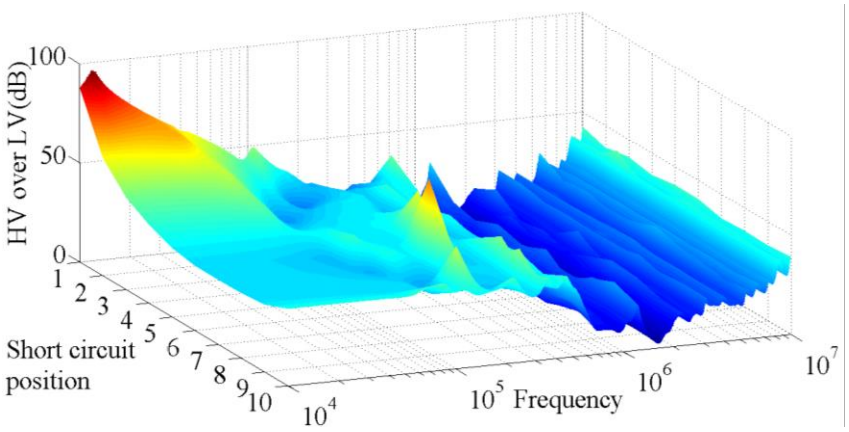

a)

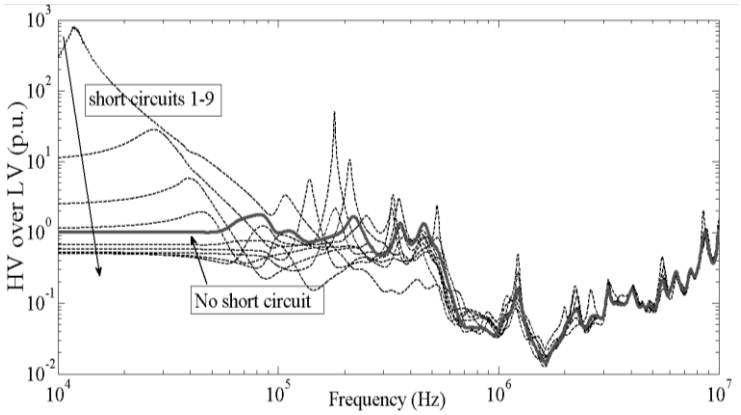

b)

Figure 4-26: *HV/LV* transfer function, (a): 3D plot, (b): 2D plot (the long arrow indicates the trend of the curves for short circuits #1 to #9. The solid curve corresponds to healthy winding).

Figure 4-27 shows that the difference factor, with respect to transfer voltage, decreases for faults in the outer layers. This means that frequency responses of transformers whose faults are located in the outer layers are closer to the frequency response of a healthy transformer. Observing the trends shown in Figure 4-26 and the difference factor in Figure 4-27, it can be determined that HV/LV magnitude is quite sensitive to faults that occur in the inner layers, although, it is less sensitive to those faults that occur in the outer layers.

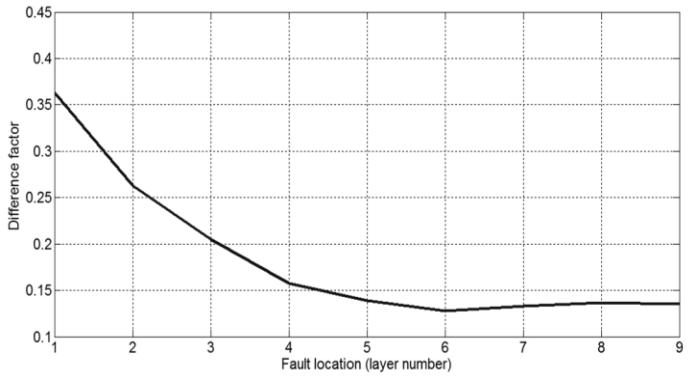

Figure 4-27: Difference factor of HV/LV transfer voltage versus fault location.

4.5.2 LV/HV Transfer voltage

Figure 4-28 shows the LV voltage over HV voltage transfer function (voltage transfer from HV side to LV side). It can be observed that at 10 kHz, the transfer voltage magnitude drastically decreases by moving the fault from inner layers to middle ones, this trend continues by moving the fault to outer layers but with a lower slope. The range of these changes is from 70.8 dB for the innermost fault to 9.5 dB for the outermost fault. On the other hand, minimum values of transfer voltages (the first anti-resonance values) and their frequencies increase by moving the short circuit location from outer layers to inner ones. Finally, in both Figure 4-26 and Figure 4-28, frequency response curves show interpretable differences up to 1 MHz while beyond that frequency; responses are almost the same for all fault locations.

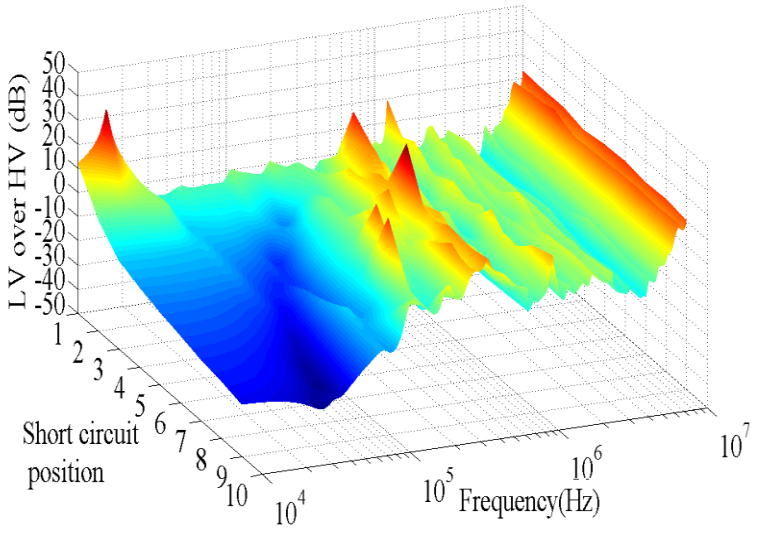

a)

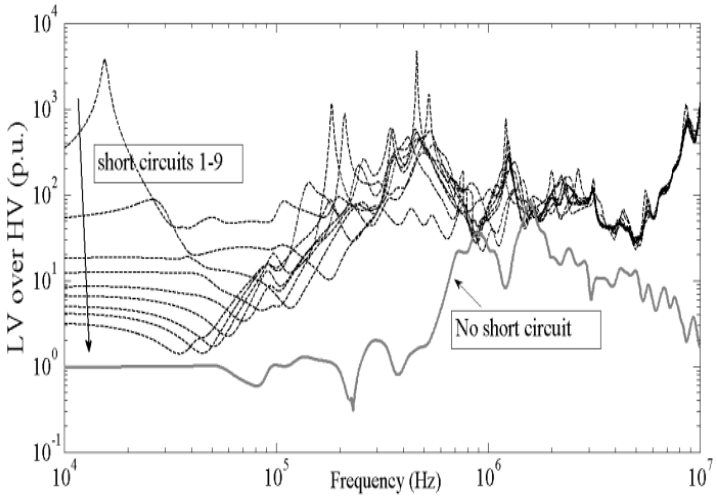

b)

Figure 4-28: *LV/ HV* transfer function, (a): 3D plot, (b): 2D plot (the long arrow indicates the trend of the curves for short circuits #1 to #9. The solid curve corresponds to healthy winding).

Similar to what is shown in Figure 4-27, Figure 4-29 shows that the difference factor decreases by moving the short circuit location to outer layers. This implies that detecting inter-turn short circuits in inner layers can easily be identified by comparing FRA responses. Furthermore, the overall higher value of difference factor in Figure 4-29 compared to that in Figure 4-27 reveals that inter-turn short circuits can be detected more promisingly using LV/HV transfer function compared to an HV/LV one.

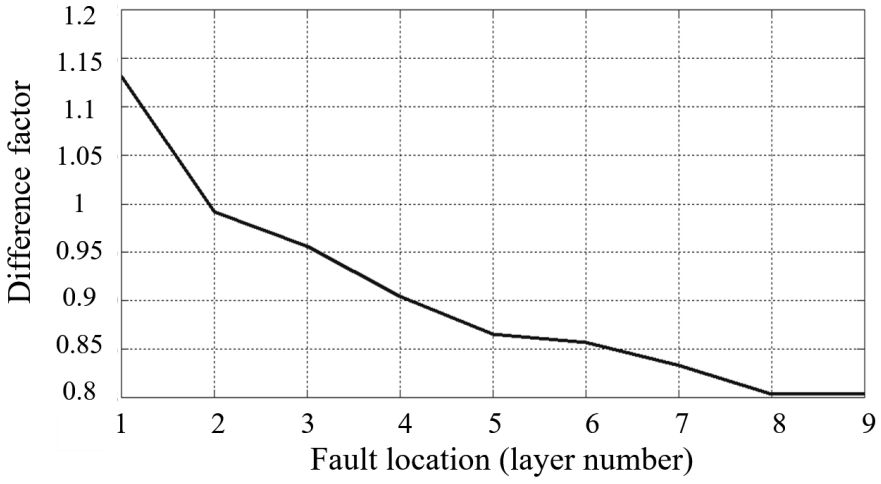

Figure 4-29: Difference factor of LV/HV transfer voltage versus fault location.

4.5.3 Input impedance from HV side

Figure 4-30 shows the frequency spectra of input impedance from HV side for internal faults at different locations in the winding. Unlike what was observed in the transfer voltage graphs (Figure 4-26 to Figure 4-29), a symmetrical pattern exists between input impedance responses of short circuits associated with faults in inner and outer layers. The trends observed with input impedance also match with the variation in the difference factor calculated (Figure 4-31). As a result, a quantitative index can be generated for quick evaluation on fault location evaluation from FRA data.

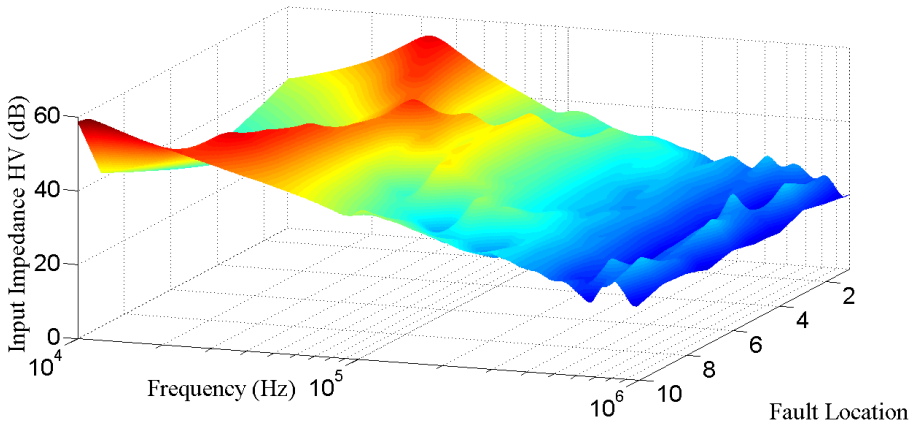

a)

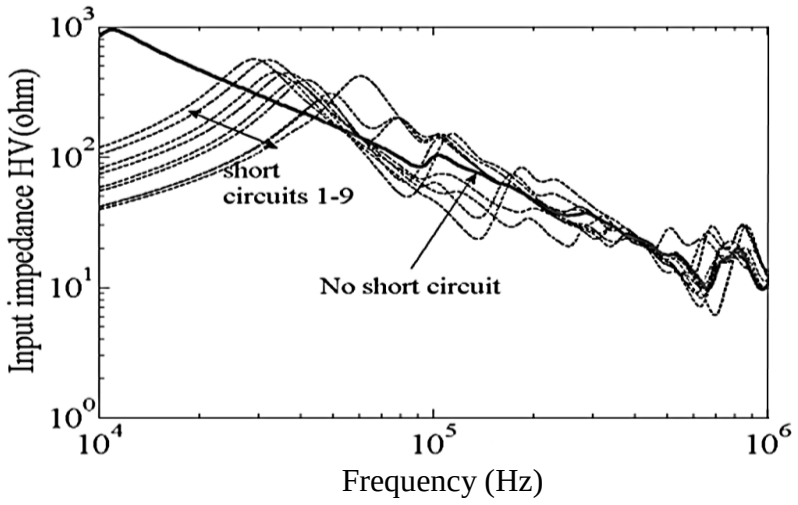

b)

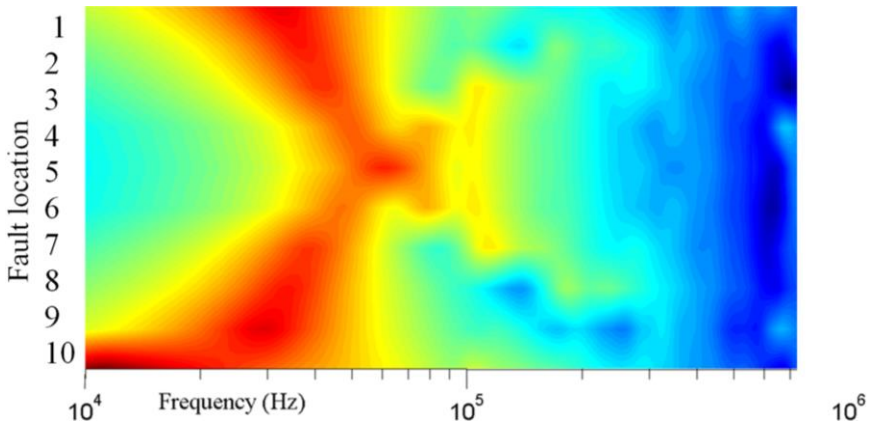

c)

Figure 4-30: Magnitude of input impedance from HV side (LV terminal short circuit). (a): 3D view, (b): 2D plot, (c): colored map representation.

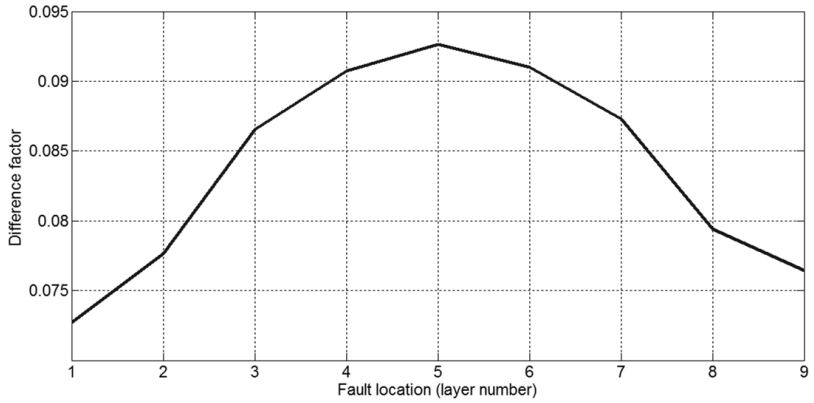

Figure 4-31: Difference factor of input impedance from HV side versus fault location (LV terminal open circuit).

4.5.4 Verification of SFRA approach

To evaluate the applicability of the proposed method on different transformers, the FRA analyses conducted on T5 are repeated on T1 and T3. Results obtained from transfer function and impedance measurements show that similar trends exist in the FRA of T1 and T3 when the fault location moves from inner layers to the outer ones. Input impedance from the HV side of T1 and T3 are presented here as an example. Figure 4-32 shows that similar symmetric patterns as in Figure 4-30 for T5 can also be seen for T1 and T3. Existence of systematic trends in frequency response of three model transformers despite huge differences in their designs (core designs, insulation systems, power ratings and voltage levels), verifies the applicability of the proposed method as a diagnostic approach for estimating internal fault locations.

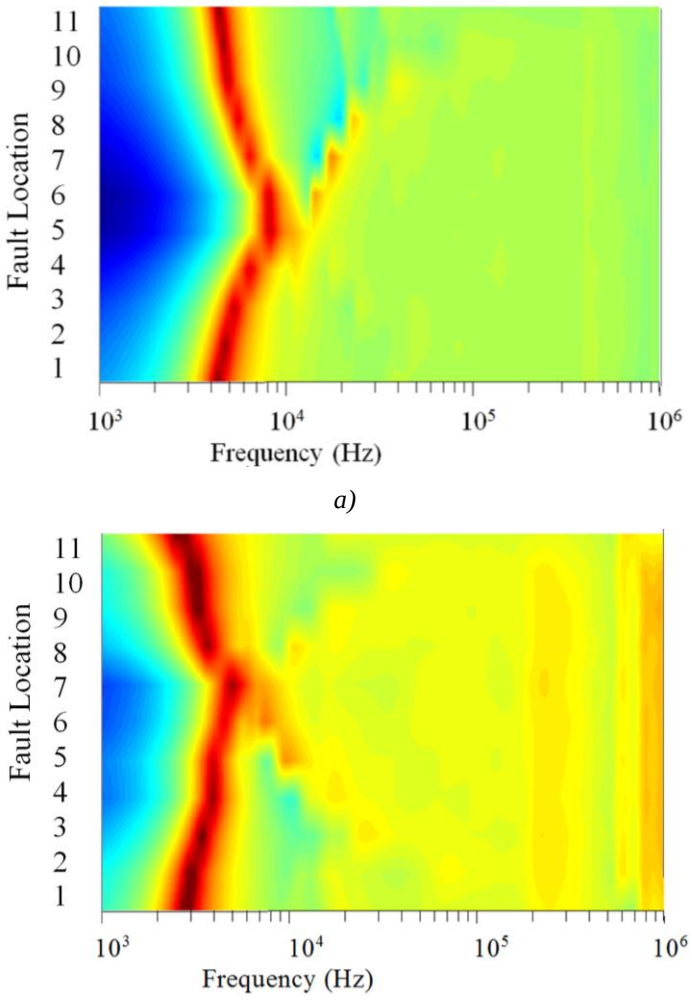

Figure 4-32: Magnitude of input impedance from HV side (LV terminal short circuit), (a): colored map representation for 1 kVA transformer, (b): colored map representation for 9 kVA transformer.

Chapter 5
Discussion

This chapter discusses the findings presented in this thesis. The ageing results for identical transformers and the interpretation of the changes in each parameter are explained in the first section. The second section provides an examination of the phenomena observed with respect to PD under high-dV/dt voltages. Subsequent sections cover transformer scaling, shielding performance, and fault location in light of frequency response analysis, and the final section includes a discussion of the compatibility of a transformer with its installation destination, based on the results reviewed in the previous sections.

5.1 Transformer ageing

This work has demonstrated that high-dV/dt distortion has a strong influence on transformer insulation properties under accelerated ageing. For accelerated ageing, the voltages applied on both transformers were 20 % higher than the rated voltage, with distortions higher than that defined by the standard for transformers in renewable energy plants: e.g., 14 % THD in the applied voltage used in this research as opposed to the 5 % THD limit specified in the IEC standard [54]. However, it is important to note that the 14 % THD defined in this work is considering a significantly broader frequency range than the THD defined by the standard, which only covers up to the 50^{th} harmonic.

Temperatures of transformers T1 and T2 were monitored throughout the duration of the ageing. The low temperature values measured imply that the insulation degradation is not related to thermal ageing. It is also shown that, although the voltage waveforms applied from source-1 and source-2 are hugely different, the transformer temperatures recorded are in the same range (Figure 4-2), indicating that the observed effects under studied conditions were related to localized degradations.

Of the parameters measured, PD showed the greatest sensitivity to ageing under distorted voltages, escalating drastically to one order of magnitude higher than that in T1 by the end of the ageing period (Figure 4-1). This finding is in agreement with the results reported in [71], for experiments on motor insulation samples, and with those published in [32], for experiments on oil-impregnated paper samples.

With respect to dissolved gas analyses, the results indicated higher hydrogen, acetylene and carbon oxide contents in T2. Higher acetylene values are associated mainly with arcing, and large quantities of hydrogen are associated mainly with PD (Figure 5-1) [72]. Therefore, the relatively high content of

acetylene and hydrogen in the oil sample from the inverter-fed transformer could be a result of PD, followed eventually by internal low-energy arcing. An additional factor is that, when accompanied by an increase in carbon monoxide and carbon dioxide, an increase in hydrogen content is known to be a result of PD in cellulose transformer insulation [73]. Based on the presence of the above gases in the inverter-fed transformer (Table 4-1), it can be inferred that PD has taken place in the inter-layer paper insulation of T2 rather than in oil. This conclusion is contrary to the idea presented by the author of [8], who claimed that gas generation with wind-farm converter-fed transformers occurs in the oil at the edges of the transformer core, due to a charge accumulation effect.

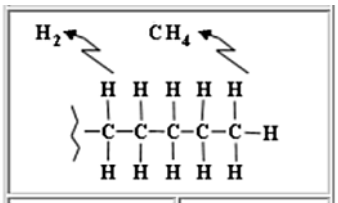

H_2	88%
$C0_2$	1
C0	1
CH_4	6
C_2H_6	1
C_2H_4	0.1
C_2H_2	0.2

PD in oil

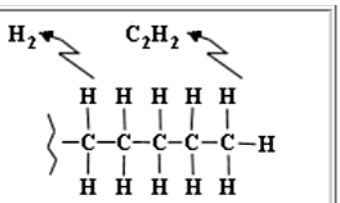

H_2	39%
$C0_2$	2
C0	4
CH_4	10
C_2H_4	6
C_2H_2	35

Arcing in oil

Figure 5-1: Generation of gases as result of PD and arcing [73].

Based on the higher dissipation factors observed for transformer T2 compared to T1 in both medium-range and low-range frequencies, it can be inferred that overall degradation occurred more quickly under high-frequency high-dV/dt distorted voltages than under power-frequency voltages. Although PD caused the paper insulation to deteriorate, the dielectric frequency responses did not demonstrate differences as large as those evident in the PD results. This observation can be explained considering the fact that the areas with tracks of carbon residuals were quite narrow compared to total winding insulation area, and since the windings are short-circuited in the DFR test, the degradation in inter-turn and inter-layer insulation would not have a strong impact on the DFR. This consideration could constitute further evidence of localized electric fields at specific transformer winding positions.

The results presented in [74] also showed that PD by-products alone will not lead to a significant change in the UST DFR of a transformer because the simulation results revealed that PD by-products, i.e., positive and negative charges, tend to diffuse into the bulk of oil-paper insulation. Therefore,

changes in the dielectric response curve due to PD by-products occurred mainly in the middle- and low-frequency regions and can be better observed through GST mode tests. This phenomenon can be also observed when the low-frequency regions of Figure 4-6 (UST mode) are compared with those in Figure 4-9 (GST mode), where the difference between the %DF values in Figure 4-9 is four times greater than that in Figure 4-6.

With reference to Figure 4-10, under a 2 kV excitation, the dissipation factor values are greater than those under a 200 V excitation, and the difference between T1 and T2 is clear. Due to the small size of the model transformers of this research, their geometrical capacitance and conductance are low. Applying a higher voltage, and hence inserting a higher current, is thus required for more stable dielectric spectroscopy. When a high voltage is applied for UST test, the dissipation factor is almost the same for high- and mid-range frequencies but is greater toward lower frequencies and DC. This effect is attributable to the fact that, in dielectric materials, conductance increases when the applied field is increased, but this phenomenon is more pronounced when the frequency is low, hence giving more time for free charge migration.

5.2 Effect of impulse train parameters on partial discharge

As shown in Table 4-4, temperatures recorded in the vicinity of paper samples are nearly the same for all tests, revealing that PD energy is low but highly localized. Similar observations have been noticed with chamber 2, with oil bath average temperatures ranging from 24.1º to 25.2º C. Based on this observation, the effect of thermal decomposition of oil can be neglected; hence, like the ageing case of T1 and T2, the detected hydrogen can be related solely to PD.

The linear increase of hydrogen content in the small controlled chambers, as the key point of this experimental study, owes to the fact that the constant increase in accumulated PD energy is directly reflected in the amount of hydrogen dissolved in oil. Based on this linear relation between hydrogen content and frequency, it can be inferred that a linear relationship also exists between PD energy of individual impulses and the corresponding amount of dissolved hydrogen. The phenomenon observed is in agreement with that described in [75] by Popa, who studied the correlation between the PD and the DGA of a power transformer. While Popa examined PD under power-frequency AC, in this research, experiments were carried out under pulse voltages in a small controlled chamber with transformer paper samples immersed in oil to find the correlation between PD energy and hydrogen content. All the results in section 4.3 use the linearity between PD energy and hydrogen content as a means for comparing PD energies under impulses with different RORs and peak values. However, it

has to be noted that linearity does not exist for hydrogen levels closer to the saturation point as saturation operates as a strong negative feedback against the increase of dissolved gas content.

A comparison of the PDGIV trends for different rise-times shown in Figure 4-17 and Figure 4-18, reveals that slower rise-times result in a lower PDGIV, especially for rise-times slower than 1 μs, for which the effect of rise-time is stronger. This phenomenon can be attributed to the greater time available for electric charges to accumulate, increasing the probability of surface discharge occurrence. These findings are in agreement with conclusions reached by Wang *et al.* [76], based on their experiments with crossed wire samples for a machine insulation study.

As shown in Figure 4-17, PD gas inception voltage is not sensitive to the impulse frequency for lower frequencies (below 200 Hz), but it shows a decreasing trend for increasing frequency when the dead time between impulses becomes comparable to impulse duration. When the impulse frequency is relatively low, the dead time is much greater than the impulse-on time; as such, accumulated charges from previous PD can disappear. When the frequency is increased, dead time becomes comparable to impulse-on time; hence, charges from the previous impulse affect the PD of the next impulse strongly. In Figure 4-18, trends mentioned can be seen in the primary flat part of the rod-plane electrodes (when dead time is much longer than impulse time), and in the secondary falling part (when dead time becomes comparable to impulse time). For plane-plane electrodes, the PDGIV curves shown in Figure 4-17 are less sensitive to frequency changes than those for rod-plane electrodes. The effect of electrode geometry can be related to the sharpness of the electrodes and also their contact with the surface of the paper. For plane-plane electrodes, a lower charge generates during the impulse time, and because of its wide physical contact with the paper, most of the charge neutralizes during dead time. In this case, neutralization can occur even during shorter dead times. On the other hand, for rod-plane electrodes, due to the sharp edge of the rod, an electric charge with a higher density is generated around the electrode on the surface of the paper. The charge that accumulates in the surrounding area, however, is less efficiently collected by the rod electrode than by the plane electrode. The effect of shorter dead times (higher frequency) is thus more noticeable for rod-plane electrodes.

Figure 4-19 and Figure 4-20 show that the application of pulses with faster rate of rise resulted in partial discharge with higher energy. Since, in this study, the effective impulse time (around 70 μs) is much longer than the slowest rise time (6 μs), changes in PD energy can be solely attributed to changes in ROR rather than changes in impulse time. PD energy test results show that although a faster ROR increases PD inception voltage, when PD begins to occur, it has more energy under faster RORs than

under slower ones. Findings with respect to the effect of the ROR on the PD energy is in agreement with conclusions drawn by Moonesan *et al.* [44] about the effect of ROR on inter-turn insulation under pulse conditions. It was observed that rise-time has a noticeable effect on the ageing of the dielectric only when the duty cycle of the square waveform is reduced. Since the impulse trains applicable to this research can be assumed to be pulse trains with almost negligible duty cycles, it is expected that this study would demonstrate the effect of rise-time at its strongest.

5.3 Effect of scaling on the high-frequency behaviour of transformers

The results of the modelling verification tests showed good agreement between the calculated and measured resonance frequencies both at the terminals and inside the transformers. The difference observed in the magnitudes of the impedance responses (Figure 4-12), which was evident even in the lower frequency range, is due to the fact that transformers comprise series resistances that can be formulated generally as follows:

$$R = \frac{\rho l}{A} \qquad [R] = \left[\frac{\oint \rho . dl}{\iint ds}\right] \tag{5.1}$$

The above basic relation for resistance matrix means that, when a transformer is scaled, the one-dimensional length parameter scales by *Scl* while the two-dimensional area parameter scales by Scl^2. This result leads to the following relation between T1 and T3 resistance matrices as follows:

$$\frac{Resistance_{Scaled\ (T3)}}{Resistance_{Original\ (T1)}} = \frac{1}{Scl} \tag{5.2}$$

This effect can be best seen at the resonance points because those are the points at which the resistance matrix, i.e., the real part of impedance, strongly affects the magnitude of the frequency response. With reference to Figure 4-12, the change in the magnitude of the main resonance can be calculated based on the scaling factor.

The results observed with respect to the voltage transfer to the layers of HV winding (Figure 4-13) indicate that the scaling method can also work for estimating the internal stresses as functions of frequency. The measurement of internal stresses is less accessible with actual-size transformers; hence, obtaining the measurements for a small transformer using such scaling methods would be beneficial at the design stage and would facilitate the achievement of a more robust transformer design.

5.4 Effect of electrostatic shielding

Based on the experimental studies on two model transformers; with and without electrostatic shielding, it was shown that a single electrostatic shield may not necessarily attenuate all the high-frequency components of the voltage with the same effectiveness. This is due to the fact that, from the resonance point of view, inserting an electrostatic shield may reform the high-frequency equivalent circuit of transformer windings resulting in suppressing certain frequency components but intensifying some other frequency components inside transformer winding. This phenomenon is illustrated in Figure 5-2 where internal resonance in location 1 at a frequency of f_1 by inserting an electrostatic shield moves to location 2 at a frequency of f_2. Such changes can be seen in high-frequency regions of Figure 4-21 and Figure 4-22.

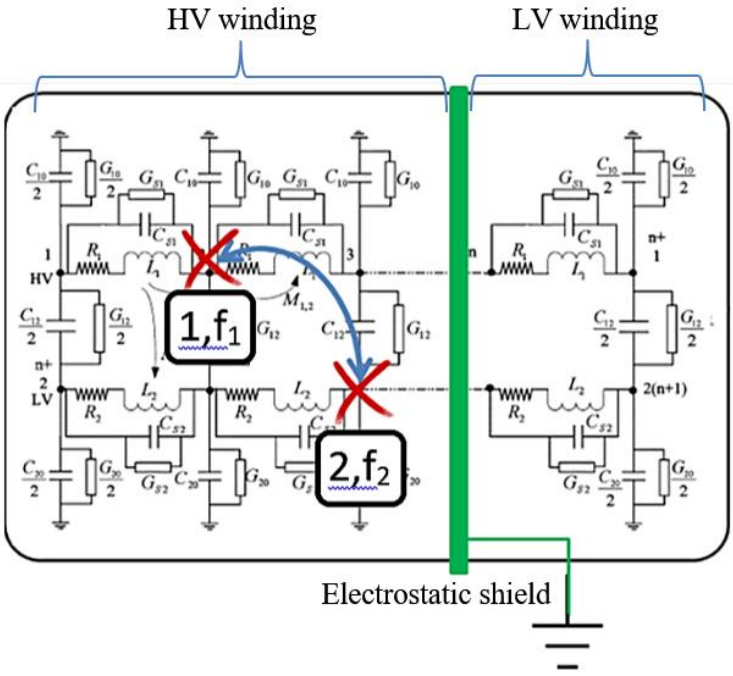

Figure 5-2: Change of internal resonance location (presented by red crosses) and frequency due to installation of electrostatic shield; illustrated with the aid of equivalent circuit.

5.5 Fault location study

Today, the FRA method is widely used to detect a variety of faults in transformers using commercially available instruments that have been developed for field tests. The high sensitivity of this method, allows one to detect even gentle displacements of windings on transformer core [77]. Compared to defects such as winding displacement and deformation, internal short circuits cause

significant changes in the frequency response of power transformers. For instance, the difference between frequency responses of a healthy winding with 20% deformed winding is limited to only 5% frequency difference in resonance frequency [78]. In contrast, the difference between the HV impedance frequency response of the winding with a fault in the first layer and the winding with a fault in the second layer is near 90% in magnitude and 10% difference in resonance frequency. Thus, changes in frequency response that occur due to internal short circuits dominate changes that occur due to other defects such as displacement and deformation.

FRA test results reveal that when a short circuit is located in the innermost layer of the winding, very high voltage amplifications can be expected for certain frequencies. For the case of model transformer T5, the highest voltage amplification happened with a fault between layers #1 and #2, where the *HV/LV* transfer voltage tends to be enormously high at 11.8 kHz. Such high magnitudes with resonant cases have also been observed in [79]; where high magnitudes were recorded for transfer functions at certain frequencies. This high amplitude can be related to the formation of an equipotential cylinder composed of shorted turns of HV winding close to the LV winding. The high capacitance between this virtual cylinder and the LV winding results in high resonance for transferred voltage. From the insulation point of view, such phenomena can result in very high stresses inside the transformer even when a very low content of the associated frequency exists in the feeding voltage. With respect to practicality, when such high gains in transfer voltages are observed (Figure 4-26 and Figure 4-28), there may be an argument that saturation of the core may affect measurements. That said, since frequencies are much higher than power-frequency and excitation voltage is too low, flux density is very low and is not significant to cause any core saturation.

Further investigation of Figure 4-32 (input impedance from HV side, when LV terminal is shorted) reveals that connections of non-tested windings are influential on the trend of frequency response changes as a function of fault location. When impedance measurements are performed with LV side short-circuited, the effect of magnetization inductance through the core and LV winding space can be neglected. This means the flux path generated by HV winding is mainly restricted to the space out of LV winding and within the HV winding itself. As a result, and due to the symmetry of the HV winding, the winding with a fault just next to one end of the winding (i.e. outermost layer fault) shows the same impedance frequency response as the winding with a fault just next to the other end of the winding (i.e. innermost layer fault). The same trend exists for other faults equally distant from the terminals.

Comparing trends in transfer ratios and input impedances, it was observed that these two parameters do not follow the same pattern with respect to fault location. This observation is in agreement with what can be concluded from the literature stating that transfer voltages have no direct relationship with input impedance measurement [55]. Therefore, it would be beneficial to perform both tests for transformer diagnosis as the observations complement each other.

5.6 Compatibility of transformers with wind-farms

One option for preventing premature failure and gassing associated with transformers at wind-farm is to examine the compatibility of the transformer with its destination installation network. One of the compatibility issues is the overlapping of the resonance frequency of the WTSU transformer and its excitation frequency contents. Such precautions can minimize the stresses on the transformer insulation.

With the results presented in the previous sections regarding the transfer functions of actual-size transformers and the characteristics of transient oscillatory voltages at transformer terminals as background, the following sub-sections discuss the compatibility of a sample transformer with the wind-farm where it is installed.

5.6.1 Compatibility with the voltage source

The performance of a transformer in light of the distortions in its voltage source is discussed in this section. Utilizing the frequency response of the transformer and the frequency spectrum of its voltage source makes it possible to estimate the frequency spectrum of the transformer output voltage and its critical frequency contents on the secondary side. To verify the practicality of this approach, an experimental sample was tested as described below.

As the first step, the output voltage of the sample inverter was measured and its frequency spectrum was extracted using fast Fourier transform (FFT). The next step employed the transformer transfer function to check its compatibility with the frequency spectrum of the inverter voltage. For comparison purpose, the transfer function spectrum and the voltage FFT are shown on the same axis and in the same frequency range (Figure 5-3). There are significant contents in inverter voltage around 180 Hz, 4 kHz and 10 kHz. The 180 Hz component coincides with a region of the transfer function that is equal to the nominal transfer ratio of the transformer. The 4 kHz component overlaps with the resonance frequency of the transfer function, which has an amplification factor 23 dB higher than the power-frequency transfer ratio. This overlapping translates into the anticipation that the 4 kHz component amplifies 14.1 times more than the power-frequency components, thus extending its 2 % content in the

primary side voltage spectrum to a 28.2 % content in the secondary side of the transformer. Conversely, the 10 kHz component overlaps with an area of the transfer function that shows a 24 dB attenuation, suppressing the 10 kHz content of 1.5 % in the primary side to 0.1 % in the secondary side. Based on consideration of the above three cases, only the 4 kHz component voltage source output is marked as critical content.

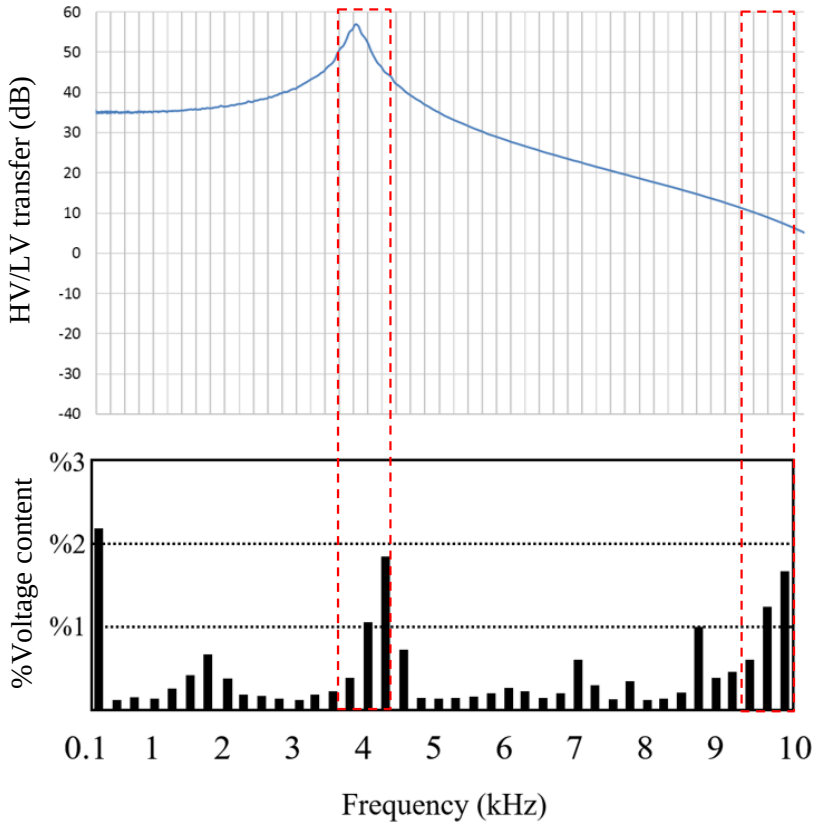

Figure 5-3: Overlap of transformer resonance frequency and major frequency contents of voltage source, (top): transfer function of model transformer, (bottom): power converter voltage spectrum.

The FFT of the transformer output voltage verifies the conclusion drawn from the above discussion. As shown in Figure 5-4, while the frequency content around 10 kHz is attenuated, the 4 kHz content is amplified in the delivery to the secondary side of the transformer. In this case, the transformer and its voltage source converter are shown to be incompatible. However, if the transformer were designed in such a way that its resonance frequencies were slightly different so that they would not fall within the proximity of 4 kHz, the resonance of the high-frequency content would be avoided. Knowing the critical frequencies also helps with the design of an adequate filter that can effectively filter such unwanted contents.

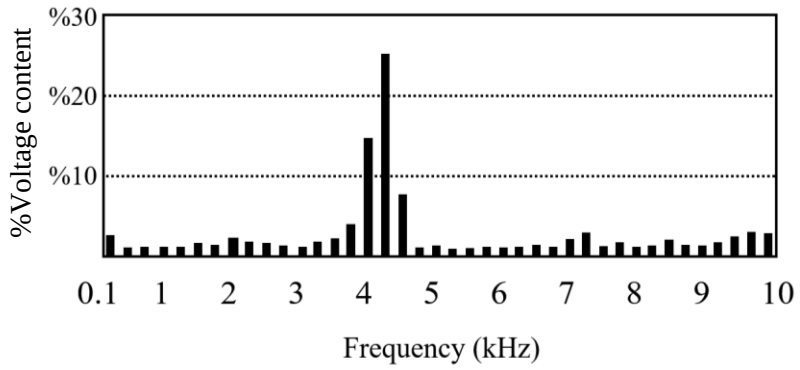

Figure 5-4: The frequency spectrum of the voltage measured at the secondary side of the transformer.

5.6.2 Compatibility with the operation of wind-farm circuit breaker

Based on reports from wind-farm developers, identical transformers installed in the same wind-farm show different gassing behaviours and failure rates. The only parameter that differs with respect to such transformers is their location in the wind-farm chain and the length of the cables connecting them to circuit breakers. Considering the dependency of the repetition frequency and dV/dt of oscillating waveforms on the connection of a breaker to a transformer, switching transient studies, explained in section 3.3.2, can help wind-farm developers choose appropriate lengths for the connecting cables. Cable lengths should be selected so that the WTSU transformers will be compatible with the switching transients of the wind-farm.

The transfer function of an actual WTSU transformer (Figure 5-5) is considered here as an example of the identification of its compatibility with the simulated wind-farm described in [62]. Based on the results presented in section 3.3.2 and the transfer functions in Figure 5-5, none of the oscillation frequencies of the possible cases overlaps the critical resonance frequencies of the transformer, which are mostly in the range of 8-12 kHz. In such cases, it can be expected that the planned arrangement is safe for the transformer with respect to terminal voltage. However, the internal resonances cannot be ensured with only a terminal study.

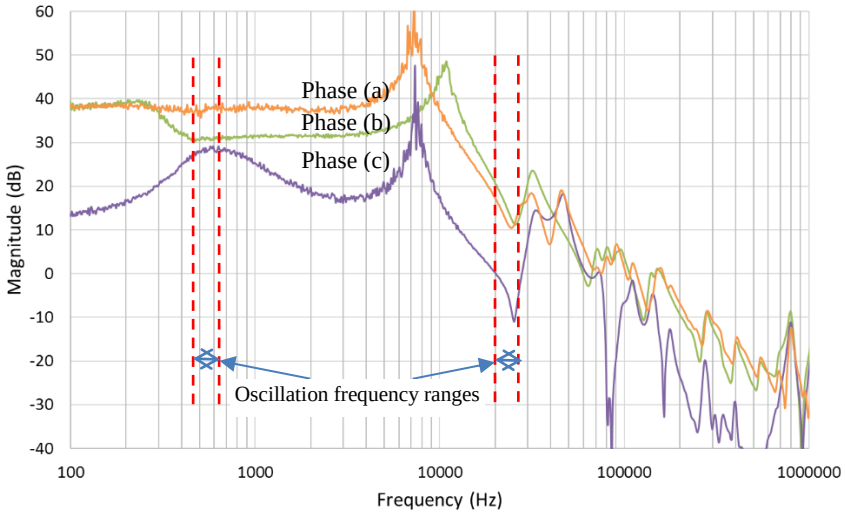

Figure 5-5: Transfer function of a 2.6 MVA 34.5/690 (DY) wind turbine transformer, measured between phase (a) of LV and three phases on HV (frequency ranges between dashed lines shows the oscillation frequency ranges obtained by simulation of circuit breaker operation).

Based on this background, provisional studies for the selection of wind-farm components and layout, with consideration of the interactions between the WTSU transformer and its surrounding equipment, is an important factor in the enhanced reliability and long-term performance of such valuable sources of renewable energy.

Chapter 6
Summary and Conclusion

6.1 Summary

Recently documented gassing problems and premature insulation failures with wind turbine transformers indicate concerns about the reliability of the insulation in such converter-fed devices. Due to the relatively young age of the majority of fully inverter-fed wind turbine generators, little has yet been published about the associated issues. This research involved the investigation of the effects of distorted voltages on wind turbine step-up transformers as well as the acquisition of an insight into the impact of internal resonance and high-frequency dielectric effects. Model transformers were aged under a converter PWM and a power grid sinusoidal voltage in order to evaluate the effect of distorted voltage on the transformer. In this regard, parameters were monitored as indications of the condition of the transformer insulation and were compared throughout the ageing period. The study of transformer behaviour under high-frequency high-dV/dt voltages required a detailed high-frequency model. The work presented in this theis resulted in the proposal of a modelling approach that includes consideration of the high-frequency behaviour of a scale down model transformer, and then relates it to the behaviour of an actual-size transformer. To verify the proposed modelling method, an experimental study was conducted as a means of investigating the correlations between the frequency responses of two model transformers with different power ratings and sizes. To analyze the switching transients imposed on wind turbine transformers due to the operation of adjacent vacuum circuit breakers, a linear wideband black-box model of an actual wind turbine transformer was prepared in order to represent a wind turbine step-up transformer for a system study in PSCAD. Based on the simulation results for impulsive voltage oscillations at transformer terminals, an experimental study was performed in order to examine the effects of impulse voltage characteristics, such as rate of rise and repetition frequency, on PD in oil-impregnated paper samples. To avoid interference from fast oscillations and other electromagnetic-related issues, in this work, a chemical approach was used for comparing PD, based on the rate of hydrogen generation in a controlled test chamber containing oil/paper samples. Finally, the installation of an electrostatic shield for improving the high-frequency performance of a transformer was analyzed, and alternative approaches were suggested for target-oriented insulation reinforcement based on a fault location study and consideration of transformer compatibility with its installation network.

6.2 Conclusion

The ageing experiment on two identical oil-filled transformers energized with different voltages for 960 hours led to the following conclusions:

- Variations in the monitored parameters revealed a severe degradation in the insulation system of the inverter-fed transformer, compared to those fed from power frequency, confirming that the exposure of transformer to high-frequency distorted voltage has a strong influence on transformer insulation properties.
- Of the measured parameters, PD showed the highest changes during the ageing under distorted voltages, compared to that in the transformer energized by non-distorted AC voltage.
- The relatively high contents of hydrogen, acetylene and oxides of carbon in the inverter-fed transformer could be caused by extensive partial discharge in winding insulation followed by internal low-power arcing.
- Dielectric response spectroscopy can be utilized as a means of insulation degradation assessment to investigate transformer paper/oil performance under various voltage waveforms. Discrepancies in %DF were observed in both medium range and low range frequencies which can be interpreted as difference in levels of winding insulation degradation and partial discharge byproducts.

The investigation of the relationship between the frequency responses of two transformers that were scaled versions of each other led to the following conclusions about the use of scaling method for modelling purposes:

- The overall trends with measured frequency responses of the original and scaled transformers, for both transfer function and input impedance, matched very closely.
- The calculated frequency responses of the scaled transformer are in close agreement with those measured. The results validated the linear scaling procedure used for studying the frequency response of the two model transformers.
- The adopted scaling approach showed that the studies on model transformers are extendable to larger transformers for high-frequency behaviour study, e.g. for wind farm transformers.

As the main ageing cause for transformer insulation degradation, partial discharge under impulse voltages were analyzed in details. The following conclusions are drawn from the experimental studies on PD in oil/paper insulation under impulse trains with different rates of rise and repetition frequency:

- Presence of hydrogen in oil can be adopted as an alternative method for indication of PD initiation in the test samples, especially under pulse waveforms, where noises from voltage source are high.
- In a small controlled oil chamber, a linear correlation exists between the generation of dissolved hydrogen and the PD energy of applied pulse train. Hydrogen-content/PD-energy relationship, can be used for comparing PD energy under pulses with different characteristics where conventional electromagnetic PD detection methods are difficult to use.
- PD gas inception voltage is not sensitive to the impulse frequency for lower frequencies, but it shows a decreasing trend for increasing frequency when dead time between impulses becomes comparable to impulse duration.
- PD gas inception voltage is higher for impulse trains with shorter rise-times (faster rate of rise).
- Application of impulses with faster rate of rise resulted in partial discharge with higher energy.

Based on the experimental studies on two model transformers; with and without electrostatic shielding, the following conclusions are drawn:

- A single electrostatic shield may not necessarily attenuate all the high frequency components of the voltage with the same effectiveness. Although the presence of an electrostatic shield between the LV and HV windings showed a good performance for deduction of high-frequency transfer from LV to HV and HV to LV, it did not positively influence the resonance frequency of internal voltage gradients. However, the shielding increased the peak value of voltage gradient by 49 % for the model transformer used in this research.
- Majority of frequency contents in the voltage waveform at transformer terminals due to converter and breaker operations must be taken into account for the effective design of electrostatic shielding.

As an approach to detection of short circuit location in transformer winding, transformers with artificial faults at different locations were experimented. Comparisons between frequency responses for faults at different locations led to the following conclusions:

- Changes in the location of internal faults result in identifiable trends in the frequency response as functions of the fault distance from the core, which can be classified into two categories: close-to-core faults and close-to-terminal faults.
- Although trends observed in the responses of input impedance and transfer voltages are independent, the results can be used complementarily in the detection of fault location. Quantitative analysis of statistical parameters, such as the difference factor, could also be used in addition to visually observed trends in FRA patterns.

6.3 Potential contribution

Conducted with the goal of designing transformers with improved ability to withstand the high stresses created by switching devices, the present research presented in this thesis has laid the ground work for establishing comprehension of the effects of high-frequency high-dV/dt stresses on transformers connected to wind-farms. The results of this project can lead to an understanding of the extent of the influence of high-dv/dt voltages on the gassing and failure of WTSU transformers. An additional important finding is that detecting the locations of field enhancements in transformer winding can help enhance the design of insulation systems by enabling the insulation to be reinforced at precise critical spots where the reinforcement is needed. Finally, this research can also contribute to the development of a standard for the qualification of transformers for installation in wind-farms.

Because it enables experimenting a scale down model transformer and relating it to an actual-size transformer, the proposed scaling method can help transformer manufacturers obtain an estimate of the high-frequency performance of to-be-built transformers as well as detemine critical frequencies and positions inside the windings of full-size transformers.

The proposed method for partial discharge analysis, and the linear relationship shown between PD energy and hydrogen content can be used for comparing the energy and destructive effect of PD in a variety of circumstances, especially in situations in which electromagnetic detection methods are not viable.

This research has highlighted the fact that transformer design modifications such as the insertion of an electrostatic shield should be studied with consideration of both its effect at the terminals and its

internal impacts. The proposed method for measuring the frequency response of inter-layer stress can help transformer designers take into account the impact of any design modification on winding insulation.

The proposed method for locating internal faults benefits transformer manufacturers by reducing the cost and time required for repairs, and also by providing statistical information about the areas of the windings where internal faults most often occur. The latter would prove useful for ensuring more effective insulation reinforcement in future designs.

6.4 Future work

The long-term full monitoring of a number of wind turbine step-up transformers from the beginning of their operation in wind-farm is suggested as future work. The high-resolution monitoring of the voltage and current at transformer terminals, together with the online monitoring of transformer condition parameters such as DGA and PD, can reveal useful information about the performance of transformer insulation based on the energization voltage and operation conditions. The use of such simultaneous measurements enables voltage and current events to be correlated with changes in the health condition of a transformer.

The use of hydrogen monitoring approach permits an examination of the effects of resonance on transformer PD and associated insulation ageing. It is suggested that distortions with different frequencies, including the resonance frequencies of a model transformer, be superimposed on power-frequency AC voltage and applied on a model transformer. Comparing hydrogen contents under voltages with differrent frequency contents can help provide an understanding of the effect of resonance on PD in a transformer.

A further suggestion is that ageing studies be performed for two similar transformers, with and without an electrostatic shield. The effectiveness of electrostatic shield can be better analyzed if the model transformers are energized using conventional power converters and the degradation speeds of transformers with and without shielding are then observed.

As experimental proof of a new approach, the fault location study demonstrated that the location of an internal fault has a systematic effect on the frequency responses of a transformer. To develop this method for practical application, a transformer model that has the capability of internal fault simulation should be compiled. With such a high-frequency model of a transformer, one can input the frequency response of a failed transformer into a program which can compare the actual frequency response of

the failed transformer with the simulated responses of that transformer having faults at different locations. The program can provide an estimated location of the fault based on the similarity of the response from the faulty transformer and that from the simulated faults.

A suggestion for future work is simulation of a full wind-farm considering the interaction between the units connected through the secondary sides of their step-up transformers. With such simulations, one can study the effects of geometrical dimensions on the propagation of high-frequency high-dV/dt oscillations between WTSU transformers. By focusing on the transformers at the beginning and end of wind-farm chain, where the harshest transients are expected, defining a safe design criterion for a wind-farm is possible.

Bibliography

[1] A. Beainy, C. Maatouk, N. Moubayed, and F. Kaddah, "Comparison of different types of generator for wind energy conversion system topologies," in *2016 3rd International Conference on Renewable Energies for Developing Countries (REDEC)*, 2016, pp. 1–6.

[2] L. S. L. S. Christensen, M. J. M. J. Ulletved, P. E. Sørensen, T. Sørensen, T. Olsen, and H. K. H. K. Nielsen, "GPS Synchronized high voltage measuring system," *Nord. Wind Power Conf. 2007*, no. November, pp. 1–2, 2007.

[3] H. C. Sorensen, L. K. Hansen, and J. M. Larsen, "Middlegrunden 40 MW offshore wind farm Denmark - Lessons Learned," *Renew. realities–offshore Wind Technol.*, no. October, pp. 1–7, 2002.

[4] M. Nagel and T. Leibfried, "Investigation on the high frequency , high voltage insulation properties of mineral transformer-oil Power source for test signal generation," pp. 226–228, 2006.

[5] A. Hayati Soloot, H. K. Høidalen, and B. Gustavsen, "Resonant overvoltage assessment in offshore wind farms via a parametric black-box wind turbine transformer model," *Wind Energy*, vol. 18, no. 6, pp. 1061–1074, Jun. 2015.

[6] C. Collins and R. T. R. Pe, "GASSING IN WIND FARM TRANSFORMERS," 2013.

[7] T. Committee of the IEEE Power and E. Society, "IEEE Std C57.104™-2008 (Revision of IEEE Std C57.104-1991), IEEE Guide for the Interpretation of Gases Generated in Oil-Immersed Transformers," 2009.

[8] Philip J Hopkinson, "Wind Power Transformer Design," in *Life of a Transformer*, 2013, pp. 1–37.

[9] PES Transformers, *IEEE C57.159 - IEEE Guide on Transformers for Application in Distributed Photovoltaic (DPV) Power Generation Systems*, no. May. 2016.

[10] R. Bi, K. Qian, C. Zhou, D. M. Hepburn, and J. Rong, "International Journal of Smart Grid and Clean Energy A survey of failures in wind turbine generator systems with focus on a wind farm in China."

[11] P. Tchakoua, R. Wamkeue, M. Ouhrouche, F. Slaoui-Hasnaoui, T. A. Tameghe, and G. Ekemb, "Wind turbine condition monitoring: State-of-the-art review, new trends, and future challenges," *Energies*, vol. 7, no. 4, pp. 2595–2630, 2014.

[12] "The Weather Network - Weather forecasts, maps, news and videos." [Online]. Available: https://www.theweathernetwork.com/ca. [Accessed: 03-Mar-2017].

[13] B. Gustavsen, "Study of transformer resonant overvoltages caused by cable-transformer high-frequency interaction," *IEEE Trans. Power Deliv.*, vol. 25, no. 2, pp. 770–779, 2010.

[14] T. Bengtsson *et al.*, "Repetitive fast voltage stresses-causes and effects," *IEEE Electr. Insul. Mag.*, vol. 25, no. 4, pp. 26–39, Jul. 2009.

[15] L. Paulsson *et al.*, "High-frequency impacts in a converter-based back-to-back tie; the Eagle Pass installation," *IEEE Trans. Power Deliv.*, vol. 18, no. 4, pp. 1410–1415, 2003.

[16] J. H. M. (Kmek) Larsen, H. C. (Spok) Soerensen, E. Christiansen, S. Naef, and P. Vølund, "Experiences from Middelgrunden 40MW Offshore Wind Farm," *Copenhagen Offshore Wind Conf.*, no. October, 2005.

[17] P. A. P. De Lima and S. H. L. Cabral, "A comparative analysis of performance of well-known methods for conforming distribution of impulsive voltage along regulating winding," *2013 IEEE Electr. Insul. Conf. EIC 2013*, no. June, pp. 168–172, 2013.

[18] M. Melfi, A. M. Jason Sung, S. Bell, and G. L. Skibinski, "Effect of surge voltage risetime on

the insulation of low-voltage machines fed by pwm converters," *IEEE Trans. Ind. Appl.*, vol. 34, no. 4, pp. 766–775, 1998.
[19] M. Khanali, S. Jayaram, and J. Cheng, "Effects of voltages with high-frequency contents on the transformer insulation properties," in *2013 IEEE Electrical Insulation Conference (EIC)*, 2013, pp. 235–238.
[20] M. Reza, K. Srivastava, T. Abdulahovic, A. Marinopoulos, and H. Breder, "High Frequency Transients in Large Wind Farm - Advanced Measurement and Characterization," no. April, 2012.
[21] C. H. Ng, L. Ran, and J. Bumby, "Unbalanced-grid-fault ride-through control for a wind turbine inverter," *IEEE Trans. Ind. Appl.*, vol. 44, no. 3, pp. 845–856, 2008.
[22] C. Han, D. E. Martin, and M. R. Lezama, "Transient over-voltage (TOV) and its suppression for a large wind farm utility interconnection," *1st Int. Conf. Sustain. Power Gener. Supply, SUPERGEN '09*, 2009.
[23] A. H. Soloot, H. K. Høidalen, and B. Gustavsen, "Frequency domain investigation of switching transients in Offshore Wind Farms," *2011 IEEE PES Trondheim PowerTech Power Technol. a Sustain. Soc. POWERTECH 2011*, pp. 1–5, 2011.
[24] V. Behjat, A. Vahedi, A. Setayeshmehr, H. Borsi, and E. Gockenbach, "Diagnosing shorted turns on the windings of power transformers based upon online FRA using capacitive and inductive couplings," *IEEE Trans. Power Deliv.*, vol. 26, no. 4, pp. 2123–2133, 2011.
[25] A. Soloot, H. Høidalen, and B. Gustavsen, "Influence of the winding design of wind turbine transformers for resonant overvoltage vulnerability," *IEEE Trans. Dielectr. Electr. Insul.*, vol. 22, no. 2, pp. 1250–1257, Apr. 2015.
[26] S. M. Hassan Hosseini, M. Vakilian, and G. B. Gharehpetian, "Comparison of transformer detailed models for fast and very fast transient studies," *IEEE Trans. Power Deliv.*, vol. 23, no. 2, pp. 733–741, 2008.
[27] H. Al-Amin, J. O'Brien, and M. Lashbrook, "Synthetic ester transformer fluid: A total solution to windpark transformer technology," *Renew. Energy*, vol. 49, pp. 33–38, 2013.
[28] M. Bradt *et al.*, "Power transformer application for wind plant substations," *2010 IEEE PES Transm. Distrib. Conf. Expo. Smart Solut. a Chang. World*, pp. 0–19, 2010.
[29] I. Power and E. Society, *IEEE Guide to describe the occurrence and mitigation of switching transients induced by transformers, switching device, and system interaction*, no. April. 2011.
[30] B. Gao, G. N. Wu, J. Y. He, and K. G. Lei, "Investigation on aging mechanism of winding insulation used in inverter-fed traction motors," *Annu. Rep. - Conf. Electr. Insul. Dielectr. Phenomena, CEIDP*, pp. 107–111, 2007.
[31] Yin Yi, Tu Demin, Lei Qinquan, Wang Xuan, and K. C. Kao, "The application of TSC/TSL-United-Spectra in the investigation of electrical aging in polymer," in *2001 Annual Report Conference on Electrical Insulation and Dielectric Phenomena (Cat. No.01CH37225)*, pp. 177–182.
[32] T. L. Koltunowicz, G. Bajracharya, D. Djairam, and J. J. Smit, "Investigation of the effects of fast transients on a transformer's paper insulation," in *2010 IEEE International Symposium on Electrical Insulation*, 2010, pp. 1–5.
[33] T. L. Koltunowicz, R. Kochetov, G. Bajracharya, D. Djairam, and J. J. Smit, "Repetitive transient aging, the influence of repetition frequency," *2011 Electr. Insul. Conf. EIC 2011*, no. June, pp. 444–448, 2011.
[34] T. Koltunowicz, G. Bajracharya, D. Djairam, M. Al-Suhaily, and J. Smit, "The effects of prolonged exposure of paper insulation to fast repeating transients," *2010 Int. Conf. High Volt. Eng. Appl. ICHVE 2010*, pp. 180–183, 2010.
[35] T. K. Saha, "Review of modern diagnostic techniques for assessing insulation condition in aged

transformers," *IEEE Trans. Dielectr. Electr. Insul.*, vol. 10, no. 5, pp. 903–917, Oct. 2003.
[36] A. M. Emsley, M. Ali, X. Xiao, and R. J. Heywood, "Degradation of cellulosic insulation in power transformers. Part 4: Effects of ageing on the tensile strength of paper," *IEE Proc. - Sci. Meas. Technol.*, vol. 147, no. 6, pp. 285–290, Nov. 2000.
[37] C. Zhang and J. K. Macalpine, "Furfural Concentration in Transformer Oil as an Indicator of Paper Ageing: Field Measurements," in *2006 IEEE/PES Transmission & Distribution Conference and Exposition: Latin America*, 2006, pp. 1–6.
[38] J. S. Simons and M. T. Richards, "Non-destructive electrical test methods for evaluating high-voltage stator insulation," *Proc. IEE Part A Power Eng.*, vol. 109, no. 3S, p. 71, 1962.
[39] C. F. Ten, M. A. R. M. Fernando, and Z. D. Wang, "Dielectric properties measurements of transformer oil, paper and pressboard with the effect of moisture and ageing," in *2007 Annual Report - Conference on Electrical Insulation and Dielectric Phenomena*, 2007, pp. 727–730.
[40] D. Linhjell, L. Lundgaard, and U. Gäfvert, "Dielectric response of mineral oil impregnated cellulose and the impact of aging," *IEEE Trans. Dielectr. Electr. Insul.*, vol. 14, no. 1, pp. 156–169, 2007.
[41] IEC 60270, "High-voltage test techniques - Partial discharge measurements," 2001.
[42] B. Florkowska, J. Roehrich, P. Zydroń, and M. Florkowski, "Measurement and analysis of surface partial discharges at semi-square voltage waveforms," *IEEE Trans. Dielectr. Electr. Insul.*, vol. 18, no. 4, pp. 990–996, 2011.
[43] T. Koltunowicz, A. Cavallini, D. Djairam, G. C. Montanari, and J. Smit, "The influence of square voltage waveforms on transformer insulation break down voltage," *Annu. Rep. - Conf. Electr. Insul. Dielectr. Phenomena, CEIDP*, pp. 48–51, 2011.
[44] M. S. Moonesan, S. H. Jayaram, and E. A. Cherney, "Time to failure of medium-voltage form-wound machine turn insulation stressed by unipolar square waves," *IEEE Trans. Dielectr. Electr. Insul.*, vol. 22, no. 6, pp. 3118–3125, 2015.
[45] K. Wu, T. Okamoto, and Y. Suzuoki, "Effects of discharge area and surface conductivity on partial discharge behavior in voids under square voltages," *IEEE Trans. Dielectr. Electr. Insul.*, vol. 14, no. 2, pp. 461–470, 2007.
[46] A. Müller, M. Beltle, S. Coenen, and S. Tenbohlen, "Correlation of DGA, UHF PD Measurement and Vibration Data for Power Transformer Monitoring," *Symp. High Volt. Eng. Hann.*, no. October 2014, 2011.
[47] F. Endo, S. Yamamoto, T. Sadakane, A. Yamagishi, K. Miyagi, and H. Okubo, "Analysis of gasses generated by electrical discharges in low viscosity silicone oil," *Proc. 2008 Int. Conf. Cond. Monit. Diagnosis, C. 2008*, vol. 1, pp. 272–275, 2007.
[48] E. Bjerkan, *High frequency modeling of power transformers*, no. May. 2005.
[49] D. Konig and K. Kress, "Study of power coil resonance phenomena based on traveling wave theory," *IEEE Trans. Electr. Insul.*, vol. 26, no. 3, pp. 349–357, Jun. 1991.
[50] M. Popov, L. van der Sluis, R. P. P. Smeets, and J. Lopez Roldan, "Analysis of Very Fast Transients in Layer-Type Transformer Windings," *IEEE Trans. Power Deliv.*, vol. 22, no. 1, pp. 238–247, Jan. 2007.
[51] A. De, D. Debnath, and A. Chakrabarti, "A study on the impact of low-amplitude oscillatory switching transients on grid connected EHV transformer windings in a longitudinal power supply system," *IEEE Trans. Power Deliv.*, vol. 24, no. 2, pp. 679–686, 2009.
[52] T. V. Craenenbroeck, H. De Herdt, J. De Ceuster, J. P. Marly, D. Van Dommelen, and R. Belmans, "Detailed study of fast transient phenomena in transformers and substations leading to an improved system design," *15th Int. Conf. Electr. Distrib.*, pp. 1–6, 1999.
[53] C. A. Banda and J. M. Van Coller, "Resonant overvoltages in wind turbine transformers," *2015 IEEE Eindhoven PowerTech, PowerTech 2015*, 2015.

[54] IEC/IEEE International Draft Standard - "Power Transformers - Part 16: Transformers for Wind Turbine Application," in P60076-16_D3, February 2017 , vol., no., pp.1-24, Jan. 1 2017.
[55] J. R. Secue and E. Mombello, "Sweep frequency response analysis (SFRA) for the assessment of winding displacements and deformation in power transformers," *Electr. Power Syst. Res.*, vol. 78, no. 6, pp. 1119–1128, 2008.
[56] A. Wilk and D. Adamczyk, "Investigations on sensitivity of FRA method in diagnosis of interturn faults in transformer winding," *Proc. - ISIE 2011 2011 IEEE Int. Symp. Ind. Electron.*, pp. 631–636, 2011.
[57] P. Gómez, F. P. Espino-Cortés, and F. De León, "Computation of the dielectric stresses produced by PWM type waveforms on medium voltage transformer windings," *Annu. Rep. - Conf. Electr. Insul. Dielectr. Phenomena, CEIDP*, pp. 199–202, 2011.
[58] P. G. Blanken, "A lumped winding model for use in transformer models for circuit simulation," *IEEE Trans. Power Electron.*, vol. 16, no. 3, pp. 445–460, May 2001.
[59] A. Holdyk, B. Gustavsen, I. Arana, and J. Holboell, "Wideband modeling of power transformers using commercial sFRA equipment," *IEEE Trans. Power Deliv.*, vol. 29, no. 3, pp. 1446–1453, 2014.
[60] B. Gustavsen, "Wide band modeling of power transformers," *IEEE Trans. Power Deliv.*, vol. 19, no. 1, pp. 414–422, 2004.
[61] A. H. Soloot, H. K. Hoidalen, and B. Gustavsen, "The effect of winding design on transformer frequency response with application on offshore wind farm energization," *2012 Int. Conf. Renew. Energy Res. Appl. ICRERA 2012*, pp. 1–2, 2012.
[62] M. Devgan, "Investigation of High Frequency Switching Transients on Wind Turbine Step Up Transformers," 2015.
[63] Ohlen Matz, "A better way for transformer condition assessment," *Megger*. [Online]. Available: http://en.megger.com/support/technical-library/electrical-tester-online/2014/july-2014/a-better-way-for-transformer-condition-assessment/. [Accessed: 15-Jan-2017].
[64] Megger, "The Complete Guide to Electrical Insulation Testing," p. 67, 2006.
[65] A. A. Reykherdt and V. Davydov, "Case studies of factors influencing frequency response analysis measurements and power transformer diagnostics," *Electr. Insul. Mag. IEEE*, vol. 27, no. 1, pp. 22–30, 2011.
[66] N. Abeywickrama, Y. V Serdyuk, and S. M. Gubanski, "Frequency Response Analysis (FRA) for Characterization of Power Transformer Insulation," vol. 21, no. 3, pp. 1–6, 2005.
[67] B. Badrzadeh, "High-Frequency Modeling and Simulation of Wind Turbine Transformer With Doubly Fed Asynchronous Generator," vol. 27, no. 2, pp. 746–756, 2012.
[68] T. Committee and E. Society, "Draft Guide on Transformers for Application in Distributed Photovoltaic (DPV) Power Generation Systems," no. May, 2015.
[69] J. Merrikhi, J. S. Moghani, and E. Fallah, "Laminated Iron Core Inductor Model with Flux Skin Effect," in *2006 2nd International Conference on Power Electronics Systems and Applications*, 2006, pp. 77–78.
[70] J.-W. Kim, B. Park, S. C. Jeong, S. W. Kim, and P. Park, "Fault Diagnosis of a Power Transformer Using an Improved Frequency-Response Analysis," *IEEE Trans. Power Deliv.*, vol. 20, no. 1, pp. 169–178, 2005.
[71] J. C. G. Wheeler, "Effects of converter pulses on the electrical insulation in low and medium voltage motors," *IEEE Electr. Insul. Mag.*, vol. 21, no. 2, pp. 22–29, 2005.
[72] E. Lee and W. Meng, "Dissolved Gas Analysis (DGA) of mineral oil used in transformers," *Singapore Eng.*, vol. 1, no. May, pp. 4–5, 2009.
[73] J. B. Digiorgio, "Dissolved Gas Analysis of Mineral Oil Insulating Fluids," *North. Technol. Test.*, no. 916, 2013.

[74] R. C. Kiiza, M. G. Niasar, R. Nikjoo, X. Wang, and H. Edin, "The effect of partial discharge by-products on the dielectric frequency response of oil-paper insulation comprising of a small cavity," *IEEE Trans. Dielectr. Electr. Insul.*, vol. 22, no. 5, pp. 2923–2930, 2015.
[75] I. Craiova, "TRANSFORMER DIAGNOSIS CORRELATING DGA WITH," no. 30, pp. 103–107, 2006.
[76] P. Wang, A. Cavallini, G. Montanari, and G. Wu, "Effect of rise time on PD pulse features under repetitive square wave voltages," *IEEE Trans. Dielectr. Electr. Insul.*, vol. 20, no. 1, pp. 245–254, 2013.
[77] M. Bagheri, M. Naderi, T. Blackburn, and T. Phung, "Frequency response analysis and short-circuit impedance measurement in detection of winding deformation within power transformers," *IEEE Electr. Insul. Mag.*, vol. 29, no. 3, pp. 33–40, 2013.
[78] A. P. Purnomoadi and D. Fransisco, "Modeling and diagnostic transformer condition using sweep frequency response analysis," *Proc. IEEE Int. Conf. Prop. Appl. Dielectr. Mater.*, pp. 1059–1063, 2009.
[79] S. M. Islam and G. Ledwich, "Locating transformer faults through sensitivity analysis of high frequency modeling using transfer function approach," *Conf. Rec. 1996 IEEE Int. Symp. Electr. Insul.*, vol. 1, pp. 38–41, 1996.

Appendix A
Transformer black-box modelling

A.1 Measurement procedure

The applied method assumes the transformer as a linear time-invariant and frequency-dependent black-box with six terminals. Frequency responses are obtained via on-site measurements as a set of current-voltage ratios (admittance matrix) over a wide band of frequency.

$$\begin{bmatrix} I_1 \\ I_2 \\ I_3 \\ I_4 \\ I_5 \\ I_6 \end{bmatrix} = \begin{bmatrix} Y_{11} & Y_{12} & Y_{13} & Y_{14} & Y_{15} & Y_{16} \\ Y_{21} & Y_{22} & Y_{23} & Y_{24} & Y_{25} & Y_{26} \\ Y_{31} & Y_{32} & Y_{33} & Y_{34} & Y_{35} & Y_{36} \\ Y_{41} & Y_{42} & Y_{43} & Y_{44} & Y_{45} & Y_{46} \\ Y_{51} & Y_{52} & Y_{53} & Y_{54} & Y_{55} & Y_{56} \\ Y_{61} & Y_{62} & Y_{63} & Y_{64} & Y_{65} & Y_{66} \end{bmatrix} \begin{bmatrix} V_1 \\ V_2 \\ V_3 \\ V_4 \\ V_5 \\ V_6 \end{bmatrix}$$

Where [Y] represents the admittance matrix, and [I] and [V] represent current and the voltage vectors, respectively. As shown in Figure A-1, applying a voltage of V_i and zero voltage to the remaining terminals produces i^{th} column of [Y], where Y_{ji} can be determined by finding the ratio between I_j to V_i. Similarly, the other five columns can be determined for a three-phase transformer.

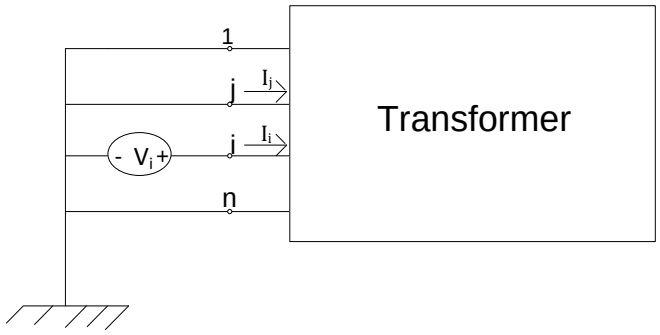

Figure A-1: N-Terminal transformer model.

Figure A-2 shows the measurement of admittances on the low and high voltage sides of the WTSU transformer.

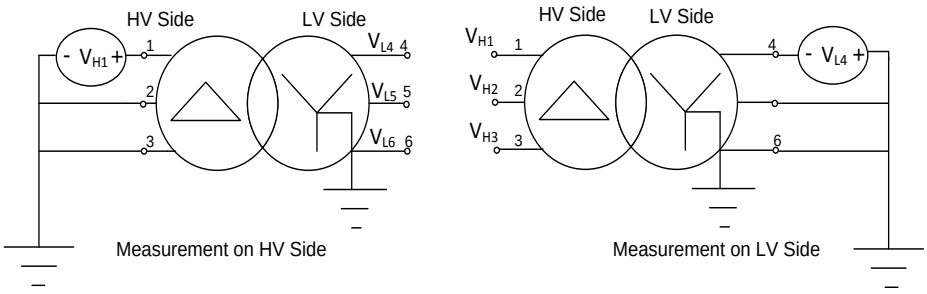

Figure A-2: Admittance matrix measurements on the HV and LV side of the transformer.

A.2 Transformer modelling

The admittance data measured as function of frequency is approximated using rational functions and vector fitting technique. Figure A-3 shows the measured and fitted curves of admittance magnitude across the transformer terminals. The graphs show the rational approximation of 36 elements of WTGSU transformer with an approximation order of 23, over 1201 frequency points in the frequency range of 20 Hz to 1 MHz. Although the fitting in low-frequency segment up to around 600 kHz is near perfect, the approximation resolution slightly drops at higher frequencies. The total rms-error of approximation, in this case, is as low as 0.013563.

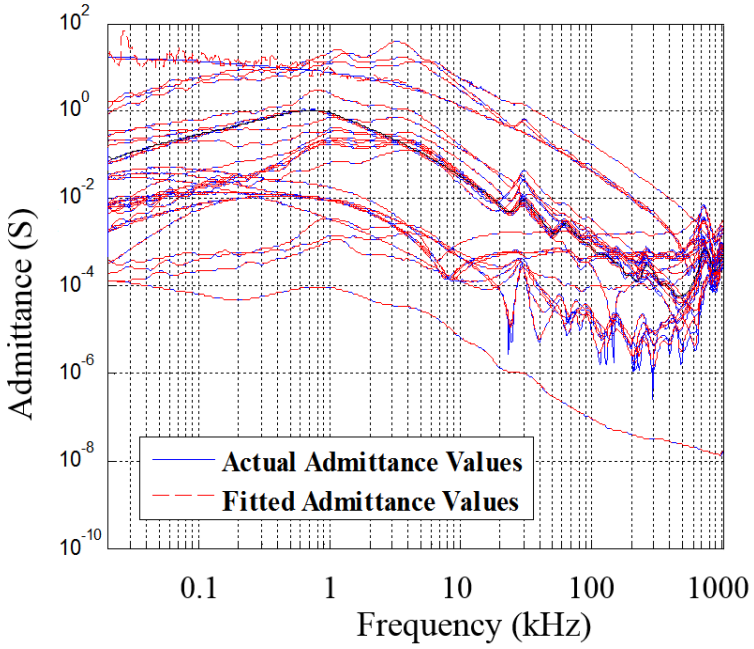

Figure A-3: Measured and calculated values of admittance matrix of the transformer.

A.3 System modelling

This section summarizes the simulation results of transient voltages generated in events of circuit breaker operation for a sample wind-farm in Ontario, Canada. The results are fully explained in [62]; hence the parts of results that are used for paper/oil PD study are mentioned here.

Figure A-4 describes the test circuit, which represents a type-IV wind-farm unit connected to the grid, simulated in PSCAD. Generation system is an approximated model of doubly-fed induction generator (DIFG) equipped with generator converter and grid converter controls. The length of low-voltage cable is 65 meters and the length of high-voltage cable is 120 meters, which are typical in connecting WTGSU transformers to circuit breakers. The short circuit ratio of the grid is 5, *X/R* ratio is 2.5, P_{base} is 150 MW and V_{base} is 130 kV.

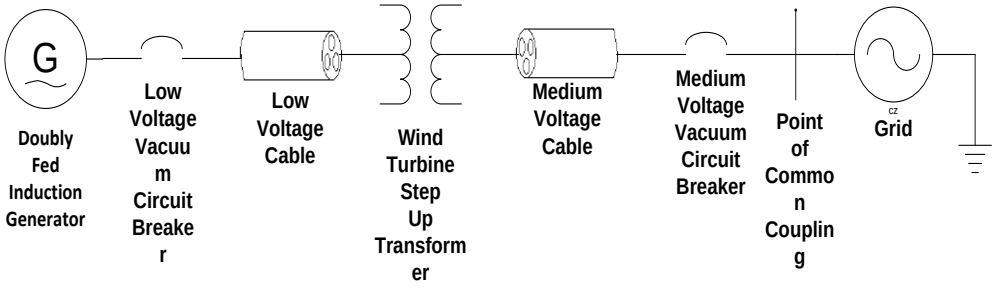

Figure A-4: Illustration of test circuit simulated in PSCAD.

The following scenarios are considered to analyze transient overvoltages in the proposed set-up:

- Case 1: VCB opening on LV side of WTSU transformer under no load
- Case 2: VCB opening on LV side of WTSU transformer under an inductive load
- Case 3: VCB closing on LV side of WTSU transformer under no load
- Case 4: VCB closing on LV side of WTSU transformer under inductive load
- Case 5: VCB opening on HV side of WTSU transformer under no load
- Case 6: VCB opening on HV side of WTSU transformer under inductive load
- Case 7: VCB closing on HV side of WTSU transformer under no load
- Case 8: VCB closing on HV side of WTSU transformer under inductive load

On the basis of these scenarios, analyses are done to determine the switching oscillation. Table A-1 summarizes the results of transient voltage simulation for the studied cases.

Table A-1: Comparison of oscillations for the studied cases.

Case Study	Peak Voltage (p.u.)	Maximum rate of voltage rise (kV/µs)	Frequency of oscillations (kHz)	Number of reignitions (Phase with highest reignitions)
1	1.4	----	0.59	----
2	3.5	7.5	0.47	73
3	1.72	----	22.1	----
4	2.1	1.1	20.3	71
5	2.9	2.3	0.66	4
6	3.03	28	0.56	74
7	1.8	----	22	----
8	1.1	5.5	24	64